Profiling cell envelope-antibiotic interactions reveals vulnerabilities to β-lactams in a multidrug-resistant bacterium

Short title: Cell envelope-antibiotic interactions and β-lactam vulnerability

Andrew M Hogan [1], Dustin T Maydaniuk[1], Aakash Natarajan [1], Beltina Léon [2], Zayra Batun [1], Anna Motnenko [1], Alejandra Bosch [2], Silvia T Cardona [1,3]*

1. Department of Microbiology, University of Manitoba, Winnipeg, Manitoba, Canada
2. CINDEFI, CONICET-CCT La Plata, Facultad de Ciencias Exactas, Universidad Nacional de La Plata, La Plata, Buenos Aires, Argentina
3. Department of Medical Microbiology and Infectious Diseases, University of Manitoba, Winnipeg, Manitoba, Canada

*To whom correspondence should be addressed: Silvia.Cardona@umanitoba.ca

Keywords: Transposon mutagenesis, antibiotic combinations, β-lactam, undecaprenyl phosphate, β-lactamase, avibactam

Author Contributions

STC and AMH conceived the idea and design of the research; AMH and BL designed and constructed the randomly-barcoded transposon mutant library; AMH performed the chemogenomics experiments, analysed the sequencing data, performed targeted validation studies, and wrote and edited the manuscript; AK constructed CRISPRi mutants related to cefiderocol activity; AM performed the lipopolysaccharide analyses; ZB assessed β-lactam susceptibility of *B. cenocepacia* clinical isolates; STC edited the manuscript, and together with AB, supervised the work and provided financial support.

Abstract

The cell envelope of the Gram-negative *Burkholderia cepacia* complex (Bcc) presents unique restrictions to antibiotic penetration. As a consequence, Bcc species are notorious for causing recalcitrant multidrug-resistant infections in immunocompromised individuals, such as those living with cystic fibrosis. To systematically identify cell envelope-associated resistance and susceptibility determinants at the genome level, we constructed a high-density, randomly-barcoded transposon mutant library in the clinical isolate *B. cenocepacia* K56-2 and exposed it to a panel of more than twenty cell envelope-targeting antibiotics. By quantifying relative mutant fitness with BarSeq, followed by validation with CRISPR-interference, we profiled over a hundred new chemical-genetic interactions and identified novel mediators of antibiotic susceptibility in the Bcc cell envelope. We first reveal new connections between broad-spectrum β-lactam susceptibility, peptidoglycan synthesis, and blockages in undecaprenyl phosphate metabolism, highlighting a β-lactam critical vulnerability associated with sharing this common lipid intermediate. We then show that the clinically relevant synergy of the β-lactam/β-lactamase inhibitor combination ceftazidime/avibactam is primarily mediated by inhibition of the PenB carbapenemase, over more than twenty other putative β-lactamases. Importantly, avibactam more strongly potentiates the activity of aztreonam and meropenem than ceftazidime in a panel of Bcc clinical isolates. Finally, we characterize for first time in the Bcc the iron and receptor-dependent activity of the novel siderophore cephalosporin antibiotic, cefiderocol. Overall, our work has implications for antibiotic target prioritization, and for using additional combinations of β-lactam/β-lactamase inhibitors that can extend the utility of our current clinical arsenal of antibacterial therapies.

Author Summary

While the Gram-negative cell envelope is a major barrier to antibiotic action, we have an incomplete picture of how each component contributes to antibiotic resistance. To answer this question from a genome-wide perspective in a model of antibiotic-resistant bacteria, we constructed a library of randomly-barcoded transposon mutants in *Burkholderia cenocepacia* and exposed it to subinhibitory concentrations of a panel of diverse cell envelope-targeting antibiotics. We identified individual genes and whole pathways associated with antibiotic resistance, including several novel players. Our work revealed how connections between cell envelope biogenesis pathways can be exploited to increase antibiotic susceptibility. Focusing on clinically relevant antibiotics, our strategy dissected how the important β-lactam/β-lactamase inhibitor combination ceftazidime/avibactam acts synergistically. Additionally, we are the first to characterise the molecular basis of the antibiotic mechanism of cefiderocol in *Burkholderia*, a new and very potent siderophore-cephalosporin conjugate drug. Overall, we highlight several avenues that can be taken to enhance or develop new therapeutic strategies against *Burkholderia* infection.

Introduction

Antimicrobial resistance is a major threat to global public health. In 2019, an estimated 4.95 million deaths were associated with drug-resistant infections (Murray et al. 2022), and the toll is expected to rise in the future (O'Neill 2014). Gram-negative bacteria consistently top the list as priorities for antibiotic development as they are a leading cause of antibiotic-resistant infections (Arzanlou et al. 2017).

A significant driver of antibiotic resistance in Gram-negative bacteria lies in the double membrane composition of their cell envelope. The outer membrane is an asymmetric bilayer composed of phospholipids on the inner leaflet and lipopolysaccharide (LPS), decorated with O-antigen units, on the outer leaflet. Asymmetry is maintained by the action of the Mla pathway, which transports excess phospholipids from the outer membrane back to the inner membrane (Powers et al. 2020). Together, the inner and outer membranes have orthogonal permeability requirements: small hydrophilic compounds (generally <600 Da; (Decad and Nikaido 1976) are able to diffuse through water-filled porins in the outer membrane, while hydrophobic compounds are able to diffuse through the inner membrane (Masi et al. 2017). The peptidoglycan sacculus is not involved in envelope permeability *per se*, but rather performs the essential function of maintaining cell shape and structural integrity (van Teeseling et al. 2017). Indeed, many components of the bacterial cell envelope are essential and have no human homologue, thus are attractive targets for a variety of antibiotics. Moreover, the use of small-molecule potentiators has gained traction as a route to increase membrane permeability and the activity of other antibiotics (Klobucar and Brown 2022).

Bacteria of the genus *Burkholderia* are notorious for their high levels of intrinsic antibiotic resistance due in part to the unique characteristics of the cell envelope (Rhodes and Schweizer 2016). Among them, the lineage known as *Burkholderia cepacia* complex (Bcc) are

opportunistic pathogens that primarily infect immunocompromised individuals. Some species, such as *B. cenocepacia*, may cause a form of pneumonia and bacteremia known as cepacia syndrome (Isles et al. 1984). Near uniform resistance to several antibiotic classes severely limits treatment options (Aaron et al. 2000; Abbott et al. 2016), and eradication protocols often require weeks to months of antibiotic cocktails (Kitt et al. 2016; Garcia et al. 2018). Furthermore, although new therapies (e.g. the CFTR modulators) are available to treat the symptoms of cystic fibrosis, there may be limited benefit in pathogen clearance (Durfey et al. 2021), but this has not yet been assessed for Bcc infection. Thus, developing new antibiotic therapies for Bcc infections remains a high priority.

The majority of our knowledge of cell envelope biogenesis comes from model organisms. However, there are noted structural differences in the Bcc cell envelope that alter its function and confer high levels of antibiotic resistance, such as LPS modifications (Isshiki et al. 1998; Hamad et al. 2012), highly restrictive porins (Parr et al. 1987), and an array of efflux pumps (Scoffone et al. 2021). The demonstrated differences between the Bcc cell envelope and common models limits the utility of broad inferences from homology and highlights the need for specific studies of the Bcc cell envelope and its effect on antibiotic action.

Here, we performed a genome-wide, transposon mutant screen in *B. cenocepacia* K56-2, a previous epidemic isolate and model for Bcc research, against a wide array of cell envelope-targeting antibiotics. We reasoned that transposon insertion in certain genes would create specific deficiencies in the cell envelope, thus revealing mechanisms of cell envelope-related antibiotic resistance and susceptibility in K56-2. Using BarSeq to quantify mutant fitness in 22 conditions (Wetmore et al. 2015), we identified over a hundred new chemical-genetic interactions that were validated by CRISPRi. We uncovered new modulators of antibiotic

susceptibility in cell envelope biogenesis pathways and dissected the vulnerable connectivity between undecaprenyl phosphate utilisation pathways. Analysis of the synergistic ceftazidime/avibactam combination revealed that the potentiation is primarily through inhibition of the PenB β-lactamase, which guided us to more potent combinations with aztreonam and meropenem. Additionally, we provide the first detailed characterisation of the activity of the novel siderophore-cephalosporin conjugate antibiotic cefiderocol, in the Bcc. Overall, we demonstrate how the analysis of genome-wide antibiotic-genetic interactions can identify susceptibility determinants and antibiotic combinations that may be exploited to bolster current antibiotic therapies.

Results

Identifying the genome-wide response of B. cenocepacia K56-2 to antibiotics targeting cell envelope processes

Rationale for the selected antibiotics

The Gram-negative cell envelope presents both a major permeability barrier to antibiotics and a potential source of antibiotic targets. In particular, Bcc species are known for their impermeable cell envelope (~10 fold less permeable compared to *E. coli* (Parr et al. 1987; Aronoff 1988)), which contributes to extreme resistance to membrane-disrupting detergents and multiple classes of antibiotics (Loutet and Valvano 2011; Ahn et al. 2016). Our goal was to probe important envelope biogenesis pathways to gain insight into the mechanisms governing cell envelope-related resistance in *B. cenocepacia* K56-2. We therefore assembled a diverse panel of clinical and pre-clinical antibiotics targeting many aspects of cell envelope biogenesis (Figure 1 and Figure S1; all abbreviations listed in Table 1). We also included three hydrophobic large scaffold antibiotics in this panel that are generally excluded by the Gram-negative cell envelope (rifampicin [RIF], erythromycin [ERY], and novobiocin [NOV]; molecular weight > 600 Da) (Decad and Nikaido 1976; Klobucar and Brown 2022). We expected the large scaffold antibiotics, to highlight chemical-genetic interactions in cell envelope permeability and disruptions in major cell envelope biogenesis mechanisms. In summary, we aimed to study cell envelope biogenesis and resistance mechanisms and how they may be exploited to inform novel antibiotic combinations.

Constructing and validating a randomly-barcoded transposon mutant library

To profile genome-wide contributions to antibiotic susceptibility and resistance, we turned to transposon mutagenesis and TnSeq to measure mutant abundance during antibiotic challenges.

Previously, our lab has constructed transposon mutant libraries in K56-2, a multidrug-resistant ET12 epidemic lineage clinical isolate (Darling et al. 1998), to identify the essential genome (Gislason et al. 2017b) and characterise targets and mechanisms of action for antimicrobials (Gislason et al. 2017a; Hogan et al. 2018; Nunvar et al. 2019). To leverage advances in sequencing and bioinformatic capabilities, we modified our Tn*5* transposon to contain a random 20 bp barcode (Figure S1D), greatly facilitating tracking mutant abundance in many conditions by Illumina sequencing (Wetmore et al. 2015). After linking unique barcodes to genomic insertion site (RB-TnSeq), barcodes may be simply amplified by PCR and sequenced (BarSeq) (Figure S1D).

We generated a library of ~340,000 uniquely barcoded transposon mutants in K56-2 (approximately equally divided into 10 subpools). Library statistics can be found in Table S1. The library had a median of 12 insertions per protein-coding gene and an average spacing between insertions of 18.7 bp. We found that insertion sites were more likely in low GC-content regions and genes (Figure S2) as we observed previously (Gislason et al. 2017b), which may be due to Tn*5* transposon insertion and DNA sequencing biases.

To ensure we could use BarSeq to accurately quantify mutant abundance, we performed a pilot experiment with known levels of mutant depletion. Quantification of mutant abundance demonstrated high replicate reproducibility (Figure S3A) and close agreement with expected levels of depletion (Figure S3B). Despite a ~10-fold range in barcode recovery in pools with equal mutant abundance – variation that was not due to barcode GC-content (Figure S3C) – we were able to successfully and accurately quantify barcoded mutant depletion at small scale.

<u>Antibiotic exposure and detection of broad interactions on whole pathways and processes</u>

The choice of antibiotic exposure conditions has important implications for the sensitivity of high-throughput experiments. Thus, to enable detection of specific mechanism-related interactions, antibiotic doses were selected to inhibit 20 – 30% of growth relative to growth without antibiotics (Hogan et al. 2018; Geisinger et al. 2020; Bailey et al. 2022), as measured by OD_{600} (Figure S4 and Table 1). As controls for the synergistic combination of ceftazidime/avibactam (AVI/CAZ), each component was also used at the lower concentration present in the combination as well as higher concentrations that individually inhibited 20 – 30% of growth. Ampicillin (AMP), fosfomycin (FOS), and CHIR-090 (CHIR) did not attain 20% growth inhibition so were each used at the highest concentration tested (256 µg/mL).

The entire pool of ~340,000 unique mutants was inoculated in LB medium at OD_{600} 0.025 (~75 CFU/mutant) and allowed to reach early exponential phase (OD_{600} 0.15). The cultures were then exposed to antibiotics (or 1% DMSO solvent control) for 8 hours (~10 generations), after which genomic DNA was harvested and used as template for BarSeq. High-output Illumina NextSeq flow cells were used to accommodate ~500 reads/gene for each condition and replicate. Resulting barcodes were counted and matched to insertion site, then normalized to Time 0 controls, aggregated across replicates to calculate average per-gene fitness scores (Wetmore et al. 2015; Morin et al. 2018).

Comparison between the DMSO control and each condition revealed hundreds of broad and specific factors that contribute to antibiotic susceptibility (Figure S5). As a first look to reveal effects on whole pathways and processes, the genes significantly affecting fitness in each condition were analysed for enrichment in BioCyc pathways and GO terms (Figures S6-S8) (Ashburner et al. 2000; Castillo-Davis and Hartl 2003; Karp et al. 2019; Gene Ontology Consortium 2021). For negative fitness effects, we observed an enrichment in genes in (phospho)lipid metabolism

pathways (Figures S6 and S8). Additionally, we found enrichment in many GO terms related to the cell envelope (Figures S7 and S8). These are, for example, “peptidoglycan metabolic process”, “integral component of the membrane”, and “periplasmic space”. Broadly, these findings are in line with expectations that cell envelope-targeting antibiotics will report on susceptibility determinants in the cell envelope.

Identifying similar hallmarks as other chemical genetics studies would serve as additional validation of our results. For example, although antibiotics act by distinct mechanisms based on their class, many also exert as metabolic perturbations and the induction of reactive oxygen species (ROS) (Kohanski et al. 2007; Dwyer et al. 2014). We found that disruptions in genes related to purine and pyrimidine metabolism and amino acid metabolism pathways often showed reduced susceptibility to antibiotics, especially the β-lactams (Figures S6 and S8). Inactivating these genes may slightly reduce metabolic rate and nucleotide pools, both known to affect antibiotic susceptibility (Yang et al. 2019; Lopatkin et al. 2019). Conversely, we found that disruptions in several genes related to ROS mitigation increased antibiotic susceptibility. When genes related to polyamine and reductant metabolism pathways were disrupted, susceptibility often increased (Figure S6). This was also detected by GO term enrichment of “response to oxidative stress”and “glutathione metabolic process” (Figure S7). Glutathione and polyamines, such as putrescine, are both known to be important in *B. cenocepacia* for protection against ROS (El-Halfawy and Valvano 2014; Van Acker et al. 2016). Together, the corroboration of several previous works and expected findings confirms the validity of our BarSeq approach to uncover detailed chemical-genetic interactions at the foundations of antibiotic action.

Chemical-genetic interactions with outer membrane components

The Mla, BAM, and Lol pathways are important for envelope integrity and resistance to multiple antibiotics

The Mla pathway functions in retrograde transport of excess phospholipids from the outer membrane to the inner membrane, thereby maintaining an asymmetric, and more impermeable, outer membrane enriched in LPS (Figure 2A) (Malinverni and Silhavy 2009; Powers et al. 2020). In *B. cenocepacia* and *B. dolosa*, defects in the Mla pathway are known to increase susceptibility to large-scaffold antibiotics and serum (Bernier et al. 2018). However, homologous defects in *E. coli* K-12 and *P. aeruginosa* PA14 were found to not alter susceptibility to a variety of antibiotics (Bernier et al. 2018). In K56-2, the Mla pathway is encoded by six genes organized in two operons, and possibly two accessory genes (K562_RS01610 and K562_RS01615) in an adjacent operon (Bernier et al. 2018).

In our BarSeq experiment, genes encoding components of the Mla pathway had negative fitness scores for nearly all tested antibiotic conditions (Figures S5 and Figure 2B). Disruptions in *mlaFED*, generally resulted in greater susceptibility increases, especially for the large scaffold antibiotics (ERY, NOV, and RIF), than did disruption in *vacJ* and *mlaCB* (Figure 2B). Indeed, the average fitness score of the Mla pathway genes negatively correlated with the molecular weight of the antibiotic (Figure 2C). To support these findings, we used CRISPR-interference (CRISPRi) (Qi et al. 2013; Hogan et al. 2019) to silence the *mlaFEDvacJ* and *mlaCB* operons. Using an *N*-phenyl-1-naphthylamine (NPN) uptake assay (Loh et al. 1984; Malott et al. 2012), we found that both of these mutants had substantially increased outer membrane permeability than the control (Figure 2D). Our findings of broad susceptibility profiles for mutants in the Mla pathway support a unique importance of this pathway in maintaining the permeability barrier of the outer membrane in *Burkholderia*, similar to a previous report (Bernier et al. 2018).

We next reasoned that chemical permeabilization of the membrane may also increase antibiotic susceptibility of K56-2. We found chlorhexidine (CHX), but not polymyxin B (PMB), to greatly increase outer membrane permeability (Figure S9). Consequently, in checkerboard interaction assays, CHX synergised strongly with large scaffold antibiotics and the β-lactams (Figure 2E).

Additionally, we were able to link disruptions in the BAM complex (β-barrel insertion into the outer membrane) (Wu et al. 2005) and Lol pathway (lipoprotein trafficking to the outer membrane) (Okuda and Tokuda 2011) with susceptibility to PMB and CHX, and to AVI, aztreonam (AZT), meropenem (MEM), CHX, and PMB, respectively (Figure S5). Given the transport and folding functions of the Lol and BAM pathways, it is likely that these changes in susceptibility are a consequence of improper localization of important outer membrane factors (e.g. Lpt and Mla proteins). Overall, our findings show that cell envelope impermeability severely limits antibiotic entry into *B. cenocepacia* K56-2.

<u>LPS, lipid A modifications, and RpoE regulon confer resistance to cationic antibiotics</u>

As part of their mechanisms of action, the cationic antibiotics CHX and PMB bind to and disrupt bacterial membranes. In *E. coli*, PMB binds the lipid A moiety of LPS (Pristovsek and Kidric 1999), both in the inner and outer membranes, resulting in cell lysis (Sabnis et al. 2021). CHX is reported to collapse the membrane potential (Kuyyakanond and Quesnel 1992) and disrupt only the outer membrane (Barrett-Bee et al. 1994). In Gram-negatives, such as *Salmonella enterica* and *P. aeruginosa*, cationic antibiotic resistance is inducible (Simpson and Trent 2019); however, *Burkholderia* species are intrinsically resistant to these agents, mediated both by physical protection of the membrane and by adaptive responses (Loutet et al. 2011). The

Burkholderia O-antigen, LPS core, and RpoE envelope stress regulon are known to be important for PMB resistance (Ortega et al. 2009; Loutet et al. 2011).

We thus leveraged our BarSeq experiment for a deeper look into cationic antibiotic resistance in *Burkholderia*. We identified genes important for PMB and/or CHX fitness associated with lipid A synthesis, LPS core synthesis, lipid A modification, and polymeric O-antigen synthesis (Figure 2F). To dissect the importance of the O-antigen vs. LPS core, we created unmarked deletion mutants in *wbiI* and *hldD,* genes required for O-antigen and LPS core synthesis, respectively. As expected, both mutants lacked polymeric O-antigen , and could be complemented *in trans* (Figure S10). Both the Δ*wbiI* and Δ*hldD* mutants were markedly more susceptible to PMB, colistin (COL) and CHX (Figure 2G); however, the Δ*wbiI* mutant was generally less susceptible than the Δ*hldD* mutant, and the increase in CHX susceptibility was only modest for both mutants. Only the Δ*hldD* mutant was more susceptible to AZT, CAZ, and MEM (Figure 2G). However, the Δ*hldD* mutant showed a large increase in outer membrane permeability as measured by NPN uptake (Figure 2H), demonstrating a complete LPS core, but not O-antigen, is required for outer membrane integrity. On the contrary, BarSeq gene fitness of *hldD* was not correlated with antibiotic molecular weight (P = 0.27; data not shown). Taken together, we suggest that only part of the antibiotic susceptibility caused by defects in *hldD* are due to increased permeability. These findings also support independent roles of the O-antigen and LPS core in physically protecting the cell from cationic antibiotics.

Lipid A modification with 4-deoxy-4-aminoarabinose (Ara4N) is known to provide cationic antibiotic resistance by reducing the net negative charge of LPS (Gunn et al. 1998). UndP is known to be the carrier for Ara4N (Trent et al. 2001b, 2001a) (Figure 2I). Supporting the connection between UndP and the Ara4N modification, we found that disruption of *dbcA*

increased susceptibility to PMB and CHX (Figure 2F). *dbcA* is a homologue of *E. coli uptA*, encoding a DedA-family UndP flippase critical for UndP recycling (Figure 3I) (Panta et al. 2019; Roney and Rudner 2022; Sit et al. 2022); thus, disruption of *dbcA* likely reduces the abundance of free UndP available for linkage to Ara4N. We also found that inhibition of UndP synthesis with the fosmidomycin analogue FR-900098 (FR-9) strongly synergised with both PMB and CHX (Figure 2J). These findings are in line with a previous report that *dbcA* is required for polymyxin resistance in *B. thailandensis* (Panta et al. 2019).

Cell envelope stress responses monitor the presence of unfolded outer membrane proteins in the periplasm and upregulate various adaptive responses (Hews et al. 2019). The Rcs and Cpx response genes lack strong homologues in K56-2, thus only the extracytoplasmic sigma factor (RpoE) response has been characterised in *B. cenocepacia* (Flannagan and Valvano 2008). Examining our BarSeq data, we found that RpoE itself, RseP (a protease necessary for RpoE activation), and the RpoE-regulated protein chaperones SurA and DnaK were important for fitness in the presence of PMB and/or CHX (Figure 2F). SurA has been linked to the maintenance of membrane integrity in *P. aeruginosa* (Klein et al. 2019), and disruption of these chaperones likely impairs outer membrane protein folding and the cell envelope stress response (Hews et al. 2019). Together, our findings demonstrate that both physical protective and adaptive responses are important for cationic antibiotic resistance in K56-2.

<u>Changes in susceptibility reveal new substrates for the BpeAB-OprB efflux pump and specific porins</u>

Bacteria possess a variety of efflux pumps that are associated with a diverse range of functions, including the removal of toxic compounds such as antibiotics. However, many of the

antibiotics used in the current study are not known to be substrates for *Burkholderia* efflux pumps. We hypothesized that transposon insertions in genes encoding efflux pumps would decrease fitness in the presence of each pump's range of substrates. From our BarSeq experiment, we observed that disruption of the K562_RS30055 PACE family efflux pump was important for fitness in the presence of multiple antibiotics, while disruption of the K562_RS10630 EmrE pump homologue was specifically important for fitness with CHX (Figure 3A).

B. cenocepacia K56-2 encodes 16 tripartite RND efflux pumps, of which several are important for antibiotic resistance (Bazzini et al. 2011). From our BarSeq experiment, we found that disruptions in components of the BpeAB-OprB efflux pump (also called RND-4, a homologue of the MexAB-OprM pump in *P. aeruginosa*) increased susceptibility to NOV, AVI, AVI/CAZ, PF-04753299 (PF-04) and CHIR (Figure 3A). Enhanced susceptibility was only seen for disruptions in *bpeA* and *bpeB*, but not for *oprB*, suggesting that the *bpeAB* complex may also form functional associations with other outer membrane factors. Before this study NOV, AVI, PF-04, and CHIR were not known to be effluxed by BpeAB-OprB in *B. cenocepacia*. To verify these findings, we used CRISPRi to knock down the *bpeABoprB* operon. Silencing of the operon by CRISPRi was validated by a 2-fold reduction in MIC of the known substrate chloramphenicol (CHL) (Figure 3B). Knockdown of this pump did not cause a growth defect without antibiotics (Fig S11). Upon dCas9 induction, susceptibility to NOV, PF-04, AVI, and AVI/CAZ moderately increased, but not to CAZ only (Figure 3B). We thus conclude that NOV, AVI, PF-04, and CHIR are new substrates for the BpeAB-oprB efflux pump in *B. cenocepacia*.

K56-2 encodes at least 130 putative porins and permeases, and few have been characterised in terms of their physiological importance. We observed that disruption of

K562_RS29850, encoding the PhnU putative 2-aminoethylphosphonate ABC-type permease, resulted in markedly reduced susceptibility exclusively in the presence of FR-9 (Figure 3A). The structural similarity between 2-aminoethylphosphonate and FR-9 leaves open the possibility that FR-9 may also be taken into K56-2 via this transporter. We found that other porins were important for fitness in multiple conditions (e.g. K562_RS21020 and K562_RS20540) (Figure 3A and Supporting Data 1). Some porins, such as OmpA and OmpC in *E. coli*, are known to be important for maintaining membrane integrity (Choi and Lee 2019), which may explain why the lack of porins may reduce fitness in the presence of antibiotics. On the other hand, we observed several porins that when disrupted resulted in increased fitness in at least one condition (e.g. K562_RS23650 and K562_RS25925) (Figure 3A and Supporting Data 1). There were no porins associated with fitness in all conditions, not even for all β-lactams, which is suggestive of an intricate network of minor variations in porin specificity and partial functional redundancy.

Of note, we observed that disruption of K562_RS14130, a homologue of *E. coli* K-12 *ompA* (53.4% identity, top hit by reciprocal best-hit BLAST), specifically increased fitness in the presence of NOV (Figure 3A). In *E. coli*, deletion of *ompA* does not affect susceptibility to NOV (Choi and Lee 2019). Phylogenetics revealed that the porin encoded by K562_RS14130 is conserved with greater than 60% amino acid identity among many Burkholderiaceae genera (Figure S12A). The presence of this porin appears to coincide with low MIC values of NOV compared to *E. coli* and *P. aeruginosa* (Figure S12B). In K56-2, *B. multivorans* ATCC 17616 and *B. thailandensis* E264, CRISPRi repression of the K562_RS14130 homologue modestly reduced susceptibility to NOV (2-fold increase in MIC) (Figure 3C), but not other antibiotics (Figure S12C). Of note, repressing K562_RS14130 did not increase the MIC of NOV to the level of non-susceptible Gram-negatives (e.g. *E. coli* and *P. aeruginosa*), indicating that other factors

play a role in the observed differences in NOV susceptibility between *Burkholderia* species and other Gram-negatives. Together, our findings support a different role of K562_RS14130 in K56-2 and we propose it to be annotated as *opnA* for Outer membrane Protein, Novobiocin entry A.

Chemical-genetic interactions with periplasmic components

Peptidoglycan biosynthesis factors modify susceptibility to β-lactams and cycloserine

β-lactams remain one of the few options to treat Bcc infections. We thus decided to examine the genome-wide β-lactam susceptibility profiles with a focus on their target: peptidoglycan metabolism. We also considered cycloserine (CYC) and FOS as these two molecules target peptidoglycan precursor assembly in the cytoplasm. Although both display poor inhibitory activity in K56-2 (Figure S4C), FOS and CYC are still useful for treating *E. coli* infection (Zhanel et al. 2020) and tuberculosis (Alghamdi et al. 2019), respectively. FOS is an inhibitor of MurA, a UDP-*N*-acetylglucosamine 1-carboxyvinyltransferase, which catalyzes the first committed step in peptidoglycan precursor synthesis (Kahan et al. 1974). CYC is a dual inhibitor of alanine racemases (Alr and DadX), which synthesize D-alanine from L-alanine, and D-alanine-D-alanine ligase (Ddl), which synthesizes D-Ala-D-Ala (Walsh 1989). In *E. coli* and most Gram-negatives, peptidoglycan precursors contain a pentapeptide stem of L-Ala-D-Glu-*meso*-diaminopimelate-D-Ala-D-Ala. Glutamate racemase is needed to convert L-Glu to D-Glu (Barreteau et al. 2008).

The targets of CYC are encoded by the *ddl*, *alr*, and *dadX* genes. While *ddl* is essential in K56-2 and not represented in our screen, we found that disruptions in *alr* and *dadX* caused susceptibility to CYC (Figure 4A). In *P. aeruginosa*, DadX is known to be more important for growth in nutrient-poor medium (He et al. 2011); accordingly, we observed that the fitness defect

due to *dadX* disruption was less than that of *alr*. Conversely, a disruption in *dadA*, encoding a catabolic D-amino acid dehydrogenase resulted in moderately reduced susceptibility to CYC (Figure 4A). Cells lacking DadA may have elevated pools of D-amino acids, including D-alanine, thus reducing dependence on the Alr and DadX alanine racemases.

Intriguingly, disruption of *murI*, encoding glutamate racemase, and K562_RS27665, encoding a putative fusion GntR-type transcriptional regulator and pyridoxal phosphate (PLP)-dependent aminotransferase, also rendered the cells highly susceptible to CYC (Figure 4A). K562_RS27665 bears homology with the *E. coli* PatA putrescine aminotransferase and the uncharacterized *E. coli* proteins YdcR, YJiR, and YbdL. The interactions of CYC with D-glutamate biosynthesis have not been reported before. MurI is the only glutamate racemase in *E. coli* that synthesizes D-Glu for incorporation into peptidoglycan precursors (Doublet et al. 1993). Species of *Staphylococcus* and *Bacillus* encode glutamate racemase and a PLP-dependent D-amino acid transaminase, also capable of synthesizing D-glutamate using D-alanine and α-ketoglutarate as substrates (Pucci et al. 1995; Fotheringham et al. 1998). With a score above 0.95, ProteInfer (Sanderson et al. 2021) confidently predicts that K562_RS27665 is associated with amino acid metabolic GO terms such as L-aspartate: "α-ketoglutarate aminotransferase activity" and "alanine catabolic process". We therefore suggest that both MurI and K562_RS27665 are each able to synthesize enough D-glutamate for peptidoglycan synthesis, as both are non-essential in K56-2 (Gislason et al. 2017b). It is possible that inhibition of Alr/DadX/Ddl by CYC renders the peptidoglycan biosynthesis pathway highly susceptible to further disruption, or that MurI and K562_RS27665 are themselves inhibited by CYC. Together, these results hint at the fine balance of D-amino acid metabolism required for peptidoglycan synthesis.

As the primary target of the β-lactams are penicillin-binding proteins (PBPs), we also expected that disruption of specific PBPs may expose weaknesses in peptidoglycan matrix biosynthetic processes. The PBP targets of the β-lactams used here have not been determined for *Burkholderia* species; thus, we drew on similarities to other Gram-negative pathogens (Sanders et al. 1997; Davies et al. 2008; Papp-Wallace et al. 2012; Asli et al. 2016; Ito et al. 2017; Sutaria et al. 2018) (Figure 1). We observed that disruption of only two PBP-encoding genes altered β-lactam susceptibility: K562_RS05010 (encoding a homologue of the DacB DD-carboxypeptidase, also called PBP4) and K562_RS01445 (encoding a homologue of *E. coli mrcA/pbp1a* we are referring to as *mrcA2*) (Figure 4A). Only a disruption in *dacB* resulted in very low fitness in the presence of AVI-H and MEM. Only a disruption in *mrcA2* impaired fitness in the presence of AZT, tazobactam (TAZ), CYC, FOS, and cefiderocol (CFD). Transposon disruptions in either *mrcA2* and *dacB* increased susceptibility to cefotetan (CTT), CAZ-H, and AVI/CAZ (Figure 4A). Upon CRISPRi knockdown of *dacB*, we found that susceptibility only increased to MEM and AVI. These were the conditions in the BarSeq experiment that resulted in the greatest fitness defect when *dacB* was disrupted.

Notably, the findings from our BarSeq experiment contrast results obtained in *P. aeruginosa* (Moya et al. 2009), *Yersinia enterocolitica* (Liu et al. 2017), and *Aeromonas hydrophila* (Tayler et al. 2010), which show that inactivation of DacB causes β-lactam resistance. In *P. aeruginosa*, the disruption of DacB leads to activation of AmpR and the CreBC/BlrAB two-component system, resulting in AmpC overexpression (Moya et al. 2009). Disruption of the K56-2 CreBC/BlrAB homologues (K562_RS27235-40) did not affect fitness in any condition tested here (Supporting Data 1); the effect of *penR* disruption will be discussed later. Overall, we suggest

that inactivation of DacB, and the consequences of its inactivation, may play a different physiological role in *B. cenocepacia*.

Deficiencies in peptidoglycan recycling cause susceptibility to *β*-lactams

Peptidoglycan recycling and trimming occur simultaneously with peptidoglycan synthesis and has substantial implications for β-lactam resistance. In *E. coli*, a variety of endopeptidases, lytic transglycosylases, and transporters are required for peptidoglycan recycling (Dik et al. 2018). Lytic transglycosylases and endopeptidases cleave (muro)peptides from peptidoglycan chains, which are then transported into the cell for recycling (Dik et al. 2018). In in *E. coli*, lytic transglycosylases are thought to mediate protection from β-lactams by removing aberrant peptidoglycan crosslinks formed by β-lactam-poisoned PBP complexes (Cho et al. 2014). However, very little is known about peptidoglycan recycling in *Burkholderia*. Analysis of the BarSeq data for homologues of genes associated with peptidoglycan recycling revealed several as important for fitness in the presence of β-lactams (Figure 4A). Disruptions in *slt* (encoding a soluble lytic transglycosylase), and in *mltD* and *mltG* (each encoding a membrane-bound lytic transglycosylase) all resulted in susceptibility to many β-lactams, but not the early peptidoglycan synthesis inhibitors CYC and FOS (Figure 4A). To validate our findings from the BarSeq experiment, we silenced *slt*, *mltD*, and *mltG* with CRISPRi, which variably increased susceptibility to AZT, CAZ, CTT, MEM, TAZ, and AVI (Figure 4B). Silencing expression of these genes did not cause a growth defect in the absence of antibiotics (Figure S11). While other endopeptidases and transglycosylases are encoded in K56-2 in addition to *slt*, *mltD*, and *mltG*, they did not contribute to fitness in the conditions used for the BarSeq experiment, perhaps due to partial functional redundancy, as recently demonstrated in *V. cholerae* (Weaver et al. 2022).

The balance of various peptidoglycan degradation products has important implications for β-lactamase expression. In the model *Citrobacteri freundii*, β-lactam exposure causes lytic enzymes to liberate GlcNAc-anhydroMurNAc-pentapeptide fragments, which enter the cytoplasm through the AmpG permease (Jacobs et al. 1994) then are processed by NagZ into anhydroMurNAc-pentapeptide, then into anhydroMurNAc by AmpD (Jacobs et al. 1995). The AmpR transcriptional activator of β-lactamase genes binds both the substrate and product of NagZ, but not the product of AmpD (Bartowsky and Normark 1991; Balcewich et al. 2010); thus, AmpD activity reduces β-lactamase expression. In *B. cenocepacia,* while mutations in *ampD* are known to confer β-lactamase resistance (Hwang and Kim 2015), the contributions of AmpG have not been experimentally characterised. Here, we observed that disruption of *ampG* increased susceptibility to many β-lactams, while disruption of *ampD* reduced susceptibility to many β-lactams and no effect was observed with disruption of *nagZ* (Figure 4A). Upon silencing of *ampD* with CRISPRi, susceptibility was reduced to CAZ, CFD, and MEM, while silencing of *ampG* increased susceptibility to AZT, CAZ, TAZ, CTT, and MEM (Figure 4B). Knocking down either *ampD* or *ampG* did not produce a growth defect in the absence of antibiotics (Figure S11). Our findings support the role of AmpG as a permease for peptidoglycan degradation products, and of AmpD as reducing the accumulation of anhydroMurNAc-pentapeptides in K56-2.

The DSB system of periplasmic disulfide bond formation

The folding and stability of secreted proteins is aided by disulfide bond (DSB) formation via the periplasmic DSB system. In *E. coli*, this system is encoded by four genes organized in two pathways, the DsbAB pathway and the DsbCD pathway, required for efficient disulfide bond formation and isomerization, respectively, in periplasmic proteins (Figure 4C) (Landeta et

al. 2018). Reports from the pre-genomic era have associated DsbAB in *Burkholderia* with pleiotropic effects on protease activity, motility, and resistance to multiple antibiotics (Abe and Nakazawa 1996; Hayashi et al. 2000). We confirmed that disruptions in *dsbA* and *dsbB* resulted in large changes in susceptibility to many β-lactams and large scaffold antibiotics, while disruptions in *dsbC* and *dsbD* did little to alter the susceptibility profile (Figure 4D). To assess the possibility of membrane integrity defects, we measured NPN uptake in targeted CRISPRi mutants. Only knockdown of *dsbB* increased outer membrane permeability as measured by NPN uptake (Figure 4E). B-lactamases have previously been implicated as substrates of DsbA in *P. aeruginosa* (Furniss et al. 2022). Additionally, given the susceptibility to non-β-lactam antibiotics (e.g. ERY, CHX, NOV), the Dsb system may be important for the function of other resistance mechanisms, such as efflux pumps (Hayashi et al. 2000; Vezina et al. 2020). Thus, we suggest that antibiotic susceptibility caused by defects in the DSB system is multifactorial.

The interconnection of cell envelope processes opens avenues for overcoming β-lactam resistance

<u>Antagonising undecaprenyl phosphate recycling causes β-lactam susceptibility, hinders growth, and affects cell morphology</u>

Polysaccharides are important structural and functional components of bacterial cell envelopes, including exopolysaccharides, the O-antigen, peptidoglycan, and protein *O*-glycosylation. From the BarSeq data, we observed that mutants with disruptions in LPS/O-antigen synthesis (e.g. *hldD*, *wbiGH*, and K562_RS30805) and protein glycosylation (e.g. *ogcABE* and *pglL*) had altered susceptibility to several β-lactam antibiotics (Figure 2F, 5A, and S5). To examine if defects in outer membrane permeability were the source of increased antibiotic susceptibility, we assessed NPN uptake of CRISPRi mutants in genes/operons highlighted by the BarSeq experiment. We found that knockdown of genes related to LPS core

and O-antigen synthesis and protein glycosylation did not significantly impair outer membrane integrity (Figure 5B), except for *hldD* which was in line with the effect observed for *hldD* deletion (Figure 2H). Thus, increased antibiotic susceptibility is not simply due to increased antibiotic influx alone.

Closer examination revealed that cell envelope glycan pathways are linked by the shared lipid carrier UndP (Figure 5C) (Manat et al., 2014). In *E. coli*, both *de novo* UndP synthesis and UndP recycling are essential for viability (El Ghachi et al. 2005; Baba et al. 2006). As a carrier, UndP is recycled after a cleavage step removes the linked glycans. UndP intermediates are present at low levels in Gram-negative membranes (<1% of total membrane lipids) (Trent et al. 2001a; Barreteau et al. 2009; Wang et al. 2009). Previous reports in *E. coli* and *Shigella flexneri* have found that disruptions in O-antigen and enterobacterial common antigen pathways cause morphological defects (Jorgenson et al. 2016; Jorgenson and Young 2016; Maczuga et al. 2022). It was suggested that disruptions cause pathway intermediate accumulation and prevent UndP recycling, thus sequestering UndP away from the essential process of peptidoglycan synthesis.

While inhibition of *de novo* UndP synthesis is known to render *B. cenocepacia* and *E. coli* cells more susceptible to β-lactams (Sass et al. 2018; Jorgenson et al. 2019), the link between UndP utilization pathways and β-lactam susceptibility has not been examined. We reasoned that due to the connection with peptidoglycan synthesis, disruptions preventing or reducing the efficiency of UndP recycling would increase susceptibility to the β-lactams, FR-9, and bacitracin (BAC). Supporting this hypothesis, in the competitive conditions of the BarSeq experiment, disruption of *dbcA*, encoding a UndP flippase important for UndP recycling, resulted in susceptibility to β-lactams, FR-9, and BAC (Figure 2F and S5). To validate the findings of the BarSeq experiment, we assessed susceptibility of the same CRISPRi mutants to AZT, CAZ, and

MEM, as representatives of the β-lactams used in the BarSeq experiment. Susceptibility moderately increased upon knockdown of cytoplasmic steps in the protein *O*-glycosylation pathway (encoded by *ogcABEI*) and LPS core synthesis (encoded by *hldD* and *wabRwaaLwabQP*) (Figure 5D). Knockdown of LPS core synthesis genes may cause an accumulation of UndP-O-antigen intermediates in the periplasm as the O-antigen cannot be ligated to a heavily truncated core, thus possibly reducing UndP recycling. To support our genetic evidence for the interactions among UndP utilisation pathways, we leveraged antibiotics as inhibitors of specific processes in checkerboard assays. We used the LpxC inhibitor PF-04, which prevents lipid A formation. We reasoned that exposing cells to PF-04 may cause accumulation of UndP-O-antigen intermediates in the periplasm, similar to knockdown of core biosynthetic genes *hldD* and *wabRwaaLwabQP*. Indeed, PF-04 strongly synergised with MEM, CTT, CAZ, AZT, and the isoprenoid synthesis inhibitor FR-9 (Figure 5E). Interaction with FR-9 suggests PF-04 may cause sequestration of UndP-linked intermediates, while the resulting stress on peptidoglycan synthesis is supported by synergism of PF-04 with the β-lactams. We argue that the observed synergy was not likely due to increased outer membrane permeability as PF-04 did not synergise with the large scaffold antibiotics ERY, NOV, or RIF.

When we silenced LPS core and *O*-glycosylation genes, we noticed that the antibiotic susceptibility profiles were very similar, regardless of the β-lactam used (Figure 5D). This may indicate an independence from which peptidoglycan synthesis complex is targeted and instead points to an interaction with UndP levels itself. If UndP sequestration causes β-lactam susceptibility by reducing flux through peptidoglycan synthesis, we also expect that reducing the total amount of UndP would produce a similar effect. To achieve this, we targeted *ispDF* (encoding early genes in isoprenoid/UndP synthesis) and *uppS* (also called *ispU*, encoding

UndPP synthase) with CRISPRi. As *uppS* is an essential gene and repression strongly suppresses growth (Figure S11), we carefully titrated the concentration of rhamnose to suppress growth by 20-30% for further assays. Indeed, knockdown of *ispDF* and *uppS* increased susceptibility to AZT, CAZ, and MEM (Figure 6A). However, knockdown of *ispDF* moderately increased membrane permeability (Figure 5C), suggesting that the β-lactam susceptibility of that mutant may be partly due to increased antibiotic influx. In addition to genetically depleting levels of UndP, we also investigated antibiotic interactions with FR-9 and BAC. FR-9 is an inhibitor of Dxr, which catalyzes an early step in isoprenoid biosynthesis (Kuzuyama et al. 1998), while BAC binds UndPP and prevents its recycling (Siewert and Strominger 1967) (Figure 1). FR-9 and BAC synergised with many β-lactams, in addition to with each other (Figure 6B), demonstrating that double targeting at different points within UndP metabolic pathways greatly increases the inhibitory effect. Overall, both chemical and genetic evidence supports our assertion that depletion of free UndP pools causes β-lactam susceptibility.

Following the BarSeq experiment, we expected that mutants in the O-antigen synthesis operons *wbiFGHI* and *vioAwbxFED* would be more susceptible to β-lactams; however, the CRISPRi mutants we constructed displayed no change in susceptibility (Figure 5D). As CRISPRi silencing is polar, we decided to create unmarked deletion mutants in six genes (*bacA*, *bceB*, *wzm-wzt*, *waaL*, *hldD* and *wbiI*) to link phenotype to individual genes. The K56-2::dCas9 background was used to permit additional perturbation with CRISPRi. BacA has a role in UndP recycling as the major UndPP phosphatase responsible for 75% of that activity in *E. coli* (El Ghachi et al. 2004). BceB is the initiating enzyme for cepacian synthesis, an exopolysaccharide also built on the UndP carrier (Ferreira et al. 2011). Wzm and Wzt are components of the ABC-type transporter that translocates the UndPP-linked O-antigen to the periplasmic leaflet. The

encoding genes *wzm* and *wzt* are adjacent and were both deleted. WaaL cleaves the O-antigen from UndPP and ligates the glycan chain to the LPS core (Ortega et al. 2009). In *E. coli*, cells with blockages in UndP utilisation pathways develop severe morphological defects and frequently lyse (Jorgenson and Young 2016; Jorgenson and Bryant 2021). However, we found in K56-2 that either individual deletion or overexpression of *bacA*, *bceB*, *wzm-wzt*, *waaL*, *hldD* and *wbiI* resulted in only minor growth reductions and no major cell morphology defects, except for overexpression of *wbiI* (Figure S14).

We thus hypothesized that the physiology of K56-2 may be more robust to UndP metabolism disruptions than that of *E. coli*, which has been used previously as a model. To enhance stress on UndP metabolism and peptidoglycan synthesis we constructed double mutants to trigger synthetic genetic interactions. In deletion mutant backgrounds we selected genes for silencing with CRISPRi or overexpression from a plasmid and then assessed growth. As UndP is an essential molecule for peptidoglycan synthesis, perturbations that further reduce UndP availability would be expected to inhibit growth (synthetic lethality/sickness). Supporting a block in UndP metabolism, the Δ*hldD* and Δ*waaL* mutants were more susceptible to knockdown of *ispDF* and *uppS*, and to overexpression of *wbiI* (Figure 7A and B). We reasoned that overexpression of *wzm-wzt* in the Δ*waaL* mutant may reduce free UndP pools by causing accumulation of periplasmic UndPP-linked O-antigen intermediates. As expected, this mutant, displayed morphological changes, such as bulging, that are indicative of defects in the peptidoglycan matrix (Figure 7C). Furthermore, this mutant was also more susceptible to AZT, CAZ, and MEM (Figure 7D).

Overall, we have shown by complementary chemical, genetic, and physiological methods that disruption of UndP synthesis and utilisation pathways increases susceptibility to β-lactams.

We propose a tentative model to fit our results within the literature (Figure 7E) (Jorgenson et al. 2016, 2019; Jorgenson and Young 2016). In wild-type cells, recycling is important to replenish the UndP pools available for the essential process of peptidoglycan synthesis (Figure 7E). However, blockages in UndP utilisation cause sequestration of UndP-glycan intermediates, reducing the efficiency of recycling and the levels of free UndP available. We then reason that impaired peptidoglycan synthesis results in a weaker matrix and increases susceptibility to β-lactams.

TnSeq reveals the basis for β-lactam/avibactam synergy and rationalizes new effective combinations

AVI/CAZ is a current front-line treatment for many infections caused by multidrug-resistant Gram-negative bacteria. The synergy of the combination is due to avibactam inhibiting a broad spectrum of β-lactamases that degrade ceftazidime (Ehmann et al. 2012; Lahiri et al. 2014). Studies on *Burkholderia* β-lactamases have focused on the Ambler class A PenB carbapenemase and the Ambler class C AmpC β-lactamase, of which only PenB is inhibited by AVI (Poirel et al. 2009; Becka et al. 2018). However, K56-2 encodes a further 19 putative β-lactamase-fold proteins, and it is unknown how/if each contributes to β-lactam resistance and if they are inhibited by AVI.

We reasoned that if the targets of AVI are the β-lactamases that degrade CAZ, transposon mutants of said β-lactamases would have a fitness defect in the presence of CAZ because CAZ cannot be degraded. The same mutants would also have no fitness differences between AVI/CAZ and CAZ only as in either case the β-lactamase target is chemically inhibited or genetically disrupted (Figure 8A). Using the data from our BarSeq experiment, we compared pairs of

conditions involved in the AVI/CAZ combination to identify genes important for fitness in one or both of the constituent conditions. For all comparisons, there were more genes unique to each condition than shared between any two, highlighting strong concentration-dependent physiological effects, even for the same antibiotic (Figure S15). Pair-wise comparison revealed that *bla*$_{PenB}$ was important for fitness in both CAZ only and AVI/CAZ, while K562_RS32470 (encoding a putative metallo-β-lactamase (MBL); Pfam 00753) was important for fitness in CAZ only (Figure S15 and 8B). None of the other 20 putative β-lactamase-fold proteins were important for fitness in any condition tested here (Supporting Data 1). Thus, our findings suggest that PenB and K562_RS32470 are the only possible candidate β-lactamase targets of AVI in K56-2.

We next asked whether *bla*$_{PenB}$, K562_RS32470, and *penR* (the positive regulator of *bla*$_{penB}$ and *bla*$_{AmpC}$) contribute to resistance against other β-lactam antibiotics. We saw that transposon disruptions in *penR*, *bla*$_{PenB}$, and K562_RS32470 increased susceptibility to AZT, AMP, CAZ-H, and MEM (Figure 8B). Notably, neither disruption increased susceptibility to CFD, and only a disruption in *penR* increased susceptibility to CTT. Although K562_RS32470 is annotated as an MBL, the interactions with AVI and AZT make us question this assignment. AZT is a poor substrate for most MBLs (Felici et al. 1993), and MBL activity is not generally inhibited by AVI (Abboud et al. 2016), both of which seem to contradict our findings. However, we did not conduct further experiments to investigate this.

For validation, we assessed β-lactam susceptibility of CRISPRi knockdown mutants in *bla*$_{AmpC}$, *bla*$_{PenB}$, and K562_RS32470. In the absence of antibiotics, neither were important for growth (Figure S11). Knockdown of either *bla*$_{AmpC}$ or K562_RS32470 did not alter the MIC of any of the tested β-lactams (Figure 8C and Table S2). On the other hand, knockdown of *bla*$_{PenB}$

resulted in marked susceptibility to AMP, TAZ, CAZ, AZT, and MEM (up to 32-fold reduction in MIC) (Figure 8C and Table S2). We reasoned that if PenB is the major β-lactamase responsible for the degradation of AZT, CAZ, and MEM, then knockdown of bla_{PenB} would result in the same MIC as adding AVI. In other words, the cells would be "blind" to the addition of AVI as the primary target is already knocked down. Indeed, in the presence of AVI, there was no change in MIC upon bla_{PenB} knockdown for CAZ and MEM (Figure 8C); however, knockdown of *penB* still reduced the MIC of AZT by 2-fold, suggesting that in the absence of PenB, K562_RS32470 may have a minor contribution to AZT resistance. Taken together, these results demonstrate that in K56-2, PenB is the predominant β-lactamase responsible for degrading clinically relevant β-lactams. Our findings also demonstrate that BarSeq can be used to elucidate the mechanisms and targets of antibiotic potentiation.

The marked β-lactam susceptibility of knockdown mutants in bla_{PenB}, together with the ability of avibactam to inhibit PenA-family β-lactamases in *Burkholderia* species (Zeiser et al. 2019), made us curious about the broader applicability of AVI/AZT and AVI/MEM combinations. AVI/AZT and AVI/MEM are not commonly used to treat Bcc respiratory infection. We assembled a panel of 41 clinical Bcc isolates (including *B. gladioli*) spanning the last two decades and representing the most commonly recovered species across Canada. We also included isolates of other CF pathogens: *P. aeruginosa*, *Achromobacter xylosoxidans,* and *Stenotrophomonas maltophilia*. Susceptibility to AZT, CAZ, and MEM was assessed with and without 8 µg/mL AVI (Table S3). For the three non-Bcc species, there was minimal potentiation by AVI, except with highly β-lactam resistant *P. aeruginosa* and with AZT against *S. maltophilia* (Table S3). Among Bcc species, MIC values of the β-lactams alone varied widely: 2 – >256 µg/mL for AZT; 0.5 – 32 µg/mL for MEM; 2 – >128 µg/mL for CAZ. Potentiation by

AVI was strongest for AZT and MEM (up to 64-fold MIC reduction) (Figure 9). These trends are in line with the changes in susceptibility upon *bla*$_{PenB}$ knockdown (Figure 8C). Consequently, and in the context of clinical breakpoints, without AVI 24/41 of the Bcc isolates were resistant to AZT, which was reduced to 2/41 with AVI. For MEM and CAZ, 9/41 and 4/41 of the Bcc isolates were resistant without AVI, respectively, and all Bcc isolates were sensitive with AVI (Figure 9).

The activity of AZT, CAZ, and MEM was not uniformly potentiated by AVI in all Bcc isolates. Even for K56-2, in which we have demonstrated the importance of PenB, AVI does not potentiate the activity of all β-lactams or even all cephalosporins (Table S4). Moreover, even if AVI potentiated the activity of one β-lactam, it did not guarantee potentiation for the others (Table S3). Thus, although alternative β-lactamases that are not inhibited by AVI may contribute to β-lactam resistance, they likely only play minor roles in most isolates. Overall, our findings suggest that, in addition to AVI/CAZ, combinations of AVI/AZT and AVI/MEM may be valuable therapeutic options for treating Bcc infection. Additionally, as the potentiation of AZT, CAZ, and MEM by AVI was generally weaker in other common CF pathogens, this highlights the differences in β-lactamase arsenals and demonstrates the need to perform genome-wide investigations in each species to uncover novel resistance mechanisms. Consequently, we suggest that among CF pathogens, combinations of AVI/AZT, AVI/CAZ, and AVI/MEM may be more tailored for use against Bcc infections.

<u>Cefiderocol enters K56-2 through a PiuA receptor homologue and requires physiological levels of iron for activity</u>

Cefiderocol is a novel antibiotic with a catechol siderophore conjugated to a cephalosporin structurally similar to ceftazidime. The siderophore chelates ferric iron and enables active transport into cells, resulting in substantially increased potency against a variety of Gram-negative pathogens (Kohira et al. 2016). However, except for a few cases of compassionate care (Shionogi Inc. 2019) and general Gram-negative panels (Hackel et al. 2017, 2018), there are no other reports on the activity of CFD in *Burkholderia* species. We thus tested the susceptibility of the Bcc clinical panel we assembled to CFD. Of the 41 isolates, the MIC_{50} was 0.5 µg/mL and only eight (20%) were resistant to CFD (Figure 9 and Table S3), demonstrating very potent activity. Susceptibility of the Bcc isolates to CFD was generally not affected by the addition of AVI (Table S3).

To explore the antibiotic mechanism of CFD, we analysed our BarSeq data for chemical-genetic interactions specific to CFD activity. Broadly, interactions were enriched in pathways related to iron and heme metabolism, which was not observed for other β-lactams (Figures S6-S8). Additionally, disruptions of β-lactamase genes bla_{PenB} and K563_RS32470 did not affect fitness in CFD (Figure 8B). Thus, while the active warhead of CFD is a β-lactam closely related to CAZ, the conjugation with a siderophore changes important chemical-genetic interaction signatures.

From previous work in *P. aeruginosa,* we expected to identify TonB-dependent siderophore receptors (TBDRs) affecting fitness in CFD (Ito et al. 2017; Luscher et al. 2018). We saw that disruptions in K562_RS04910 (encoding a TonB-related protein) and K562_RS23150 (encoding a homologue of the *P.aeruginosa* PAO1 *piuA* TBDR) reduced susceptibility to CFD (Figure 10A). Of 24 putative TBDRs encoded by K56-2, *piuA* was the only TBDR identified by the screen with significantly enhanced fitness (Supporting Data 1). We

confirmed the link to *piuA* with CRISPRi knockdown, showing reduced susceptibility to CFD (but not the structurally related CAZ) and demonstrating that this TBDR is a receptor for CFD in K56-2 (Figure 10B and C). Of note, even with *piuA* knocked down the cells remain much more susceptible to CFD than to the related β-lactam CAZ (MIC of 8 µg/mL vs 32 µg/mL).

Iron is an essential micronutrient for microbial growth and is often growth-limiting in infection settings. In low iron conditions, iron acquisition mechanisms, such as TBDRs, are upregulated (Butt and Thomas 2017). We thus reasoned susceptibility to CFD in K56-2 would inversely correlate with the concentration of iron in the medium, as in *P. aeruginosa* (Luscher et al. 2018). For low-iron medium, we used a minimal medium without added iron (M9 salts + 0.3% low-iron casamino acids; M9+CAA). Using ICP-MS, we determined the concentration of total iron in our batches of M9+CAA and CAMHB to be 0.61 µM (± 0.07 µM) and 6.75 µM (± 0.71 µM), respectively. Curiously for K56-2, the MIC of CFD was 8-fold higher in M9+CAA than in CAMHB (Figure 10C). Furthermore, the FDA-approved iron chelator deferiprone strongly antagonised CFD in both CAMHB and M9+CAA (Figure 10D). Reduced susceptibility was not due to *piuA* receptor repression, as we observed an additional 4-fold increase in MIC when *piuA* was knocked down in M9+CAA (Figure 10C). These findings suggest that while *piuA* is expressed in M9+CAA, there may be other receptors for CFD that were not detected in the BarSeq experiment. Additionally, the reduced susceptibility in low-iron conditions demonstrates that there is a critical threshold of iron required for CFD activity.

The concentration of iron in the sputum of individuals with severe CF is several fold higher than normal lung sputum (18 µM vs. on average 62 µM, but can go up to 125 µM) (Hunter et al. 2013). To address if CFD would be active at these higher iron concentrations, we performed checkerboard assays with CFD and $FeCl_3$. For K56-2, supplementing CAMHB with

iron antagonised CFD and raised the MIC by 4-fold at 100 µM $FeCl_3$ (Figure 10E). Conversely, supplementing M9+CAA with iron lowered the MIC (Figure 10E). Overall, while CFD susceptibility of K56-2 is strongly dependent on the concentration of iron, we highlight that MIC values remain well below those of other β-lactams (Table S3), even at the elevated iron concentrations present in CF infection settings.

Discussion

The alarming rate of antibiotic resistance among Gram-negative organisms requires immediate attention. NGS-based assays provide scalable high-throughput approaches that can be applied to virtually any organism. Chemical-genetic interaction profiles can be created and examined to inform on antibiotic resistance and susceptibility determinants to guide rational antibiotic combinations. Here, using *B. cenocepacia* K56-2 as a model, we measured genome-wide fitness contributions in the presence of 22 antibiotic conditions primarily targeting the cell envelope. Generation of thousands of chemical-genetic interactions allowed confident assignment and validation of over a hundred new functional annotations for many genes not previously associated with antibiotic susceptibility in K56-2. By screening with compounds that target the cell envelope, the majority of the identified factors play roles in cell envelope biogenesis and represent approaches to overcome antibiotic resistance.

High levels of cationic antibiotic resistance in *B. cenocepacia* are suggested to stem from a “two-tier” model involving contributions from LPS and adaptive responses to cell envelope damage (Loutet et al. 2011). We confirmed previous findings that disruptions in many genes along the O-antigen, LPS core, and lipid A modification pathways caused susceptibility to PMB (Ortega et al. 2009; Hamad et al. 2012), and extend this to CHX as well (Figure 2). Together, this demonstrates that the O-antigen, LPS core, and Ara4N modification work together to electrostatically and sterically hinder cationic antimicrobials from accessing their binding sites on lipid A. Furthermore, we extended on the importance of the RpoE cell envelope stress response for PMB and CHX resistance by showing contributions of key components sensing the damage stimulus (*rpoE* and *rseP*) and responding to it (*dnaK* and *surA*) (Figure 2F). The RpoE regulon has not been fully characterised in *B. cenocepacia*, but is known in *E. coli* to include

protein chaperones, such as DnaK and SurA, that enhance outer membrane integrity (Dartigalongue et al. 2001; Calloni et al. 2012; Hews et al. 2019). Overall, the extent of resistance factors to cationic antibiotics, including the integration of the Ara4N modification into an essential network, suggests strong and long-term environmental selection for antimicrobial peptide resistance. Breaking this resistance could therefore pave new therapeutic avenues.

The centrality and essentiality of UndP for cell envelope biogenesis hints at a weakness that may be exploited for antibiotic development. In *B. cenocepacia*, at least four pathways use UndP intermediates (Figure 5C), and two are essential for growth (peptidoglycan synthesis and the Ara4N modification). Our BarSeq experiment pointed to disruptions in O-antigen synthesis and protein *O*-glycosylation causing susceptibility to β-lactams, FR-9, and/or BAC. Targeted genetic and chemical validations indicated midpoint disruptions in these pathways caused a buildup of UndP intermediates, thus reducing the free UndP available for peptidoglycan synthesis. Mutations causing accumulation of UndP-O-antigen and UndP-enterobacterial common antigen intermediates in *E. coli* (Jorgenson et al. 2016; Jorgenson and Young 2016) and *Shigella flexneri* (Maczuga et al. 2022) are known to cause substantial morphological defects from insufficient peptidoglycan synthesis. While, β-lactam susceptibility has been observed in large-scale screens for disruptions in UndP utilisation pathways in *A. baylyi* (Bailey et al. 2022), *Vibrio cholerae* (Weaver et al. 2018), and *P. aeruginosa* (Dötsch et al. 2009; Sonnabend et al. 2020); we are the first to validate these interactions with targeted genetic and chemical investigations.

An important question that remains is if targeting UndP utilisation pathways is a viable strategy for antibiotic development. Indeed, there are two documented successes: targocil and BTZ043 (Makarov et al. 2009; Swoboda et al. 2009; Lee et al. 2010). Targocil is an inhibitor of

the TarG transporter for wall teichoic acid (WTA), a surface-linked glycan constructed on UndP, in *Staphylococcus aureus.* However, as the WTA pathway is non-essential, spontaneous resistance occurs relatively frequently *in vitro* (~1 in 10^6 cells) (Swoboda et al. 2009). BTZ043 is an antimycobacterial that targets DprE1 in the essential cell wall arabinan biosynthesis (Makarov et al. 2009). In the related species *Corynebacterium glutamicum* (Alderwick et al. 2005), BTZ043 was found to inhibit growth via sequestering decaprenyl phosphate intermediates required for peptidoglycan synthesis (Grover et al. 2014). Overall however, the outlook is not favourable for targeting UndP utilisation pathways, as suppressor mutants are commonly identified when attempting to manipulate these non-essential pathways (Burrows and Lam 1999; Xayarath and Yother 2007; Jorgenson and Young 2016). Furthermore, while single genetic mutations in UndP utilisation pathways in *E. coli* substantially affect cell morphology (Jorgenson et al. 2016; Jorgenson and Young 2016), we did not see this in K56-2 (Figure S14). It was only upon deleting the *waaL* O-antigen ligase and overexpressing the *wzm-wzt* O-antigen transporter that cell morphology displayed evidence of peptidoglycan defects (Figure 7). We suggest that *Burkholderia* may be more robust to alterations in UndP levels perhaps due to higher initial abundance of UndP, as the essential Ara4N modification may otherwise place a very high burden on UndP pools. Additionally, O-antigen synthesis in *Burkholderia* may require less UndP than in *E. coli*. The Wzy-dependent pathway predominant in *E. coli* strains uses one UndP carrier for each O-antigen subunit, while the ABC transporter-dependent pathway in *Burkholderia* (and many other species (Greenfield and Whitfield 2012)) uses a single UndP carrier to assemble the entire polymeric O-antigen. Thus, species that use the ABC transporter-dependent O-antigen pathway may be less susceptible to antibiotic inhibition of UndP utilisation pathways.

In addition to developing new antibiotics, there is also a great deal of interest in discovering potentiators (also called adjuvants) that synergise with antibiotics to substantially increase potency and spare doses of the paired antibiotic. The presented transposon-based screen is well-suited to identify attractive targets for new potentiators, as gene disruption/silencing can mimic the effect of gene product inhibition with a small molecule (Anglada-Girotto et al. 2022). We found that disruption of the DsbAB, but not the DsbCD, pathway substantially increased susceptibility to many antibiotics, including β-lactams and large-scaffold antibiotics (Figure 4D). Another transposon screen by the Manoil group also found that DsbA and DsbB were important for resistance to meropenem in *A. baumannii* (Bailey et al. 2022). Recently in *E. coli*, the disulfide bonds introduced by the DsbAB pathway were found to be important for stability of periplasmic proteins such as β-lactamases and MCR enzymes (mobile colistin resistance) (Furniss et al. 2022). DsbAB has been previously linked to multiple traits in *B. pseudomallei* and *B. cepacia*, including extracellular protease activity, motility, and virulence in a murine model (McMahon et al. 2018; Hayashi et al. 2000). The pleiotropic effect of the DsbAB system on virulence and antibiotic resistance makes it an attractive target for further investigation.

In the context of antibiotic potentiation, the fitness profile of the mutant in *dbcA* deserves further attention. Disruption of *dbcA* increased susceptibility to β-lactams, BAC, FR-9, CHX, and PMB (Figure 3E). DbcA, a DedA-family UndP flippase and homologue of UptA in *E. coli* (Roney and Rudner 2022), was found to be important for the Ara4N lipid A modification in *B. thailandensis* E264 (Panta et al. 2019), and a Δ*dbcA* mutant had a colistin MIC of 8 µg/mL (compared to > 256 µg/mL in WT E264). The peak sputum concentration of some inhaled colistin therapies is above 300 µg/mL sputum (Yapa et al. 2014), well above the inhibitory concentration for a mutant lacking DbcA. We suggest that DbcA, and UndP recycling more

broadly, may be a linchpin in both β-lactam and cationic antibiotic resistance in *Burkholderia*. Thus, inhibiting UndP recycling with a small molecule may potentiate the activity of multiple clinically available antibiotics.

B-lactamase inhibitors, such as AVI and TAZ, potentiate the activity of β-lactams by protecting them from hydrolysis by β-lactamases. AVI/CAZ shows promise as a treatment for Bcc respiratory infection (Spoletini et al. 2019); however, resistance has been identified to this combination (Everaert and Coenye 2016; Papp-Wallace et al. 2017). By comparing fitness profiles of CAZ treatment in the presence or absence of AVI, we identified that the PenB serine β-lactamase and the K562_RS32470 putative metallo-β-lactamase are targets of AVI. Targeted validations then demonstrated that PenB is the predominant β-lactamase in K56-2. A similar transposon-based approach was recently used by the Manoil group in *A. baylyi* to show that AVI potentiates CAZ by inhibiting the GES-14 β-lactamase, while MEM is potentiated by inhibiting GES-14 and OXA-23 (Bailey et al. 2022).

We then exploited the dependence on PenB to demonstrate that AVI strongly potentiates AZT and MEM in a panel of Bcc clinical isolates (Figure 9 and Table S3). These combinations are not commonly reported for treatment of Bcc infection and may represent alternative therapeutic approaches. AVI/AZT is reported to be most potent against species of enterobacteria that express a serine β-lactamase (which is inhibited by AVI) and a metallo-β-lactamase (which generally cannot degrade AZT) (Biedenbach et al. 2015). However, for treatment of CF respiratory infections, inhaled formulations of aztreonam are available that can achieve concentrations over 725 µg/g sputum with new inhaler technology (Gilead Sciences Inc. 2012), which is nearly 100-fold the MIC_{50} we determined for the AVI/AZT combination. AZT is also generally-well tolerated by people with allergies to other β-lactams (Romano et al. 2011).

Although inhaled MEM has been used in some cases (Hewer 2012), no other β-lactams are currently licensed as inhaled formulations. Additionally, as we found that the BpeAB-OprB pump effluxes AVI in K56-2, it may be possible that pump overexpression in clinical isolates may break AVI/β-lactam synergy; however, this remains to be determined.

Our genome-wide view into the mechanism of action of CFD may have an impact in moving CFD forward for therapeutic uses as it is not yet indicated to treat CF infections. In K56-2, we found that CFD activity was not affected by disruptions in the major β-lactamases (Figure 8). Additionally, in the largest screen of CFD activity in Bcc isolates to date, 85% were susceptible to CFD alone and there was little benefit of combination with AVI (Figure 9). Indeed, CFD is generally stable to β-lactamase hydrolysis; however, the NDM-1 and NDM-5 metallo-β-lactamases are linked to resistance in *Enterobacter cloacae* and *Klebsiella pneumoniae*, respectively (Nurjadi et al. 2021; Lan et al. 2022). An additional consideration for CFD activity is also the concentration of iron in the growth conditions. We observed that physiological iron concentrations, even elevated levels associated with chronic CF (Hunter et al. 2013), are adequate for CFD activity. Furthermore, CFD activity was reduced by iron limitation from growth in a low-iron medium and from chelation. We therefore suggest that critical iron concentration thresholds exist that reflect the interplay between the availability of free iron for CFD to bind and the cellular responses to iron levels. In summary, we demonstrate how chemogenomics can be used to functionally annotate uncharacterised genes and prioritize targets for rational antibiotic combinations to increase effectiveness of current antibiotic therapies.

Methods and Materials

Strains, medium preparation, and growth conditions

All strains used in this study are listed in Table S5. LB-Lennox medium (Difco) was used for routine strain propagation and maintenance, unless otherwise specified. All strains and mutants of *E. coli* and *B. cenocepacia* were grown at 37°C. All clinical isolates of *P. aeruginosa*, *A. xylosoxidans*, *S. maltophilia* and Bcc species were grown at 37°C. All strains and mutants of *R. pickettii* K-288, *B. thailandensis* E264, *B. multivorans* ATCC 17616, *B. contaminans* FFH2055, and *B. cepacia* ATCC 25416 were grown at 30°C. All plasmids used in this study are listed in Table S6. The following selective antibiotics were used: trimethoprim (Sigma; 50 µg/mL for *E. coli* and 100 µg/mL for all species of *Burkholderia*), kanamycin (Fisher Scientific; 40 µg/mL for *E. coli*), gentamicin (Fisher Scientific; 50 µg/mL for all species of *Burkholderia*), and tetracycline (Sigma; 20 µg/mL for *E. coli* and 100 µg/mL for *B. cenocepacia*)

Stock solutions of D-glucose (Fisher Scientific) and L-rhamnose (Sigma) were made to 20% in de-ionized water then filter sterilized. The following antibiotics were stocked in sterile de-ionized water: kanamycin sulphate (Fisher), gentamicin sulphate (Fisher), ampicillin sodium (Sigma), ceftazidime hydrate (Sigma), ceftriaxone sodium (Sigma), cefotaxime sodium (Sigma), cephalexin hydrate (Carbosynth), cefmetazole (Sigma), cefoperazone sodium (Sigma), moxalactam sodium (Sigma), polymyxin B sulphate (Sigma), colistin sulphate (GoldBio), novobiocin sodium (Sigma), and FR-900098 sodium (Toronto Research Chemicals). The following antibiotics were stocked in 100% DMSO (Fisher): aztreonam (Alfa Aesar), cefiderocol (MedKoo Biosciences), trimethoprim (TCI America), tazobactam sodium (Alfa Aesar), cefotetan sodium (Target Mol), meropenem trihydrate (MedKoo Biosciences), avibactam sodium (MedKoo Biosciences), CHIR-090 (MedKoo Biosciences), PF-04753299 (Sigma), chlorhexidine

hydrochloride (Angene China), and rifampicin (Sigma). The following antibiotics were stocked in 95% ethanol: chloramphenicol (Sigma), tetracycline hydrochloride (Sigma), and erythromycin (Sigma). D-Cycloserine (Alfa Aesar) and fosfomycin disodium (Sigma) were both stocked in sterile Dulbecco's PBS (Sigma) pH 7.2. Ciprofloxacin hydrochloride (Sigma) and bacitracin zinc (Sigma) were both stocked in sterile 0.1M HCl.

Extraction of plasmid and genomic DNA

Plasmid DNA was routinely extracted using with the EZNA Plasmid DNA Mini Kit (Omega Bio-tek) and eluted in 10 mM Tris-HCl pH 8.5. Genomic DNA was isolated from *Burkholderia* with the PureLink Genomic DNA Mini Kit (Invitrogen) or by standard isopropanol precipitation and solubilized in 10 mM Tris-HCl pH 8.5.

Construction, maintenance, and transfer of plasmids

The desired inserts were amplified by PCR using Q5 high-fidelity DNA polymerase (NEB) with the high-GC buffer as per the manufacturer's protocols. See Table S7 for a list of all primers used in this study. The Monarch PCR and DNA Cleanup Kit (NEB) and Monarch DNA Gel Extraction Kit (NEB) were routinely used to purify the DNA fragments. For restriction cloning, the appropriate restriction enzymes and T4 ligase (NEB) were used according to the manufacturer's recommendations to digest the vector and insert. To prevent self-ligation, the vector was also treated with Antarctic phosphatase (NEB). For blunt-end ligation cloning, raw PCR product was mixed with T4 DNA ligase (NEB), DpnI (NEB), and T4 polynucleotide kinase (NEB) in a custom ligase buffer (132 mM Tris-HCl pH 7.5, 20 mM $MgCl_2$, 2 mM ATP, 15% PEG6000 in de-ionized water) and incubated for 30 mins at 37°C.

A previously published python script was used to design sgRNAs (van Gestel et al. 2021). sgRNAs were selected to bind as close as possible to the gene start, which has been shown to result in strong silencing (van Gestel et al. 2021). To mitigate the effect of off-target gene silencing, sgRNAs with a 12 bp seed region matching any other site in the genome (adjacent to a PAM site) were removed. Additionally, sgRNAs were removed if they contained any of the following features suggested to reduce silencing efficiency: 1) PAM site of ANN or TNN, 2) the sgRNA ended in GG or GA or 3) very high (>80%) GC-content. Each gene was typically targeted by two different sgRNAs within the 5' most 75 bp, and the results of the mutant that displayed the stronger phenotype were reported.

New sgRNA targeting regions were introduced into pSCB2-sgRNA by inverse PCR as previously described (Qi et al. 2013; Larson et al. 2013; Hogan et al. 2019). Briefly, the desired targeting sequence was added as a 5' extension to a primer with sequence: 5' – GTTTTAGAGCTAGAAATAGCAAGTTAAAATAAGGC – 3'. That primer was used with primer 1092 for PCR with Q5 DNA polymerase with high-GC buffer (NEB). The raw PCR product was used for blunt end ligation as above.

E. coli DH5α was used to maintain plasmids with broad-range origins of replication. *E. coli* SY327λpir^{+} was used to maintain plasmids containing the R6Kγ origin. Plasmids were introduced into these cells by standard transformation or electroporation

Electro-competent *B. cenocepacia* K56-2 was made as per (Choi et al. 2006) with some modifications. Briefly, 5 mL of overnight culture of the appropriate strain was split into 1 mL aliquots and washed by centrifugation at 6 000 x g for 5 mins followed by resuspension in sterile, room temperature 300 mM sucrose in de-ionized water. This washing was repeated twice more

and each of the aliquots were finally resuspended in 300 mM sucrose solution and used immediately.

More commonly, plasmids were introduced into Bcc species by triparental mating (Hogan et al. 2018, 2019). The *E. coli* donor strain, bearing the plasmid to be mobilized, the *E. coli* MM294/pRK2013 helper strain and the *Burkholderia* recipient were mated on an LB plate and incubated overnight (16-18 hours) at 37°C. Successful exconjugants were selected on LB plates containing the appropriate antibiotics with 50 µg/mL gentamicin to counterselect for the *E. coli* donor and helper. Colonies that appeared within 48 hours at 37°C were screened by colony PCR.

Unmarked gene deletion in K56-2

Genes were deleted as per a double homologous recombination method reported previously (Flannagan et al. 2008; Hamad et al. 2010), with some modifications. Briefly, 360 – 450 bp of the upstream and downstream regions flanking the gene(s) to be deleted were fused and ordered as a single gBlock from IDT with *Xma*I and *Xba*I restriction sites (see Table S8 for all gBlock fragments). The fragments were cloned into pGPI-SceI and transformed into *E. coli* SY327. Plasmids were confirmed by colony PCR with primers 153 and 154, then introduced into K56-2::dCas9 by triparental mating. The first recombination was confirmed by colony PCR of trimethoprim-resistant exconjugants. To promote the second recombination, pDAI-SceI-SacB (Hamad et al. 2010) was introduced by triparental mating. Trimethoprim-sensitive colonies were screened by colony PCR for successful gene deletion. To cure pDAI-SceI-SacB, colonies were patched on LB (without NaCl) + 15% sucrose (Fisher). Tetracycline-sensitive colonies were again screened by colony PCR for the deletion.

Construction of the barcoded plasposon and transposon mutant library

We wished to model our approach to barcoding on a previous report from the Deutschbauer lab (Wetmore et al. 2015). They constructed a 20 bp random barcode flanked by unique priming sites (GTCGACCTGCAGCGTACG and GAGACCTCGTGGACATC). These sequences are not found in K56-2 and were thus used for our approach. Primers 964 and 965 were used for inverse PCR of our parental plasposon pRBrhaBout. The product was circularized with In-Fusion HD Cloning (Takara Bio) as per the manufacturer's protocols. The resulting plasmid, pKS1, was sequence-confirmed to contain *Bam*HI and *Nco*I restriction sites between the inverted repeat and *dhfr*. A dsDNA fragment containing 20 random bases flanked by unique priming sites (Wetmore et al. 2015) and *Bam*HI and *Nco*I restriction sites was ordered from IDT with the sequence: 5′-GTTCAA*CCATG***GATGTCCACGAGGTCTCT**NNNNNNNNNNNNNNNNNNNN**CGTAC GCTGCAGGTCGAC***GGATCC***ACTTA - 3′. Italics show the *Nco*I and *Bam*HI restriction sites, while bold shows the unique priming sites; note that the end of the *Nco*I site (CCATGG) overlaps by one base (G) with one of the priming sites. As the fragment is used to generate the barcoded plasposon, pRBrha-Barcode, primers 972 and 973 were designed to amplify the fragment by PCR with Q5 polymerase and high-GC buffer (NEB). The barcode fragment and pKS1 were both digested with *Nco*I and *Bam*HI and ligated with T4 DNA ligase (NEB) at a 5:1 (insert:vector) ratio (100 ng total DNA/20 µL reaction) overnight at 16°C. The ligation mix was heated inactivated at 65°C for 15 mins then 5 µL was electroporated into *E. coli* SY327 and plated on LB plates with 50 µg/mL trimethoprim. Colonies were collected in subpools of 200 000 – 600 000 and frozen in PCR tubes at -80°C until needed. This process was repeated until ~6

million donor colonies were collected. A pilot BarSeq experiment (see *2.2.7* for the method) sequenced on a MiSeq with reagent kit v2 (Génome Québec, Montréal, Canada) using the first collected subpool confirmed it was highly diverse as expected.

Each subpool of *E. coli* was used only once as donor for triparental mating with K56-2. After only 4 hours of mating at 37°C (to reduce library redundancy), the mating pellicle was spread on Bioassay Qtrays (Molecular Devices) with the appropriate selective antibiotics and 0.2% rhamnose. After 2 days of growth, colonies were counted and harvested in subpools of 75 000 – 100 000 and frozen in PCR tubes at OD 2.0 – 4.0 (~100 million CFU/mL, or ~ 100 CFU/mutant) at -80°C. A pilot BarSeq experiment sequenced on a MiSeq with reagent kit v2 (Génome Québec, Montréal, Canada) was also performed on the first collected subpool of barcoded transposon mutants, which showed there were approximately half as many unique barcodes as total collected colonies.

RB-TnSeq DNA library preparation and sequencing

The transposon-genome junctions were amplified by the TnSeq-circle method as previously reported (Gallagher et al. 2011; Gislason et al. 2017b), with some modifications to accommodate the barcoding scheme (RB-TnSeq-circle). Briefly, DNA was extracted from representatives of the entire transposon mutant library (not treated with antibiotics) by isopropanol precipitation. The DNA was sheared with a Covaris M220 ultrasonicator, followed by end repair with the NEBNext End Repair Module (NEB). Adapters, consisting of annealed primers 683 and 684, were annealed with the Quick Ligation Kit (NEB). The DNA was then digested with *Pac*I (NEB) overnight. Probe 1426 in the presence of Ampligase (Lucigen) was used to selectively circularize and protect fragments containing the barcoded transposon

sequence, while all other fragments were digested with a mix of T7 *gene 6* exonuclease (ThermoFisher), Lambda exonuclease (NEB), and Exonuclease I (NEB). qPCR with iTaq Universal SYBR Green Supermix (Bio-Rad) was used to determine enrichment of transposon-genome junctions. The number of cycles corresponding to ~50% maximum product by qPCR was used to amplify transposon-genome junctions with iTaq for Illumina sequencing. All primers used for this purpose were constructed to enable 1-step PCR to add the Illumina flow cell adapter, Nextera index, and sequencing primer binding site. After clean-up with SeraMag beads (Cytiva), the final PCR product was first analysed on a TapeStation4150 (Agilent Technologies) then sequenced on an Illumina MiSeq (Donnelly Centre, Toronto, Canada) to assess library quality with a MiSeq reagent kit v2 (2x250 bp reads) and 20% PhiX spike. To increase sequencing depth, an Illumina HiSeq 2500 (The Applied Centre for Genomics, Toronto, Canada) was used on rapid run mode with a 20% PhiX spike (1x150bp reads). In both cases, the sequencing reads covered the transposon-specific sequence, barcode region, and at least 40 bp of the genome adjacent to the insertion site. In total, ~180 million reads were generated.

RB-TnSeq data analysis

To link barcodes to transposon insertion sites, the bioinformatic pipeline and scripts reported by (Wetmore et al. 2015) were used in a Conda 4.10.0 environment. These are available at https://bitbucket.org/berkeleylab/feba/src/master/. Briefly, the scripts identify reads containing the flanking priming sites and a transposon-specific sequence (terminal repeat) then map it to a genome with BLAT (Kent 2002). The priming sites flanking the barcode were the same as in the original report (Wetmore et al. 2015). The transposon-specific sequence in our construct is CATGGGCACTTGTGTATAAGAGTCAG. The default stringency and base error tolerances

were used, resulting in 86.1% of the observed barcodes being considered “usable” (primarily associated with one insertion site and filtered to remove sequencing/PCR errors). The reads were aligned to the closed K56-2 genome (RefSeq accession GCF_014357995.1) (García-Romero and Valvano 2020).

2.2.6 Transposon mutant pool antibiotic exposure

Wild-type K56-2 was used to determine the dose-response curves of the antibiotics in conditions mimicking the planned mutant pool exposure. Stationary phase cells were diluted to OD_{600} 0.025 in LB medium and grown at 37°C with 230 rpm shaking until early exponential phase (OD_{600} 0.15, about 3 hours). In 2 mL culture in glass tubes, a range of antibiotic concentrations was added (in technical duplicate) and the cells were grown for 8 hours (approximately 10-12 generations), again at 37°C with 230 rpm shaking. Then, the OD_{600} of each tube was measured to compute the dose-response curve for each antibiotic relative to cells grown without antibiotics. This assay was performed in three biological replicates. The $IC_{20\text{-}30}$ was confirmed by repeating this assay with a much narrower antibiotic concentration range around the $IC_{20\text{-}30}$.

To prepare the mutant inoculum, aliquots of the transposon mutant library were thawed and mixed in ratios according to the number of colonies contained in each aliquot to obtain approximately equal abundance of each of the ~340 000 unique mutants. This master pool was then inoculated into flasks with 50 mL of LB medium with 0.2% rhamnose at OD_{600} 0.025 (~75 CFU/mutant) and grown at 37°C with 230 rpm shaking until early exponential phase (OD_{600} 0.15, about 5-6 hours from frozen stocks). The culture was then split up into 2 mL volumes in small glass tubes, six for each antibiotic: three replicate tubes at two slightly different

concentrations to ensure at least one achieved the IC_{20-30}. A 2 mL aliquot of cells not exposed to antibiotic was taken at the Time 0 sample. The cultures were then exposed to antibiotics (or 1% DMSO solvent control) for 8 hours 37°C with 230 rpm shaking, after which the OD_{600} of the cultures were taken and cells were harvested from the tubes at the IC_{20-30}.

BarSeq DNA library preparation and sequencing

The method to amplify barcodes for sequencing followed a 1-step PCR as per (Wetmore et al. 2015) with some modifications. After antibiotic exposure, genomic DNA was extracted from cells with the PureLink Genomic DNA Mini Kit (Invitrogen). Yield for this and all subsequent steps was quantified with a Qubit (ThermoFisher) with either AccuGreen broad-range or high-sensitivity dsDNA detection kits (Biotium). To preserve mutant abundance ratios and reduce the propagation of PCR errors, semiquantitative PCR was performed. This was done for six randomly selected conditions. In each of a set of 10 µL reaction volumes, we added 40 ng of genomic DNA and 20 µM of each primer with Q5 high-fidelity DNA polymerase, the high-GC buffer, and standard Q5 reaction buffer (NEB). In an Eppendorf Mastercycler EP Gradient S, the cycling conditions were: 98°C for 4 mins, followed by cycling between 98°C for 30 s, 61°C for 30 s, 72°C for 30 s, then followed by a final extension at 72°C for 5 mins. After each cycle between 13 and 21, we quickly removed one tube and added 3 µL of Gel Loading Dye, Purple 6x (NEB) (with 10 mM EDTA) to stop the reaction. Formation of the product at 196 bp was visualized by electrophoresis through a 2.5% agarose gel in standard TAE buffer. By visual inspection of band intensities, a cycle number was chosen that resulted in ~25% of maximum product formation. This cycle number (17) was the same for all six randomly selected conditions and was thus used for all conditions. These cycling conditions were found in a small pilot

experiment, sequenced on a MiSeq with reagent kit v2 and 20% PhiX spike, to result in 96.4% of reads containing known barcodes.

We found that amplification in 10 µL matched that in 50 µL, thus the exact same PCR setup was used when scaled up to four tubes of 50 µL per condition to increase yields. For the template, 200 ng DNA was added to ensure >75 molecules of genome per mutant. We observed a minor secondary product (<10%) at 315 bp on TapeStation 4150 traces (Agilent Technologies). Thus, for each condition, 200 µL of raw BarSeq PCR product was pooled and subjected to two rounds of dual size selection with Sera-Mag Select (Cytiva) magnetic beads to purify the desired product at 196 bp. The primers were designed with Nextera-type tagmentation sequences as for the RB-TnSeq-circle sequencing primers, except that the 8 bp standard Nextera indexes were replaced with 10 bp Unique Dual Indexes (primers 2163 – 2255, Table 3). Each product was amplified with a unique i5 and i7 index, enabling greater multiplexing flexibility and higher confidence in correcting up to 2 bp errors during indexing read sequencing. Up to 24 samples were indexed together for runs of a NextSeq 550 in high-output mode (Donnelly Centre, Toronto, Canada) with reagent kit v2.5 and 20% PhiX spike, generating 410 – 510 million 30 bp single-end reads each. A custom sequencing recipe was used for dark-cycling during the first 18 bases, covering the flanking primer region, with the read output starting at the beginning of the barcode and extending 10 bp into the other flanking priming region.

BarSeq gene fitness calculations

BarSeq reads were associated with the correct barcode using the pipeline from (Wetmore et al. 2015). Reads, in fastq format, were first trimmed to contain only the 20 bp barcode using the FASTX toolkit (http://hannonlab.cshl.edu/fastx_toolkit/). Reads with any base having a

quality score below 20 were also filtered out. Artificial pre- and post-sequences, NNNGTCGACCTGCAGCGTACG and AGAGACC, respectively, were added to all barcodes so the script RunBarSeq.pl would recognize the barcodes as valid.

Following this, the barcodes were processed with scripts from (Morin et al. 2018) which are designed to compare mutant abundance between conditions (https://github.com/DuttonLab/RB-TnSeq-Microbial-interactions). A pseudocount of 0.1 was added to all barcode counts to prevent 0-value errors with log transformations. Barcodes were removed if they 1) had fewer than 3 reads in the Time 0 condition and 2) represented intergenic insertions, or insertions in the first or last 10% of a gene. Raw counts were normalized against the counts of 10 non-essential "neutral" genes randomly selected from across the genome that also showed no fitness effect in any condition. These were: K562_RS24650 (ABC-type amino acid transporter), K562_22855 (putative glycosyltransferase), K562_05000 (hydrolase family protein), K562_12100 (acyl-CoA dehydrogenase), K562_01045 (Raf kinase inhibitor-like protein), K562_06455 (putative PHA depolymerase protein), K562_13470 (GudD glucarate dehydratase), K562_16220 (DUF3025 domain-containing protein), K562_18550 (hypothetical protein), K562_28510 (hypothetical protein). Strain fitness values were then calculated as the $\log_2$(reads in Condition X / reads in Time 0). Gene fitness values were calculated as the arithmetic mean of strain fitness values for each gene. To account for artificial inflation of read count due to proximity to the replication forks, fitness values were smoothed based on genomic position using a moving window (Wetmore et al. 2015). Across the three replicates, gene fitness was calculated as the inverse-variance weighted mean. Spearman, Pearson, and Lin correlation coefficients across replicates for each condition were between 0.5 and 0.8. Lastly, the gene fitness values in each condition were compared to the DMSO control by an independent two-

sided Student's t-test. The data was also curated to remove any genes from downstream analysis that only had one reporting mutant. We used eggNOG-mapper v2 to provide functional annotations and gene names based on orthology (Huerta-Cepas et al. 2017; Cantalapiedra et al. 2021).

As many bacterial genes are organized in operons, disruptions in upstream genes may have polar effects on the downstream gene expression. Consequently, observed effects would be a combination of disrupting two or more genes. We argue that polarity may have a minimal effect on our findings due to 1) high insertion density and 2) the construction of our transposon. The large number of mutants recovered in our screen virtually guarantees insertions in every non-essential gene, thus genomic saturation would rule out polar effects by reporting fitness scores for nearly all non-essential genes. Secondly, our transposon has outward-facing promoters in both directions, the rhamnose-inducible promoter and the promoter controlling *dhfr*. As the transposon mutant antibiotic exposures were performed with added rhamnose, and the transposon terminal repeat after *dhfr* is not predicted to form an intrinsic terminator, insertion in operons may permit downstream gene expression. The parent transposon pTn*Mod*-OTp (Hunt et al. 2004) was suggested to not cause polar effects (Ortega et al. 2005). However, any expression, either upstream or downstream of the insertion, would be altered/non-native and was not directly assessed.

Microscopy

To observe the effect of β-lactam exposure on K56-2, cells were inoculated at OD 0.025 in 2 mL glass tubes and incubated at 37°C with 230 rpm shaking until early exponential phase OD 0.15, about 3 hours. Antibiotics were added and the incubation continued for 4 hours. To

observe the effect of deletion or overexpression of O-antigen-related genes, the appropriate mutants were inoculated in 2 mL glass tubes at OD 0.025 with or without rhamnose (0.05% or 0.005%) and grown at 37°C with 230 rpm shaking for 3 hours. Cells were then diluted to OD ~0.05, fixed in 3.7% formaldehyde + 1% methanol (Sigma) at room temperature for 20 minutes. The formaldehyde was quenched by addition of an equal volume of 0.5 M glycine, and the cells were washed by centrifugation and resuspended in Dulbecco's PBS (Sigma). Cells were spotted on 1.5% agarose pads with PBS to maintain turgor and imaged by DIC microscopy on an Axio Imager upright microscope (Carl Zeiss Microscopy GmbH).

LPS analysis

The general structure of the O-antigen LPS and lipid A core were analysed qualitatively by silver staining polyacrylamide gels as per (Marolda et al. 2006), with some modifications. For LPS extractions, CRISPRi mutants were grown overnight in liquid LB with 100 µg/mL trimethoprim and 0.5% rhamnose at 37°C. The mutants were subcultured at OD 0.025 and grown with 0.5% rhamnose for an additional 8 hours. For complementation, cells were subcultured to OD 0.025 and grown for 3 hours, then induced with 0.05% rhamnose for an additional 4 hours. For both types of mutants, an equivalent amount of 500 µL of OD 1.5 was harvested, washed by centrifugation, and resuspended in 150 µL lysis buffer (2% w/v SDS, 4% β-mercaptoethanol, 0.5 M Tris, pH 6.8). Cells were lysed by incubation at 95°C for 10 mins. DNase I (Worthington Biochemical) was added to 100 µg/mL and incubated at 37°C for 30 mins. Proteinase K (ThermoFisher) was added to 1.25 mg/mL and incubated at 60°C for 2 hr. An equal volume of 90% phenol (ThermoFisher) (supplemented with 0.1% β-mercaptoethanol and 0.2% 8-hydroxyquinoline) was added the tubes were incubated at 70°C for 15 mins, with vortexing

every 5 mins. The extractions were chilled on ice for 10 mins then centrifuged at 16 000 x g for 10 mins. The aqueous phase was washed with 10x volumes of ethyl ether (saturated with 10 mM Tris and 1 mM EDTA, pH 8.0) and centrifuged briefly. The top organic phase was removed by aspiration, then the aqueous phase was gently heated to 55°C for 10 mins to boil off any remaining ethyl ether. An equivalent volume of 2x loading dye (120 mM Tris-HCl pH 6.8, 4% m/v SDS, 20% glycerol, 0.04% bromophenol blue, and 10% β-mercaptoethanol) was added and the samples were stored at -20°C until needed.

The LPS banding patterns were resolved by Tricine-SDS-PAGE as per (Marolda et al. 2006), with some modifications. The gels were cast using 30% acrylamide/bis 29:1 solution (Bio-Rad) at final concentrations of 14% for the resolving gel and 4% for the stacking gel. 10 uL of each sample, diluted with an equal volume of loading buffer, was run in each lane. Gels were run at 50 V for 1 hr, then at 130 V for 3 hrs and 15 mins, then stained with the Pierce Silver Stain Kit (ThermoFisher) and imaged immediately afterwards on a Bio-Rad ChemiDoc.

Rhamnose dose-response curves

After construction, the first objective with the CRISPRi and overexpression mutants was to characterize how varying gene knockdown or overexpression affects growth. Each of the mutants were diluted to OD_{600} 0.01 in 96-well format and inoculated into a rhamnose gradient (with 100 µg/mL trimethoprim). Growth was monitored in a BioTek Synergy 2 plate reader with constant linear shaking and temperature maintained at 37°C.

Antimicrobial susceptibility testing and interaction assays

Broth microdilution susceptibility tests were used to assess and interpret MIC values as per CLSI guidelines (Clinical and Laboratory Standards Institute CLSI, 2014). Overnight cultures grown in liquid LB were used to prepare inocula for standard microdilution tests and checkerboard interactions assays. Growth was visually assessed in the antibiotic gradients after 20 hrs of static incubation. When interpretive standards for *Burkholderia* did not exist (as for cefiderocol and aztreonam), standards for *Pseudomonas aeruginosa* were used. M9+CAA medium consisted of the following: 1x M9 salts (Difco), 25 mg/L $CaCl_2$, 12.5 mg/L $MgCl_2$, 0.3% low-iron casamino acids (Fisher), and 25 mM glucose.

A similar format to the standard MIC method above was used to assess changes in antibiotic susceptibility of the CRISPRi mutants. A final concentration of 0.5% rhamnose was added to the wells to induce dCas9 expression. For fitness-associated/essential genes (e.g. *uppS*), a concentration of rhamnose to achieve 80% WT growth was used. For assays done in M9+CAA medium, 25 mM glycerol was used instead of glucose, as glucose catabolism represses the rhamnose-inducible promoter (Egan and Schleif 1993). Trimethoprim was not included in the assay plates to remove the possibility of chemical interactions. Growth was assessed after 20 hrs of static incubation by reading OD_{600} values with a BioTek Synergy 2 plate reader to record subinhibitory dose effects.

Checkerboard assays were prepared in mini 4x4 well format using antibiotic concentrations of 1/8 – 1/2 the MIC for each compound. Testing was performed in cation-adjusted MHB as per CLSI guidelines. For testing with BAC, CAMHB buffered to pH 7.2 with 100 mM PBS was used as we found the acidic solvent for BAC antagonised β-lactam susceptibility (data not shown). Checkerboard data was processed with SynergyFinder2 (http://www.synergyfinder.org/#!/) (Ianevski et al. 2020; Zheng et al. 2022) as this easily handles

biological replicates and gives mathematical interpretations of interactions even when compounds do not fully inhibit. When both the Loewe Additivity and Bliss Independence scores were below -10 (as determined from the 95% confidence intervals), the interaction was regarded as strongly antagonistic; synergy was interpreted when both scores were above +10 (as determined from the 95% confidence intervals). A weak interaction was interpreted when one score was above +10 or below -10 and the other was between -10 and +10.

NPN uptake assay

Outer membrane permeability was assessed with the NPN uptake assay as per (Loh et al. 1984; Malott et al. 2012), with some modifications. For CRISPRi mutants, overnight cultures were grown with or without 0.5% rhamnose (or 0.04% for the *uppS* mutants) then diluted to OD 0.025 and grown for an additional 8 hours (with or without the same concentration of rhamnose) until OD ~1.0. For gene deletion mutants, overnight cultures were diluted to OD 0.2 and grown for 3 hours until OD ~1.0. Cells were washed by centrifugation at 5 000 x g for 5 minutes then resuspended in 5 mM HEPES pH 7.2 with 10 mM NaN_3 (Sigma) and rested at room temperature for 30 minutes. An equal volume of cells was mixed with HEPES buffer containing 80 µM NPN (Sigma). The fluorescence signal was measured in a BioTek Synergy 2 plate reader with filter sets: Ex 360/40 nm and Em 420/40 nm. Wild-type K56-2 treated with 32 µg/mL CHX was used as a positive permeabilized control. The blank-corrected fluorescence values were normalized to the OD_{600} of each well. To easily compare between replicates, the fluorescence ratios of the mutants to K56-2 controls (with non-targeting sgRNA as appropriate) were calculated.

Statistical analysis

For RB-TnSeq and BarSeq data, the statistical analysis and normalizations built into the scripts were used (Wetmore et al. 2015; Morin et al. 2018). Only the independent Student's t-test was applied to the BarSeq data comparisons, not the false-discovery rate multiple-testing correction as it was found to be too stringent; however, samples were only compared by t-test if they passed Fisher's F-test of equal variances ($\alpha = 0.002$). As this was expected to produce false positive, only genes with fitness effects greater than 0.5 or less than -0.5 were considered for further analysis. Additionally, we performed extensive follow-up validations using CRISPRi mutants many of the effects we observed in the BarSeq data. Pearson's correlation with two-tailed p-values was used to assess the relationship between gene fitness values in AVI/CAZ and the single conditions in the combination. The NPN outer membrane permeability assay was analysed by 1-way ANOVA with a Dunnett's multiple comparison test, with K56-2::dCas9 bearing the non-targeting sgRNA (or without for the deletion mutants) set as the reference.

Data availability

Raw sequencing data is available from the NCBI Sequencing Read Archive (SRA) under the BioProject ID PRJNA859150. All gene fitness scores are available in Supplementary Data 1 (https://doi.org/10.34990/FK2/UIQTSR). Publicly available databases and servers were used for gene annotations: BioCyc (https://biocyc.org/), EggNOG-mapper v2 (http://eggnog-mapper.embl.de/), GO (http://geneontology.org/), and UniProt (https://www.uniprot.org/).

Acknowledgments

This work was financially supported by a Discovery Grant from the Natural Sciences and Engineering Research Council of Canada (NSERC), a Basic Research Grant from Cystic Fibrosis Canada, and a Research Project Grant from the Canadian Institutes of Health Research (CIHR) to STC; AMH was supported by a Vanier Canada Graduate Scholarship from CIHR; AN was supported by an Undergraduate Summer Research Award from NSERC; BL and AB were supported by the Fondo para la Investigación Científica y Tecnológica (FONCyT) Proyecto de Investigación Trianual PICT-2019-III-A, Categoría Raíces.

The authors are grateful Debbie Armstrong and Dr. Feiyue Wang from the Ultra-Clean Trace Elements Laboratory (UCTEL) at the Centre for Earth Observation Science at the University of Manitoba for ICP-MS analysis. The authors are appreciative of insightful discussions with Dr. Krisztina Papp-Wallace (Veterans Affairs Northeast Ohio Healthcare System and Case Western Reserve University) regarding the pathways and biochemistry of peptidoglycan recycling. The authors also wish to thank the Donnelly Centre (Toronto, Ontario, Canada), The Centre for Applied Genomics (Toronto, Ontario, Canada), and Génome Québec (Montréal, Québec, Canada) for sequencing services.

Conflict of Interest Statement

The authors declare no conflict of interest.

Table 1. Antibiotics used for genome-wide fitness profiling

Antibiotic	IC_{20-30} Concentration (µg/mL)	Target (Process)
Ampicillin (**AMP**) †	256†	PBP3/Divisome (Cell wall synthesis)
Aztreonam (**AZT**)	40	PBP3/Divisome (Cell wall synthesis)
Cefiderocol (**CFD**)	0.04	PBP3/Divisome (Cell wall synthesis)
Ceftazidime - High (**CAZ-H**)*	4	PBP3/Divisome (Cell wall synthesis)
Ceftazidime - Low (**CAZ-L**)*	1.5	PBP3/Divisome (Cell wall synthesis)
Tazobactam (**TAZ**)	50	PBP3/Divisome (Cell wall synthesis)
Cefotetan (**CTT**)	45	PBP3/Divisome (Cell wall synthesis) + PBP2/Rod complex (Cell wall synthesis)
Meropenem (**MEM**)	3.5	PBP2/Rod complex (Cell wall synthesis)
Avibactam - High (**AVI-H**)*	115	PBP2/Rod complex (Cell wall synthesis) + Diverse β-lactamases
Avibactam - Low (**AVI-L**)*	8	PBP2/Rod complex (Cell wall synthesis) + Diverse β-lactamases
Ceftazidime/Avibactam (**AVI/CAZ**)	1.5/8	PBP2/Rod complex (Cell wall synthesis) + Diverse β-lactamases + PBP3/Divisome (Cell wall synthesis)
Cycloserine (**CYC**)	150	Alr and Ddl (Cell wall precursor synthesis)
Fosfomycin (**FOS**) †	256†	MurA (Cell wall precursor synthesis)
Bacitracin (**BAC**)	375	Und-PP (Undecaprenol metabolism)
FR-900098 (**FR-9**)	85	Dxr (Undecaprenol metabolism)
CHIR-090 (**CHIR**) †	256†	LpxC (Lipid A synthesis)
PF-04753299 (**PF-04**)	0.18	LpxC (Lipid A synthesis)
Chlorhexidine (**CHX**)	1.8	Lipid membranes
Polymyxin B (**PMB**)	550	LPS and lipid membranes
Erythromycin (**ERY**)	100	Peptide exit tunnel/23S rRNA (Protein Synthesis)
Novobiocin (**NOV**)	1.1	GyrB (DNA gyrase)
Rifampicin (**RIF**)	5.5	RpoB (Transcription)

* Two concentrations of AVI and CAZ were used. A higher concentration that independently reached the IC_{20-30}, and a lower concentration the same as that used in the synergistic AVI/CAZ combination.

† IC_{20-30} could not be reached for AMP, FOS, and CHIR, so highest concentration tested was used (256µg/mL).

Shading groups antibiotics by broad target processes.

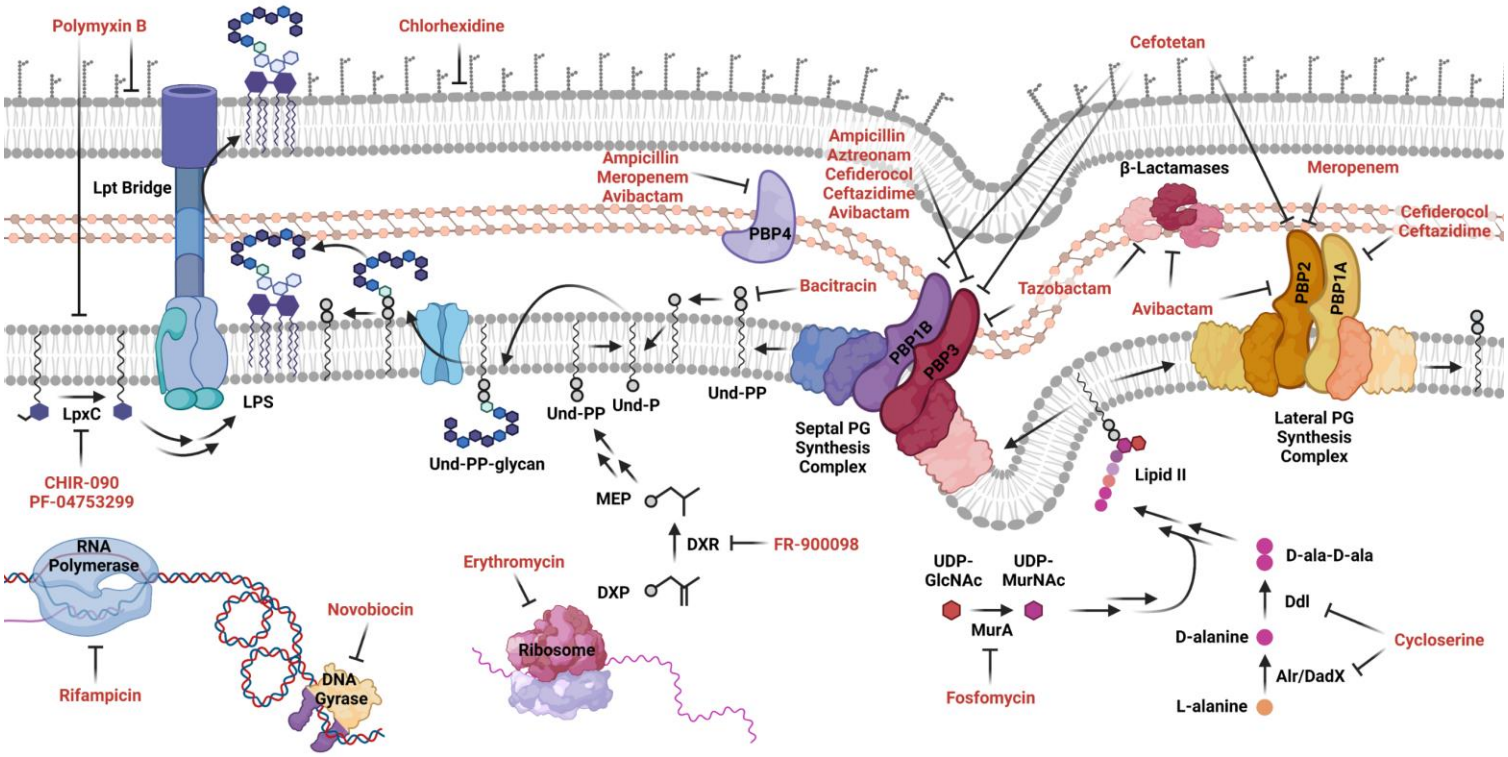

Figure 1. Schematic of the Gram-negative cell envelope and steps inhibited by the antibiotic panel. Rifampicin, novobiocin, and erythromycin are controls that do not target the envelope. Targets are shown based on previous experimental evidence from E. coli, and only if a Bcc homologue exists. High molecular weight PBPs 5, 6, 7 are omitted for clarity.

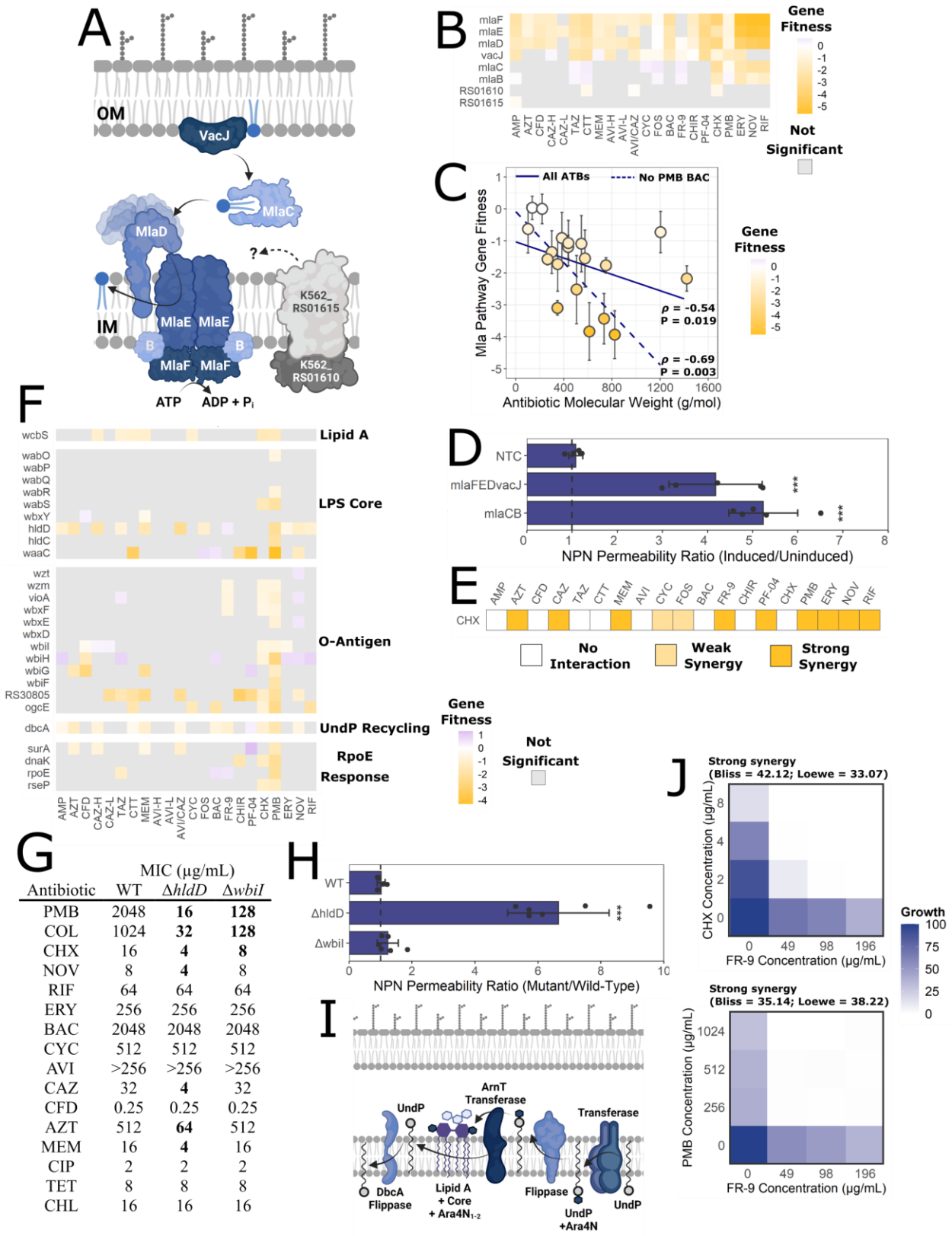
A
OM
VacJ
MlaC
MlaD
?
K562_ RS01615
IM
MlaE MlaE
B
B
MlaF MlaF
K562_ RS01610
ATP
ADP + Pi
B
mlaF
mlaE
mlaD
vacJ
mlaC
mlaB
RS01610
RS01615
AMP AZT CFD CAZ-H CAZ-L TAZ CTT MEM AVI-H AVI-L AVI/CAZ CYC FOS BAC FR-9 CHIR PF-04 CHX PMB ERY NOV RIF
Gene Fitness
0 -1 -2 -3 -4 -5
Not Significant
C
All ATBs
No PMB BAC
Mla Pathway Gene Fitness
ρ = -0.54
P = 0.019
ρ = -0.69
P = 0.003
Antibiotic Molecular Weight (g/mol)
Gene Fitness
0 -1 -2 -3 -4 -5
F
wcbS
Lipid A
wabO wabP wabQ wabR wabS wbxY hldD hldC waaC
LPS Core
wzt wzm vioA wbxF wbxE wbxD wbiI wbiH wbiG wbiF RS30805 ogcE
O-Antigen
dbcA
UndP Recycling
surA dnaK rpoE rseP
RpoE Response
AMP AZT CFD CAZ-H CAZ-L TAZ CTT MEM AVI-H AVI-L AVI/CAZ CYC FOS BAC FR-9 CHIR PF-04 CHX PMB ERY NOV RIF
Gene Fitness
1 0 -1 -2 -3 -4
Not Significant
D
NTC
mlaFEDvacJ
mlaCB
***
***
NPN Permeability Ratio (Induced/Uninduced)
E
AMP AZT CFD CAZ TAZ CTT MEM AVI CYC FOS BAC FR-9 CHIR PF-04 CHX PMB ERY NOV RIF
CHX
No Interaction
Weak Synergy
Strong Synergy
G
MIC (μg/mL)
Antibiotic WT ΔhldD ΔwbiI
PMB 2048 16 128
COL 1024 32 128
CHX 16 4 8
NOV 8 4 8
RIF 64 64 64
ERY 256 256 256
BAC 2048 2048 2048
CYC 512 512 512
AVI >256 >256 >256
CAZ 32 4 32
CFD 0.25 0.25 0.25
AZT 512 64 512
MEM 16 4 16
CIP 2 2 2
TET 8 8 8
CHL 16 16 16
H
WT
ΔhldD
ΔwbiI
***
NPN Permeability Ratio (Mutant/Wild-Type)
I
ArnT Transferase
UndP
Transferase
DbcA Flippase
Lipid A + Core + Ara4N1-2
Flippase
UndP +Ara4N
UndP
J
Strong synergy
(Bliss = 42.12; Loewe = 33.07)
CHX Concentration (μg/mL)
FR-9 Concentration (μg/mL)
Growth
100 75 50 25 0
Strong synergy
(Bliss = 35.14; Loewe = 38.22)
PMB Concentration (μg/mL)
FR-9 Concentration (μg/mL)

Figure 2. Structural defects in the outer membrane increase susceptibility to multiple antibiotics. A) Retrograde phospholipid trafficking from the outer (OM) to inner (IM) membranes by the Mla pathway, inferred by homology (Bernier et al. 2018; Powers et al. 2020). The roles of K562_RS01610 and K562_RS01615 are unclear. B) Gene fitness scores relative to DMSO control of the genes in the Mla pathway. Grey squares indicate the value was not significant ($P > 0.05$). C) Correlation of average gene fitness scores in the Mla pathway (*mlaFEDvacJ* and *mlaCB*) with antibiotic molecular weight. The points are coloured by average Mla pathway gene fitness score. The lines show a linear regression with all antibiotics (solid) vs. without PMB and BAC (dashed). Shown by each line is the Spearman's rank correlation coefficient (ρ) and P-value. D) Ratios of NPN fluorescence of the CRISPRi mutants in inducing (0.5% rhamnose) vs uninducing (0% rhamnose) conditions. Error bars represent means ± SD of six replicates. Significance was determined by 1-way ANOVA with Dunnett's post hoc test to the wild-type control. *** $P < 0.001$. The dashed lines indicate a NPN fluorescence ratio of 1. E) Summary of antibiotic checkerboard interaction assay with CHX. Interactions were assessed and interpreted with SynergyFinder as per the Materials and Methods. F) Gene fitness scores relative to DMSO control of the genes associated with LPS, lipid A modifications, and the RpoE regulon. G) MIC values of K56-2 and the Δ*hldD* and Δ*wbiI* mutants. The K56-2 and deletion backgrounds have dCas9 integrated in the chromosome. Values are medians of three biological replicates, with bold indicating at least 2-fold change from WT. H) Ratios of NPN fluorescence of the deletion mutants to the fluorescence of the wild-type control. Error bars represent means ± SD of six replicates. Significance was determined by 1-way ANOVA with Dunnett's post hoc test to the wild-type control. *** $P < 0.001$. The dashed lines indicate a NPN fluorescence ratio of 1. I) Diagram of the membrane-associated steps of the Ara4N LPS modification, inferred from

homology and experimental evidence in Burkholderia (Panta et al. 2019; Simpson and Trent 2019). J) Mini checkboard assays of FR-9 interaction with CHX and PMB. Values are normalized to the OD_{600} of growth without antibiotic.

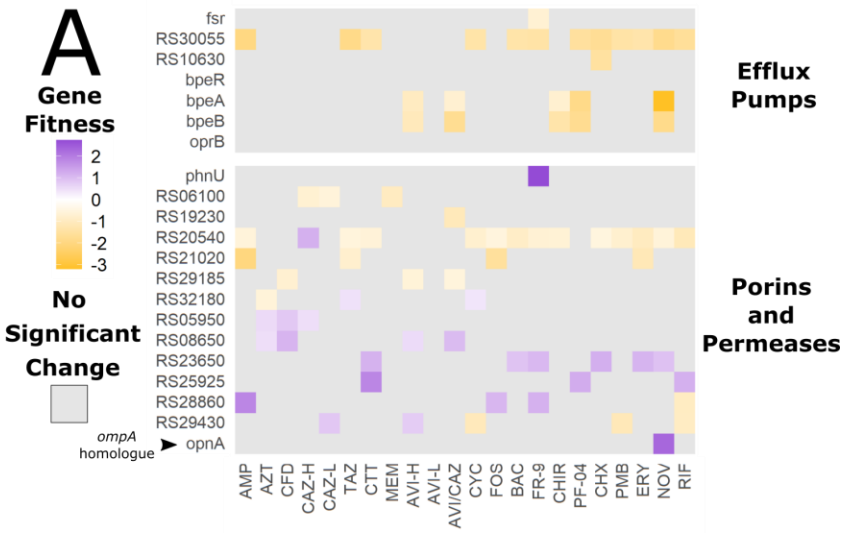

B

CRISPRi Target	MIC (µg/mL) CHL	PF-04	NOV	AVI	CAZ	AVI/CAZ
NTC	16	1	8	>256	32	8/4
bpeAB-oprB	**8**	**0.5**	**4**	**128**	32	**8/2**

C

CRISPRi Target	NOV MIC (µg/mL) *B. cenocepacia* K56-2	*B. multivorans* ATCC17616	*B. thailandensis* E264
NTC	8	8	8
opnA	**16**	**16**	**16**

Figure 3. Disruptions in efflux pumps, porins, and permeases alter antibiotic susceptibility**.** A) Gene fitness scores relative to DMSO control of the genes associated with efflux pumps, porins, and permeases. For genes not assigned names, the K562_# locus tags are given. B) MIC values of K56-2::dCas9 harbouring plasmids expressing a non-targeting sgRNA control (NTC) or an sgRNA targeting the *bpeAB-oprB* operon C) MIC values of CRISPRi mutants of *Burkholderia* species targeting *opnA*. MIC values are medians of three biological replicates, with bold indicating at least 2-fold change from the NTC with the addition of rhamnose.

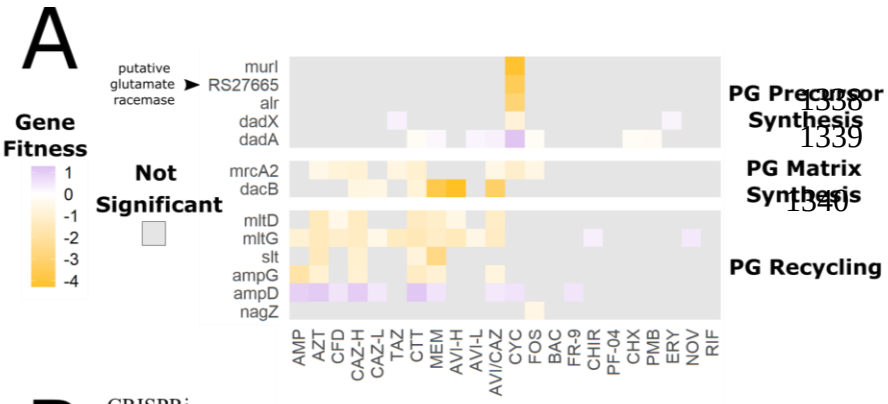

B

CRISPRi Target	AMP	AZT	CFD	CAZ	TAZ	CTT	MEM	AVI
NTC	>512	512	0.25	32	128	64	16	>256
dacB	>512	512	0.25	32	128	64	**4**	**64**
slt	>512	**32**	0.25	**8**	**32**	**16**	**8**	**128**
mltD	>512	**256**	0.25	**16**	128	64	16	>256
mltG	>512	**64**	0.25	**8**	**32**	**32**	**8**	>256
ampD	>512	512	**0.5**	**64**	128	64	**32**	>256
ampG	>512	**8**	0.25	**4**	**32**	**16**	**4**	**128**

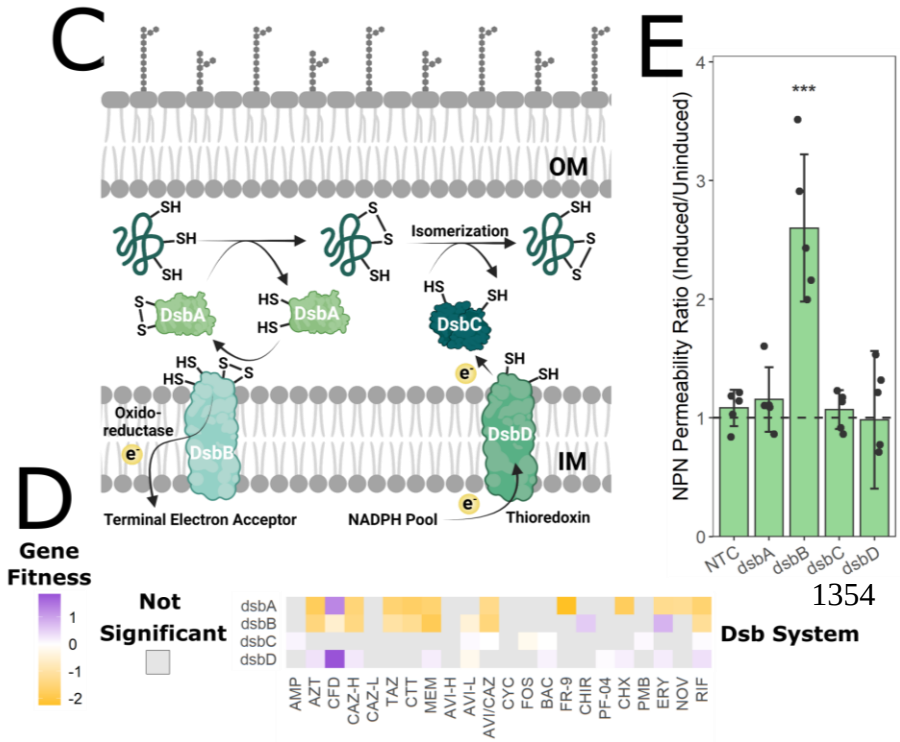

Figure 4. Chemical genetic interactions with periplasmic processes (peptidoglycan synthesis and the DSB system). A) Gene fitness scores relative to DMSO control of the genes encoding peptidoglycan precursor and matrix synthesis, and peptidoglycan recycling. B) MIC values of K56-2::dCas9 harbouring plasmids expressing a non-targeting sgRNA control (NTC) or an sgRNA targeting the indicated genes. MIC values are medians of three biological replicates, with bold indicating at least 2-fold change from the NTC with the addition of rhamnose. C) Periplasmic disulfide bond formation by DsbAB and isomerization by DsbCD (Landeta et al. 2018). D) Gene fitness scores relative to the DMSO control of the genes in the DSB system. E) Ratios of NPN fluorescence of the CRISPRi mutants in inducing (0.5% rhamnose for *dsbA*, *dsbC*, and *dsbD*; 0.05% rhamnose for *dsbB*) vs uninducing conditions (0% rhamnose). Error bars represent means ± SD of five replicates. Significance was determined by 1-way ANOVA with Dunnett's post hoc test to the wild-type control. *** $P < 0.001$. The dashed lines indicate a NPN fluorescence ratio of 1.

1375

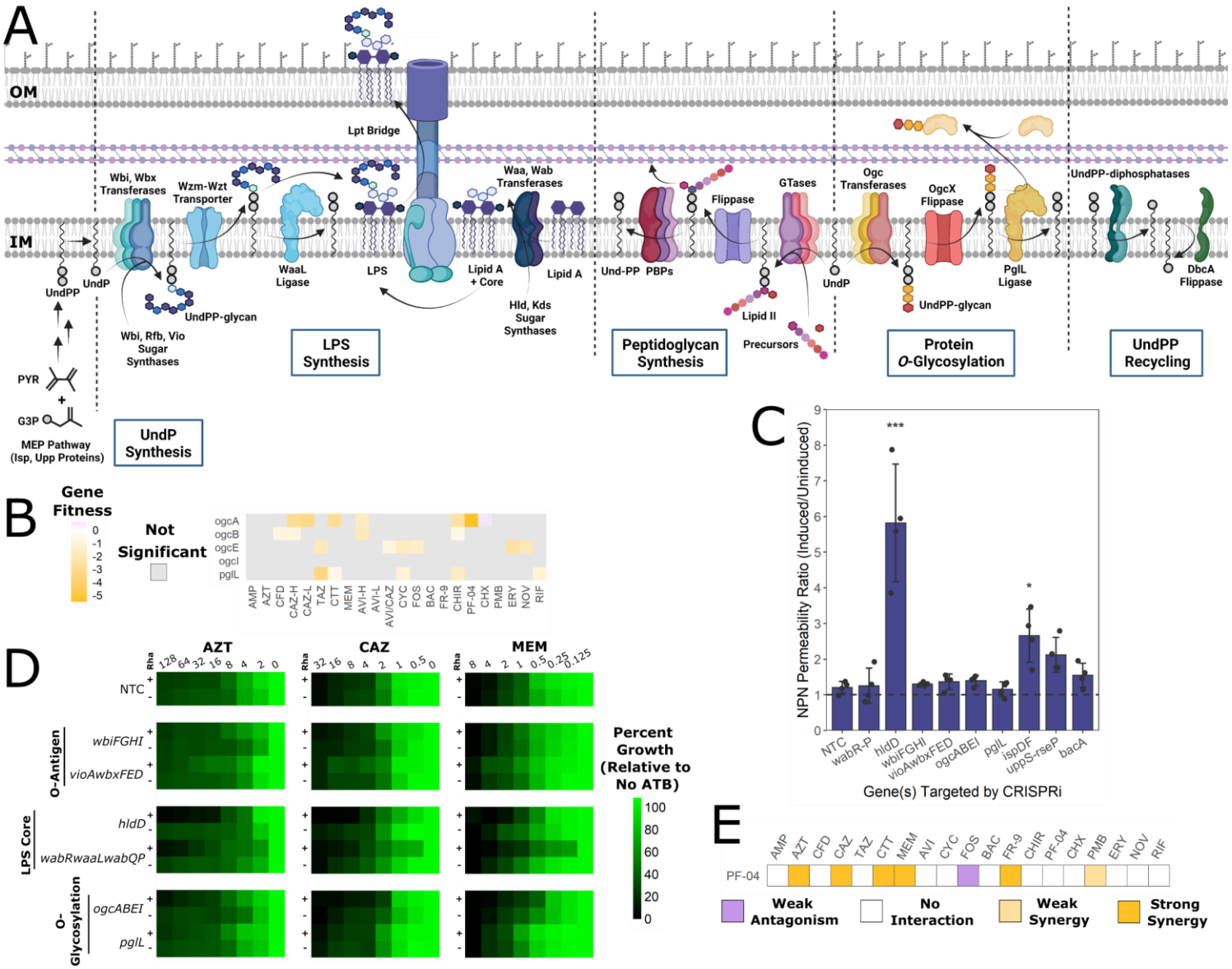
A
OM
IM
Lpt Bridge
Wbi, Wbx Transferases
Wzm-Wzt Transporter
Waa, Wab Transferases
Flippase
GTases
Ogc Transferases
OgcX Flippase
UndPP-diphosphatases
UndPP
UndP
UndPP-glycan
Wbi, Rfb, Vio Sugar Synthases
WaaL Ligase
LPS
Lipid A + Core
Lipid A
Hld, Kds Sugar Synthases
Und-PP
PBPs
Lipid II
Precursors
UndP
UndPP-glycan
PglL Ligase
DbcA Flippase
LPS Synthesis
Peptidoglycan Synthesis
Protein O-Glycosylation
UndPP Recycling
PYR
G3P
MEP Pathway (Isp, Upp Proteins)
UndP Synthesis
B
Gene Fitness
0
-1
-2
-3
-4
-5
Not Significant
ogcA
ogcB
ogcE
ogcI
pglL
AMP AZT CFD CAZ-H CAZ-L TAZ CTT MEM AVI-H AVI-L AVI/CAZ CYC FOS BAC FR-9 CHIR PF-04 CHX PMB ERY NOV RIF
C
NPN Permeability Ratio (Induced/Uninduced)
***
*
NTC
wabR-P
hldD
wbiFGHI
vioAwbxFED
ogcABEI
pglL
ispDF
uppS-rseP
bacA
Gene(s) Targeted by CRISPRi
D
AZT
CAZ
MEM
Rha
NTC
O-Antigen
wbiFGHI
vioAwbxFED
LPS Core
hldD
wabRwaaLwabQP
O-Glycosylation
ogcABEI
pglL
Percent Growth (Relative to No ATB)
100
80
60
40
20
0
E
AMP AZT CFD CAZ TAZ CTT MEM AVI CYC FOS BAC FR-9 CHIR PF-04 CHX PMB ERY NOV RIF
PF-04
Weak Antagonism
No Interaction
Weak Synergy
Strong Synergy

1376

Figure 5. Defects in UndP utilisation pathways sensitize cells to β-lactams. A) Summary of the major UndP(P) metabolic pathways in B. cenocepacia (from experimental evidence and inferred by homology), annotated with proteins names if they are known (Egan 2020; Manat et al. 2014; Mohamed et al. 2019; Ortega et al. 2005, 2009; Roney and Rudner 2022; Valvano 2015). The Ara4N modification is shown in Figure 2I. UndPP is synthesized in the cytoplasm by the methylerythritol phosphate (MEP) pathway. UndP is a lipid carrier for construction of the O-antigen, peptidoglycan building blocks (in the form of lipid I and II), and the protein O-glycan. After use as a carrier, UndPP is liberated and recycled into UndP on the cytoplasmic leaflet. IM = inner membrane, OM = outer membrane. B) Gene fitness scores relative to the DMSO control of the genes in the protein O-glycosylation (Ogc) pathway. C) Ratios of NPN fluorescence of the CRISPRi mutants in inducing vs uninducing conditions. Error bars represent means ± SD of four replicates. Significance was determined by 1-way ANOVA with Dunnett's post hoc test to the wild-type control. * $P < 0.05$; *** $P < 0.001$. The dashed lines indicate a NPN fluorescence ratio of 1. D) Antibiotic dose responses (µg/mL) of growth of CRISPRi mutants with or without induction with 0.5% rhamnose. Values are normalized to the OD600 of growth without antibiotic. NTC = non-targeting control sgRNA. E) Summary of antibiotic checkerboard interaction assay with PF-04. Interactions were assessed and interpreted with SynergyFinder as per the Materials and Methods.

A

CRISPRi Target	MIC (µg/mL) AZT	CAZ	MEM
NTC	256	32	16
ispDF	**32**	**8**	**8**
uppS	**64**	**16**	**8**

B

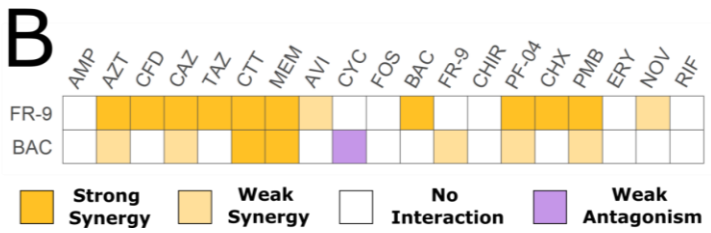

Figure 6. Inhibiting isoprenoid and UndP synthesis sensitizes cells to β-lactams. A) MIC values of K56-2::dCas9 harbouring plasmids expressing a non-targeting sgRNA control (NTC) or an sgRNA targeting the indicated genes. MIC values are medians of three biological replicates, with bold indicating at least 2-fold change from the NTC with the addition of rhamnose. B) Summary of antibiotic checkerboard interaction assay with FR-9 and BAC. Interactions were assessed and interpreted with SynergyFinder as per the Materials and Methods.

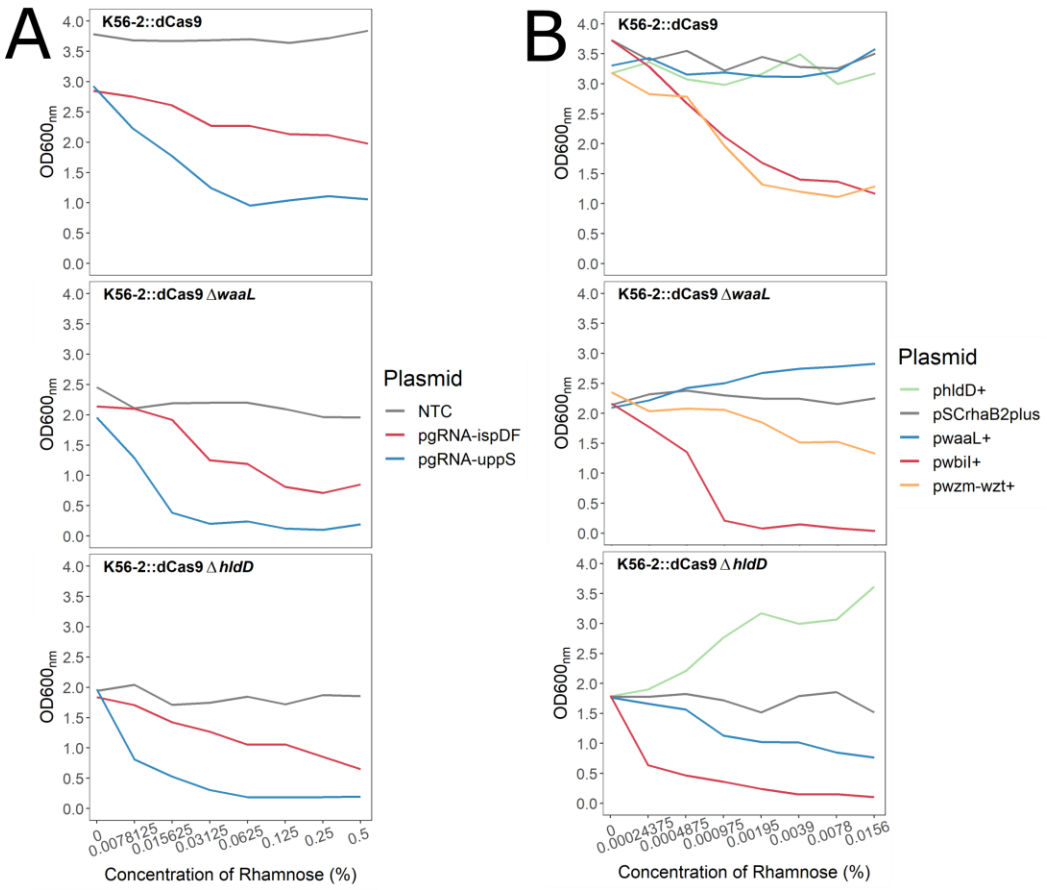
A
B
K56-2::dCas9
K56-2::dCas9 ΔwaaL
K56-2::dCas9 Δ hldD
OD600nm
Concentration of Rhamnose (%)
Plasmid
NTC
pgRNA-ispDF
pgRNA-uppS
phldD+
pSCrhaB2plus
pwaaL+
pwbil+
pwzm-wzt+

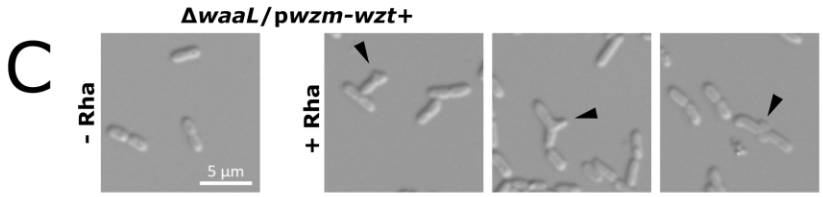
C
ΔwaaL/pwzm-wzt+
- Rha
+ Rha
5 µm

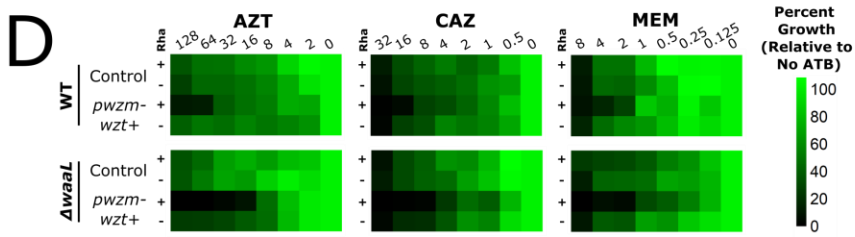
D
AZT
CAZ
MEM
Rha
WT
ΔwaaL
Control
pwzm-wzt+
Percent Growth (Relative to No ATB)

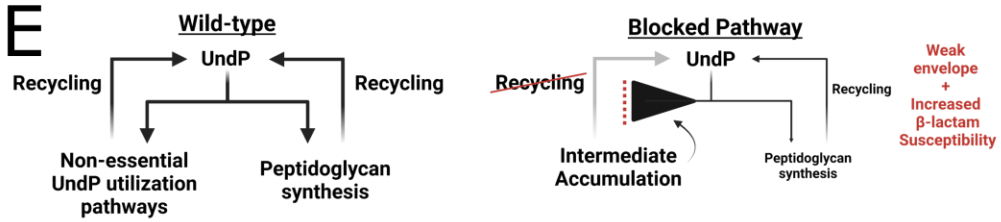
E
Wild-type
UndP
Recycling
Recycling
Non-essential UndP utilization pathways
Peptidoglycan synthesis
Blocked Pathway
UndP
Recycling
Recycling
Intermediate Accumulation
Peptidoglycan synthesis
Weak envelope + Increased β-lactam Susceptibility

Figure 7. Growth and morphology of double mutants support a model that UndP sequestration causes defects in peptidoglycan synthesis. Cultures of deletion mutants with A) CRISPRi plasmids or B) overexpression plasmids were grown with the indicated concentrations of rhamnose for 18 hours, the time at which the control strains reached the maximum OD_{600}. Panels are organized by mutant background: Values shown are averages of three biological replicates. C) Mid exponential phase cells of the Δ*waaL*/p*wzm-wzt*+ mutant were induced with 0.05% rhamnose for 3 hours then immobilized on 1% agarose pads and imaged by DIC at 100x magnification. The black arrowheads mark morphological abnormalities such as bulging. D) Antibiotic dose responses (µg/mL) of growth of the indicated mutants with or without induction with 0.005% rhamnose. Values are normalized to the OD600 of growth without antibiotic. Control strain harbours pSCrhaB2plus. E) Proposed framework for how disruptions in UndP metabolism reduce UndP recycling and flux into peptidoglycan synthesis, weakening the peptidoglycan matrix and increasing β-lactam susceptibility

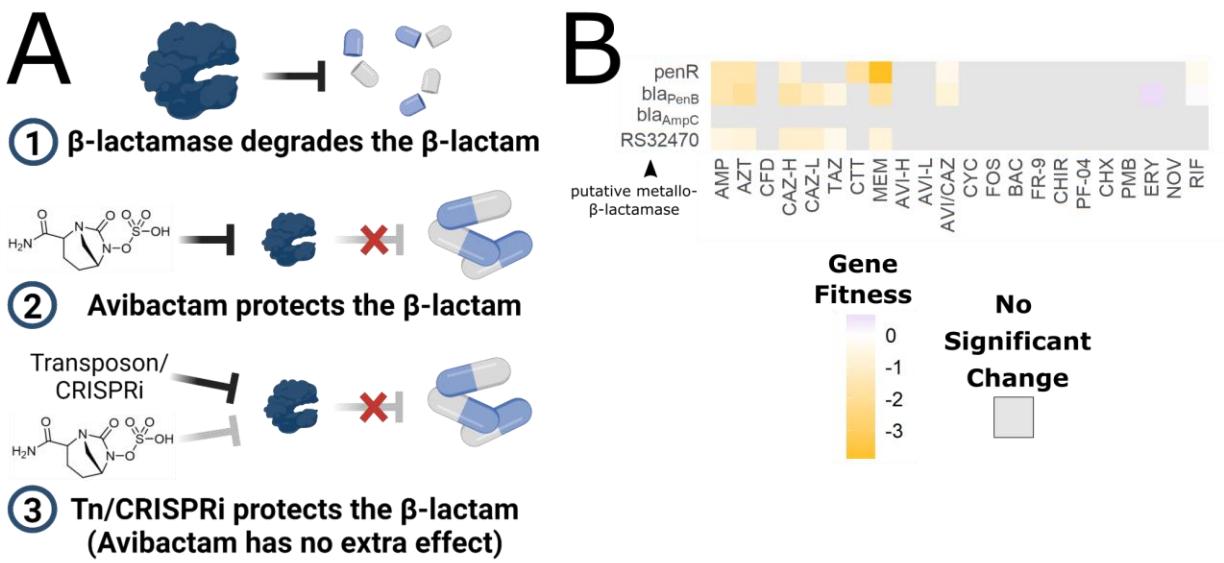

C

Antibiotic	Gene	MIC (µg/mL) -AVI*	MIC (µg/mL) +AVI*	Fold MIC†
AZT	NTC	256	4	32
	bla$_{AmpC}$	256	4	32
	bla$_{PenB}$	**8**	4	**2**
	RS32470	256	4	32
CAZ	NTC	32	4	8
	bla$_{AmpC}$	32	4	8
	bla$_{PenB}$	**4**	4	**1**
	RS32470	32	4	8
MEM	NTC	16	1	16
	bla$_{AmpC}$	16	1	16
	bla$_{PenB}$	**1**	1	**1**
	RS32470	16	1	16

Figure 8. PenB is the predominant β-lactamase in K56-2 and is inhibited by AVI. A) Rationale for identifying targets of AVI. If a target is disrupted with a transposon or repressed with CRISPRi there will be no change in β-lactam MIC when AVI is added B*)* Gene fitness scores relative to the DMSO control of β-lactamase and regulatory genes. C) MIC values of K56-2::dCas9 harbouring plasmids expressing a non-targeting sgRNA control (NTC) or an sgRNA targeting the indicated genes. MIC values are medians of three biological replicates, with bold indicating change versus the NTC. † Fold MIC is the ratio of the MIC -AVI to the MIC +AVI. * AVI kept constant at 8 µg/mL.

A

	AZT		MEM		CAZ		CFD	
	-AVI	+AVI	-AVI	+AVI	-AVI	+AVI	-AVI	+AVI
Resistant/Total Isolates	24/41	2/41	9/41	0/41	4/41	0/41	8/41	8/41
(% Resistant)	(59%)	(5%)	(22%)	(0%)	(10%)	(0%)	(20%)	(20%)

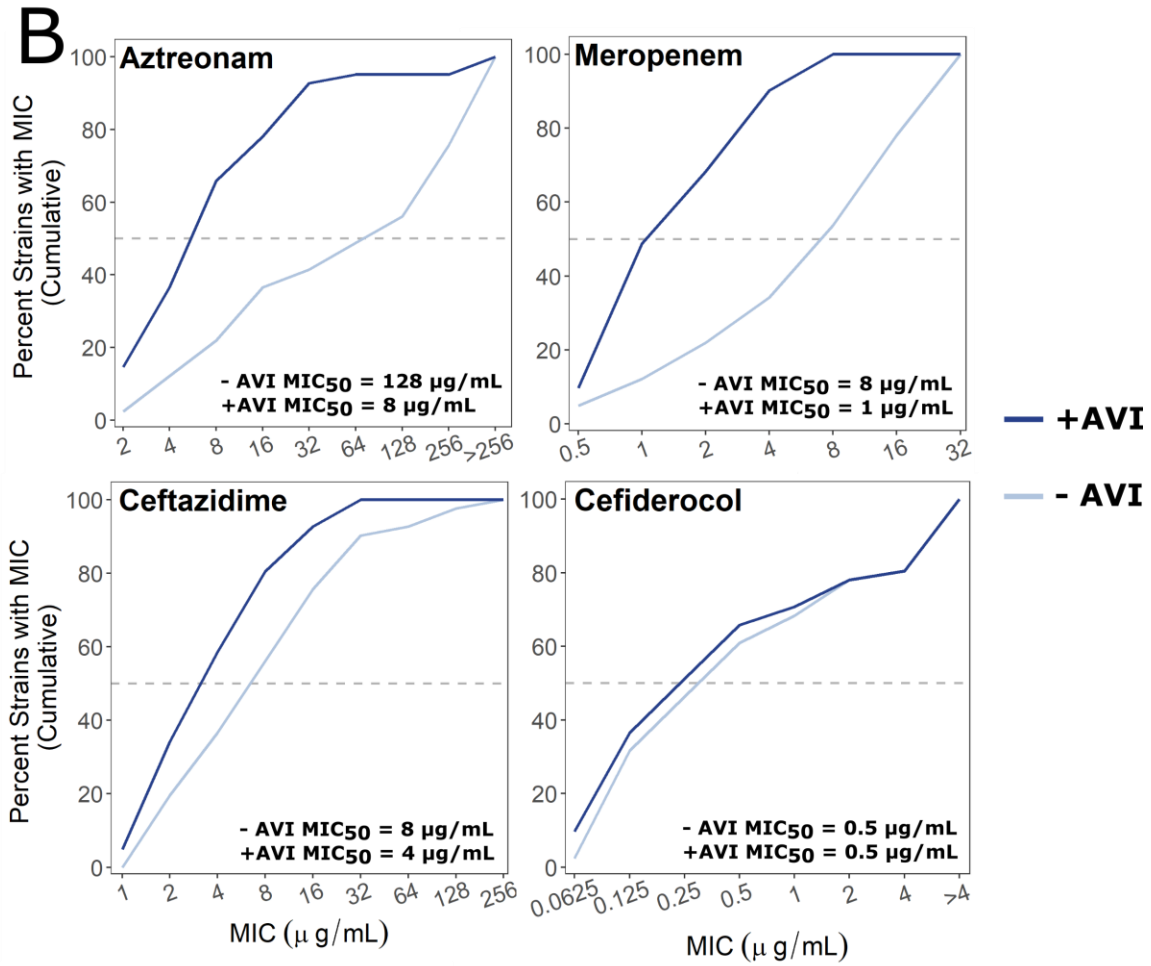

Figure 9. AVI strongly potentiates AZT and MEM in Bcc clinical isolates. A) Resistance to AZT, MEM, and CAZ with or without 8 µg/mL AVI. CLSI resistance breakpoints for Bcc: MEM ≥ 16 µg/mL; CAZ ≥ 32 µg/mL. CLSI resistance breakpoint for *Pseudomonas aeruginosa*: AZT ≥ 32 µg/mL; CFD > 4 µg/mL. B) Percent cumulative growth inhibition of 41 Bcc clinical isolates with or without AVI. Data is summarized from Table S3. The dashed line indicates the MIC_{50}, the concentration at which 50% of the isolates were inhibited.

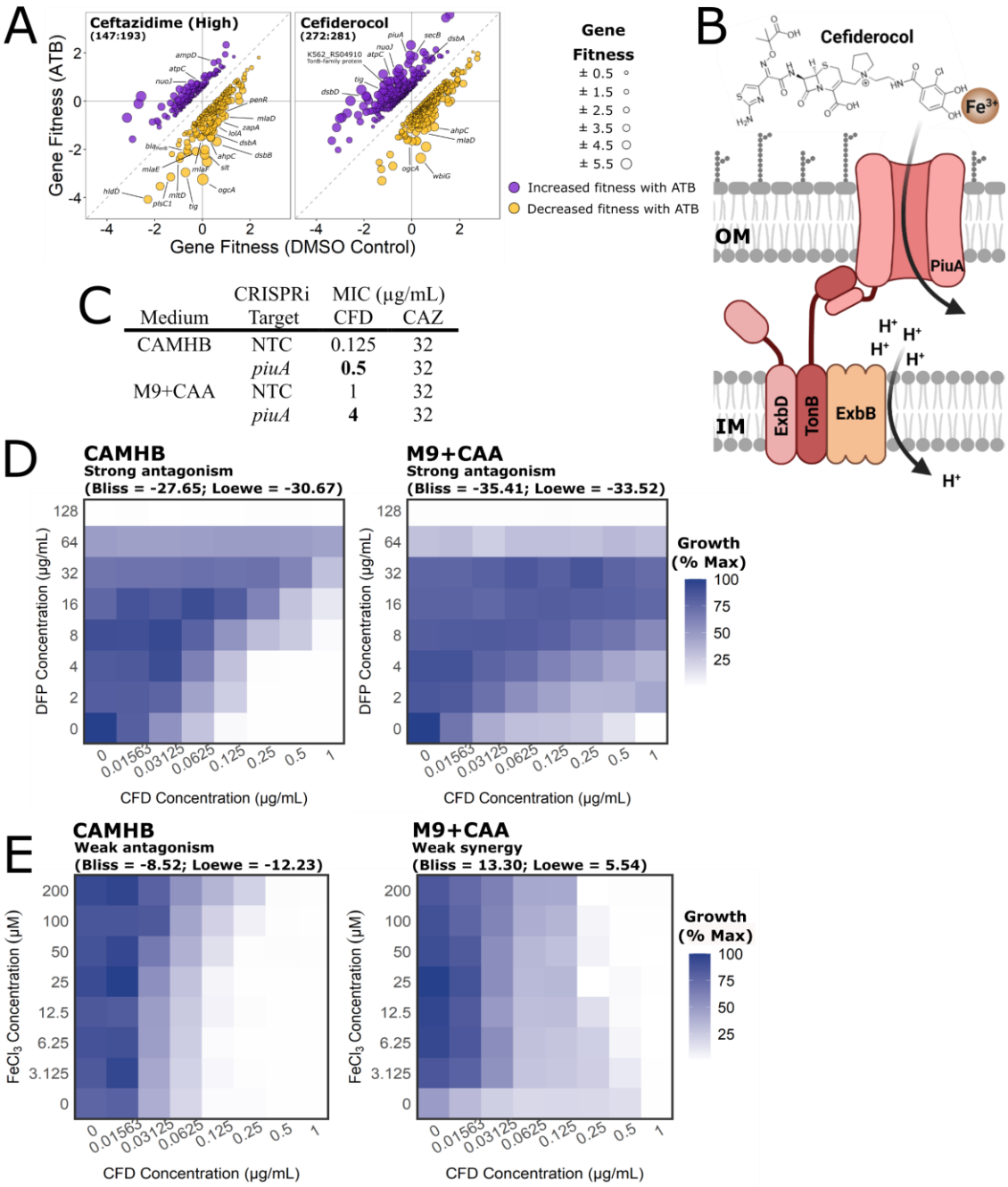

Medium	CRISPRi Target	MIC (µg/mL) CFD	CAZ
CAMHB	NTC	0.125	32
	piuA	**0.5**	32
M9+CAA	NTC	1	32
	piuA	**4**	32

Figure 10. CFD uptake in K56-2 is via the PiuA siderophore receptor and is strongly dependent on iron abundance. A) Gene fitness profiles of CAZ and CFD from Figure S5. The points are coloured based on positive (increased fitness; purple) or negative (decreased fitness; gold) interactions. B) The catechol group of CFD binds ferric iron (Fe^{3+}) and is recognized by the PiuA siderophore receptor. TonB, in complex with ExbBD, transduces energy from the proton motive force to PiuA for siderophore uptake into the cell. C) MIC values of CRISPRi mutants in *piuA* for CFD and CAZ in CAMHB and M9+CAA medium. NTC = non-targeting control sgRNA. MIC values are medians of three biological replicates, with bold indicating at least 2-fold change from the NTC with the addition of rhamnose. † Fold MIC is the ratio of the MIC -Rha to the MIC +Rha. D) Checkerboard assays of CFD crossed with deferiprone in K56-2 in CAMHB and M9+CAA. E) Checkerboard assays of CFD crossed with $FeCl_3$ in K56-2 in CAMHB and M9+CAA. Values are normalized to the OD_{600} of the well with the most growth. Interactions were assessed and interpreted with SynergyFinder as per the Materials and Methods.

REFERENCES

Aaron, S.D., Ferris, W., Henry, D.A., Speert, D.P., and Macdonald, N.E. 2000. Multiple combination bactericidal antibiotic testing for patients with cystic fibrosis infected with *Burkholderia cepacia*. Am J Respir Crit Care Med. **161**(4 Pt 1): 1206–1212. doi:10.1164/ajrccm.161.4.9907147.

Abbott, F.K., Milne, K.E.N., Stead, D.A., and Gould, I.M. 2016. Combination antimicrobial susceptibility testing of *Burkholderia cepacia* complex: significance of species. Int J Antimicrob Agents **48**(5): 521–527. doi:10.1016/j.ijantimicag.2016.07.020.

Abboud, M.I., Damblon, C., Brem, J., Smargiasso, N., Mercuri, P., Gilbert, B., Rydzik, A.M., Claridge, T.D.W., Schofield, C.J., and Frère, J.-M. 2016. Interaction of avibactam with class B metallo-β-lactamases. Antimicrob Agents Chemother **60**(10): 5655–5662. doi:10.1128/AAC.00897-16.

Abe, M., and Nakazawa, T. 1996. The *dsbB* gene product is required for protease production by *Burkholderia cepacia*. Infect Immun **64**(10): 4378–4380. doi:10.1128/iai.64.10.4378-4380.1996.

Ahn, Y., Kim, J.M., Kweon, O., Kim, S.-J., Jones, R.C., Woodling, K., Gamboa da Costa, G., LiPuma, J.J., Hussong, D., Marasa, B.S., and Cerniglia, C.E. 2016. Intrinsic resistance of *Burkholderia cepacia* complex to benzalkonium chloride. mBio **7**(6). doi:10.1128/mBio.01716-16.

Alderwick, L.J., Radmacher, E., Seidel, M., Gande, R., Hitchen, P.G., Morris, H.R., Dell, A., Sahm, H., Eggeling, L., and Besra, G.S. 2005. Deletion of Cg-*emb* in *Corynebacterianeae* leads to a novel truncated cell wall arabinogalactan, whereas inactivation of Cg-*ubiA* results in an arabinan-deficient mutant with a cell wall galactan core. J Biol Chem **280**(37): 32362–32371. doi:10.1074/jbc.M506339200.

Alghamdi, W.A., Alsultan, A., Al-Shaer, M.H., An, G., Ahmed, S., Alkabab, Y., Banu, S., Barbakadze, K., Houpt, E., Kipiani, M., Mikiashvili, L., Schmidt, S., Heysell, S.K., Kempker, R.R., Cegielski, J.P., and Peloquin, C.A. 2019. Cycloserine population pharmacokinetics and pharmacodynamics in patients with tuberculosis. Antimicrob Agents Chemother. doi:10.1128/AAC.00055-19.

Anglada-Girotto, M., Handschin, G., Ortmayr, K., Campos, A.I., Gillet, L., Manfredi, P., Mulholland, C.V., Berney, M., Jenal, U., Picotti, P., and Zampieri, M. 2022. Combining CRISPRi and metabolomics for functional annotation of compound libraries. Nat Chem Biol **18**(5): 482–491. doi:10.1038/s41589-022-00970-3.

Aronoff, S.C. 1988. Outer membrane permeability in *Pseudomonas cepacia*: diminished porin content in a beta-lactam-resistant mutant and in resistant cystic fibrosis isolates. Antimicrob Agents Chemother. **32**(11): 1636–1639. doi:10.1128/AAC.32.11.1636.

Arzanlou, M., Chai, W.C., and Venter, H. 2017. Intrinsic, adaptive and acquired antimicrobial resistance in Gram-negative bacteria. Essays Biochem **61**(1): 49–59. doi:10.1042/EBC20160063.

Ashburner, M., Ball, C.A., Blake, J.A., Botstein, D., Butler, H., Cherry, J.M., Davis, A.P., Dolinski, K., Dwight, S.S., Eppig, J.T., Harris, M.A., Hill, D.P., Issel-Tarver, L., Kasarskis, A., Lewis, S., Matese, J.C., Richardson, J.E., Ringwald, M., Rubin, G.M., and Sherlock, G. 2000. Gene Ontology: tool for the unification of biology. Nat Genet **25**(1): 25–29. doi:10.1038/75556.

Asli, A., Brouillette, E., Krause, K.M., Nichols, W.W., and Malouin, F. 2016. Distinctive binding of avibactam to penicillin-binding proteins of Gram-negative and Gram-positive bacteria. Antimicrob Agents Chemother **60**(2): 752–756. doi:10.1128/AAC.02102-15.

Baba, T., Ara, T., Hasegawa, M., Takai, Y., Okumura, Y., Baba, M., Datsenko, K.A., Tomita, M., Wanner, B.L., and Mori, H. 2006. Construction of *Escherichia coli* K-12 in-frame, single-gene knockout mutants: the Keio collection. Mol Syst Biol. **2**: 2006.0008. doi:10.1038/msb4100050.

Bailey, J., Gallagher, L., Barker, W.T., Hubble, V.B., Gasper, J., Melander, C., and Manoil, C. 2022. Genetic dissection of antibiotic adjuvant activity. mBio: e0308421. doi:10.1128/mbio.03084-21.

Balcewich, M.D., Reeve, T.M., Orlikow, E.A., Donald, L.J., Vocadlo, D.J., and Mark, B.L. 2010. Crystal structure of the AmpR effector binding domain provides insight into the molecular regulation of inducible AmpC beta-lactamase. J Mol Biol **400**(5): 998–1010. doi:10.1016/j.jmb.2010.05.040.

Barb, A.W., McClerren, A.L., Snehelatha, K., Reynolds, C.M., Zhou, P., and Raetz, C.R.H. 2007. Inhibition of lipid A biosynthesis as the primary mechanism of CHIR-090 antibiotic activity in *Escherichia coli*. Biochemistry **46**(12): 3793–3802. doi:10.1021/bi6025165.

Barreteau, H., Kovač, A., Boniface, A., Sova, M., Gobec, S., and Blanot, D. 2008. Cytoplasmic steps of peptidoglycan biosynthesis. FEMS Microbiol Rev **32**(2): 168–207. doi:10.1111/j.1574-6976.2008.00104.x.

Barreteau, H., Magnet, S., El Ghachi, M., Touzé, T., Arthur, M., Mengin-Lecreulx, D., and Blanot, D. 2009. Quantitative high-performance liquid chromatography analysis of the pool levels of undecaprenyl phosphate and its derivatives in bacterial membranes. J Chromatogr B Analyt Technol Biomed Life Sci **877**(3): 213–220. doi:10.1016/j.jchromb.2008.12.010.

Barrett-Bee, K., Newboult, L., and Edwards, S. 1994. The membrane destabilising action of the antibacterial agent chlorhexidine. FEMS Microbiol Lett **119**(1–2): 249–253. doi:10.1111/j.1574-6968.1994.tb06896.x.

Bartowsky, E., and Normark, S. 1991. Purification and mutant analysis of *Citrobacter freundii* AmpR, the regulator for chromosomal AmpC beta-lactamase. Mol Microbiol **5**(7): 1715–1725. doi:10.1111/j.1365-2958.1991.tb01920.x.

Bazzini, S., Udine, C., Sass, A., Pasca, M.R., Longo, F., Emiliani, G., Fondi, M., Perrin, E., Decorosi, F., Viti, C., Giovannetti, L., Leoni, L., Fani, R., Riccardi, G., Mahenthiralingam, E., and Buroni, S. 2011. Deciphering the role of RND efflux transporters in *Burkholderia cenocepacia*. PLoS ONE **6**(4): e18902. doi:10.1371/journal.pone.0018902.

Becka, S.A., Zeiser, E.T., Barnes, M.D., Taracila, M.A., Nguyen, K., Singh, I., Sutton, G.G., LiPuma, J.J., Fouts, D.E., and Papp-Wallace, K.M. 2018. Characterization of the AmpC β-Lactamase from *Burkholderia multivorans*. Antimicrob Agents Chemother **62**(10): e01140-18. doi:10.1128/AAC.01140-18.

Bernier, S.P., Son, and Surette, M.G. 2018. The Mla pathway plays an essential role in the intrinsic resistance of *Burkholderia cepacia* complex species to antimicrobials and host innate components. J Bacteriol **200**(18): e00156-18. doi:10.1128/JB.00156-18.

Biedenbach, D.J., Kazmierczak, K., Bouchillon, S.K., Sahm, D.F., and Bradford, P.A. 2015. *In vitro* activity of aztreonam-avibactam against a global collection of Gram-negative

pathogens from 2012 and 2013. Antimicrob Agents Chemother **59**(7): 4239–4248. doi:10.1128/AAC.00206-15.

Burrows, L.L., and Lam, J.S. 1999. Effect of *wzx (rfbX)* mutations on A-band and B-band lipopolysaccharide biosynthesis in *Pseudomonas aeruginosa* O5. J Bacteriol **181**(3): 973–980.

Butt, A.T., and Thomas, M.S. 2017. Iron acquisition mechanisms and their role in the virulence of *Burkholderia* Species. Front. Cell. Infect. Microbiol. **7**: 460. doi:10.3389/fcimb.2017.00460.

Calloni, G., Chen, T., Schermann, S.M., Chang, H., Genevaux, P., Agostini, F., Tartaglia, G.G., Hayer-Hartl, M., and Hartl, F.U. 2012. DnaK functions as a central hub in the *E. coli* chaperone network. Cell Reports **1**(3): 251–264. doi:10.1016/j.celrep.2011.12.007.

Cantalapiedra, C.P., Hernández-Plaza, A., Letunic, I., Bork, P., and Huerta-Cepas, J. 2021. eggNOG-mapper v2: Functional annotation, orthology assignments, and domain prediction at the metagenomic scale. bioRxiv: 2021.06.03.446934. Cold Spring Harbor Laboratory. doi:10.1101/2021.06.03.446934.

Castillo-Davis, C.I., and Hartl, D.L. 2003. GeneMerge--post-genomic analysis, data mining, and hypothesis testing. Bioinformatics **19**(7): 891–892. doi:10.1093/bioinformatics/btg114.

Cho, H., Uehara, T., and Bernhardt, T.G. 2014. Beta-lactam antibiotics induce a lethal malfunctioning of the bacterial cell wall synthesis machinery. Cell **159**(6): 1300–1311. doi:10.1016/j.cell.2014.11.017.

Choi, K.-H., Kumar, A., and Schweizer, H.P. 2006. A 10-min method for preparation of highly electrocompetent *Pseudomonas aeruginosa* cells: application for DNA fragment transfer between chromosomes and plasmid transformation. J. Microbiol. Methods **64**(3): 391–397. doi:10.1016/j.mimet.2005.06.001.

Choi, U., and Lee, C.-R. 2019. Distinct roles of outer membrane porins in antibiotic resistance and membrane integrity in *Escherichia coli*. Frontiers in Microbiology **10**.

Clinical and Laboratory Standards Institute CLSI. 2014. Performance standards for antimicrobial disk susceptibility testing; twenty-fourth informational supplement M100-S24. Clinical and Laboratory Standards Institute, Wayne, PA.

Darling, P., Chan, M., Cox, A.D., and Sokol, P.A. 1998. Siderophore production by cystic fibrosis isolates of *Burkholderia cepacia*. Infection and immunity **66**(2): 874–877.

Dartigalongue, C., Missiakas, D., and Raina, S. 2001. Characterization of the *Escherichia coli* sigma E regulon. J Biol Chem **276**(24): 20866–20875. doi:10.1074/jbc.M100464200.

Davies, T.A., Shang, W., Bush, K., and Flamm, R.K. 2008. Affinity of doripenem and comparators to penicillin-binding proteins in *Escherichia coli* and *Pseudomonas aeruginosa*. Antimicrob Agents Chemother **52**(4): 1510–1512. doi:10.1128/AAC.01529-07.

Decad, G.M., and Nikaido, H. 1976. Outer membrane of gram-negative bacteria. XII. Molecular-sieving function of cell wall. J Bacteriol **128**(1): 325–336. doi:10.1128/jb.128.1.325-336.1976.

Dik, D.A., Fisher, J.F., and Mobashery, S. 2018. Cell-wall recycling of the Gram-negative bacteria and the nexus to antibiotic resistance. Chem Rev **118**(12): 5952–5984. doi:10.1021/acs.chemrev.8b00277.

Dötsch, A., Becker, T., Pommerenke, C., Magnowska, Z., Jänsch, L., and Häussler, S. 2009. Genomewide identification of genetic determinants of antimicrobial drug resistance in

Pseudomonas aeruginosa. Antimicrob Agents Chemother **53**(6): 2522–2531. doi:10.1128/AAC.00035-09.

Doublet, P., van Heijenoort, J., Bohin, J.P., and Mengin-Lecreulx, D. 1993. The *murI* gene of *Escherichia coli* is an essential gene that encodes a glutamate racemase activity. J Bacteriol **175**(10): 2970–2979. doi:10.1128/jb.175.10.2970-2979.1993.

Durfey, S.L., Pipavath, S., Li, A., Vo, A.T., Ratjen, A., Carter, S., Morgan, S.J., Radey, M.C., Grogan, B., Salipante, S.J., Welsh, M.J., Stoltz, D.A., Goss, C.H., McKone, E.F., and Singh, P.K. 2021. Combining ivacaftor and intensive antibiotics achieves limited clearance of cystic fibrosis infections. mBio: e0314821. doi:10.1128/mbio.03148-21.

Dwyer, D.J., Belenky, P.A., Yang, J.H., MacDonald, I.C., Martell, J.D., Takahashi, N., Chan, C.T.Y., Lobritz, M.A., Braff, D., Schwarz, E.G., Ye, J.D., Pati, M., Vercruysse, M., Ralifo, P.S., Allison, K.R., Khalil, A.S., Ting, A.Y., Walker, G.C., and Collins, J.J. 2014. Antibiotics induce redox-related physiological alterations as part of their lethality. PNAS **111**(20): E2100–E2109. doi:10.1073/pnas.1401876111.

Egan, S.M., and Schleif, R.F. 1993. A regulatory cascade in the induction of *rha*BAD. J Mol Biol **234**(1): 87–98. doi:10.1006/jmbi.1993.1565.

Ehmann, D.E., Jahić, H., Ross, P.L., Gu, R.-F., Hu, J., Kern, G., Walkup, G.K., and Fisher, S.L. 2012. Avibactam is a covalent, reversible, non–β-lactam β-lactamase inhibitor. PNAS **109**(29): 11663–11668. doi:10.1073/pnas.1205073109.

El Ghachi, M., Bouhss, A., Blanot, D., and Mengin-Lecreulx, D. 2004. The *bacA* gene of *Escherichia coli* encodes an undecaprenyl pyrophosphate phosphatase activity. J Biol Chem **279**(29): 30106–30113. doi:10.1074/jbc.M401701200.

El Ghachi, M., Derbise, A., Bouhss, A., and Mengin-Lecreulx, D. 2005. Identification of multiple genes encoding membrane proteins with undecaprenyl pyrophosphate phosphatase (UppP) activity in *Escherichia coli*. J Biol Chem **280**(19): 18689–18695. doi:10.1074/jbc.M412277200.

El-Halfawy, O.M., and Valvano, M.A. 2014. Putrescine reduces antibiotic-induced oxidative stress as a mechanism of modulation of antibiotic resistance in *Burkholderia cenocepacia*. Antimicrob. Agents Chemother. **58**(7): 4162–4171. doi:10.1128/AAC.02649-14.

Everaert, A., and Coenye, T. 2016. Effect of β-lactamase inhibitors on in vitro activity of β-lactam antibiotics against *Burkholderia cepacia* complex species. Antimicrob Resist Infect Control **5**: 44. doi:10.1186/s13756-016-0142-3.

Felici, A., Amicosante, G., Oratore, A., Strom, R., Ledent, P., Joris, B., Fanuel, L., and Frère, J.M. 1993. An overview of the kinetic parameters of class B beta-lactamases. Biochem J **291**(Pt 1): 151–155.

Ferreira, A.S., Silva, I.N., Oliveira, V.H., Cunha, R., and Moreira, L.M. 2011. Insights into the role of extracellular polysaccharides in *Burkholderia* adaptation to different environments. Front Cell Infect Microbiol **1**: 16. doi:10.3389/fcimb.2011.00016.

Flannagan, R.S., Linn, T., and Valvano, M.A. 2008. A system for the construction of targeted unmarked gene deletions in the genus *Burkholderia*. Environmental microbiology **10**(6): 1652–1660. doi:10.1111/j.1462-2920.2008.01576.x.

Flannagan, R.S., and Valvano, M.A. 2008. *Burkholderia cenocepacia* requires RpoE for growth under stress conditions and delay of phagolysosomal fusion in macrophages. Microbiology (Reading, England) **154**(Pt 2): 643–653. doi:10.1099/mic.0.2007/013714-0.

Fotheringham, I.G., Bledig, S.A., and Taylor, P.P. 1998. Characterization of the genes encoding d-amino acid transaminase and glutamate racemase, two d-glutamate biosynthetic enzymes of *Bacillus sphaericus* ATCC 10208. J Bacteriol **180**(16): 4319–4323.

Furniss, R.C.D., Kaderabkova, N., Barker, D., Bernal, P., Maslova, E., Antwi, A.A., McNeil, H.E., Pugh, H.L., Dortet, L., Blair, J.M., Larrouy-Maumus, G., McCarthy, R.R., Gonzalez, D., and Mavridou, D.A. 2022. Breaking antimicrobial resistance by disrupting extracytoplasmic protein folding. eLife **11**: e57974. doi:10.7554/eLife.57974.

Gallagher, L.A., Shendure, J., and Manoil, C. 2011. Genome-scale identification of resistance functions in *Pseudomonas aeruginosa* using Tn-seq. MBio **2**(1): e00315-10. doi:10.1128/mBio.00315-10.

Garcia, B.A., Carden, J.L., Goodwin, D.L., Smith, T.A., Gaggar, A., Leon, K., Antony, V.B., Rowe, S.M., and Solomon, G.M. 2018. Implementation of a successful eradication protocol for *Burkholderia cepacia* complex in cystic fibrosis patients. BMC Pulm Med **18**. doi:10.1186/s12890-018-0594-8.

García-Romero, I., and Valvano, M.A. 2020. Complete genome sequence of *Burkholderia cenocepacia* K56-2, an opportunistic pathogen. Microbiol Resour Announc **9**(43). doi:10.1128/MRA.01015-20.

Geisinger, E., Mortman, N.J., Dai, Y., Cokol, M., Syal, S., Farinha, A., Fisher, D.G., Tang, A.Y., Lazinski, D.W., Wood, S., Anthony, J., van Opijnen, T., and Isberg, R.R. 2020. Antibiotic susceptibility signatures identify potential antimicrobial targets in the *Acinetobacter baumannii* cell envelope. Nat Commun **11**(1): 4522. doi:10.1038/s41467-020-18301-2.

Gene Ontology Consortium. 2021. The Gene Ontology resource: enriching a GOld mine. Nucleic Acids Res **49**(D1): D325–D334. doi:10.1093/nar/gkaa1113.

van Gestel, J., Hawkins, J.S., Todor, H., and Gross, C.A. 2021. Computational pipeline for designing guide RNAs for mismatch-CRISPRi. STAR Protocols **2**(2): 100521. doi:10.1016/j.xpro.2021.100521.

Gilead Sciences Inc. 2012. Cayston [package insert]. Foster City, California.

Gislason, A.S., Choy, M., Bloodworth, R.A.M., Qu, W., Stietz, M.S., Li, X., Zhang, C., and Cardona, S.T. 2017a. Competitive growth enhances conditional growth mutant sensitivity to antibiotics and exposes a two-component system as an emerging antibacterial target in *Burkholderia cenocepacia*. Antimicrob Agents Chemother. **61**(1): e00790-16. doi:10.1128/AAC.00790-16.

Gislason, A.S., Turner, K., Domaratzki, M., and Cardona, S.T. 2017b. Comparative analysis of the *Burkholderia cenocepacia* K56-2 essential genome reveals cell envelope functions that are uniquely required for survival in species of the genus *Burkholderia*. Microb Genom **3**(11): e000140. doi:10.1099/mgen.0.000140.

Grover, S., Alderwick, L.J., Mishra, A.K., Krumbach, K., Marienhagen, J., Eggeling, L., Bhatt, A., and Besra, G.S. 2014. Benzothiazinones mediate killing of Corynebacterineae by blocking decaprenyl phosphate recycling involved in cell wall biosynthesis. J Biol Chem **289**(9): 6177–6187. doi:10.1074/jbc.M113.522623.

Gunn, J.S., Lim, K.B., Krueger, J., Kim, K., Guo, L., Hackett, M., and Miller, S.I. 1998. PmrA–PmrB-regulated genes necessary for 4-aminoarabinose lipid A modification and polymyxin resistance. Mol Microbiol **27**(6): 1171–1182. doi:10.1046/j.1365-2958.1998.00757.x.

Hackel, M.A., Tsuji, M., Yamano, Y., Echols, R., Karlowsky, J.A., and Sahm, D.F. 2017. In vitro activity of the siderophore cephalosporin, cefiderocol, against a recent collection of clinically relevant Gram-negative bacilli from North America and Europe, including carbapenem-nonsusceptible isolates (SIDERO-WT-2014 Study). Antimicrob Agents Chemother **61**(9): e00093-17. doi:10.1128/AAC.00093-17.

Hackel, M.A., Tsuji, M., Yamano, Y., Echols, R., Karlowsky, J.A., and Sahm, D.F. 2018. *In vitro* activity of the siderophore cephalosporin, cefiderocol, against carbapenem-nonsusceptible and multidrug-resistant isolates of Gram-negative bacilli collected worldwide in 2014 to 2016. Antimicrob. Agents Chemother. **62**(2). doi:10.1128/AAC.01968-17.

Hamad, M.A., Di Lorenzo, F., Molinaro, A., and Valvano, M.A. 2012. Aminoarabinose is essential for lipopolysaccharide export and intrinsic antimicrobial peptide resistance in *Burkholderia cenocepacia*. Molecular Microbiology **85**(5): 962–974. doi:10.1111/j.1365-2958.2012.08154.x.

Hamad, M.A., Skeldon, A.M., and Valvano, M.A. 2010. Construction of aminoglycoside-sensitive *Burkholderia cenocepacia* strains for use in studies of intracellular bacteria with the gentamicin protection assay. Appl Environl Microbiol **76**(10): 3170–3176. doi:10.1128/AEM.03024-09.

Hayashi, S., Abe, M., Kimoto, M., Furukawa, S., and Nakazawa, T. 2000. The DsbA-DsbB disulfide bond formation system of *Burkholderia cepacia* is involved in the production of protease and alkaline phosphatase, motility, metal resistance, and multi-drug resistance. Microbiol Immunol **44**(1): 41–50. doi:10.1111/j.1348-0421.2000.tb01244.x.

He, W., Li, C., and Lu, C.-D. 2011. Regulation and characterization of the *dadRAX* locus for d-amino acid catabolism in *Pseudomonas aeruginosa* PAO1. J Bacteriol **193**(9): 2107–2115. doi:10.1128/JB.00036-11.

Hews, C.L., Cho, T., Rowley, G., and Raivio, T.L. 2019. Maintaining integrity under stress: Envelope stress response regulation of pathogenesis in Gram-negative bacteria. Front Cell Infect Microbiol **9**. Available from https://www.frontiersin.org/article/10.3389/fcimb.2019.00313 [accessed 8 February 2022].

Hogan, A.M., Rahman, A.S.M.Z., Lightly, T.J., and Cardona, S.T. 2019. A broad-host-range CRISPRi toolkit for silencing gene expression in *Burkholderia*. ACS Synth. Biol. **8**(10): 2372–2384. doi:10.1021/acssynbio.9b00232.

Hogan, A.M., Scoffone, V.C., Makarov, V., Gislason, A.S., Tesfu, H., Stietz, M.S., Brassinga, A.K.C., Domaratzki, M., Li, X., Azzalin, A., Biggiogera, M., Riabova, O., Monakhova, N., Chiarelli, L.R., Riccardi, G., Buroni, S., and Cardona, S.T. 2018. Competitive fitness of essential gene knockdowns reveals a broad-spectrum antibacterial inhibitor of the cell division protein FtsZ. Antimicrob Agents Chemother **62**(12): e01231-18. doi:10.1128/AAC.01231-18.

Huerta-Cepas, J., Forslund, K., Coelho, L.P., Szklarczyk, D., Jensen, L.J., von Mering, C., and Bork, P. 2017. Fast genome-wide functional annotation through orthology assignment by eggNOG-Mapper. Mol Biol Evol **34**(8): 2115–2122. doi:10.1093/molbev/msx148.

Hunt, T.A., Kooi, C., Sokol, P.A., and Valvano, M.A. 2004. Identification of *Burkholderia cenocepacia* genes required for bacterial survival *in vivo*. Infection and immunity **72**(7): 4010–4022.

Hunter, R.C., Asfour, F., Dingemans, J., Osuna, B.L., Samad, T., Malfroot, A., Cornelis, P., and Newman, D.K. 2013. Ferrous iron Is a significant component of bioavailable iron in cystic fibrosis airways. mBio **4**(4): e00557-13. doi:10.1128/mBio.00557-13.

Hwang, J., and Kim, H.S. 2015. Cell wall recycling-linked coregulation of AmpC and PenB β-lactamases through *ampD* mutations in *Burkholderia cenocepacia*. Antimicrob. Agents Chemother. **59**(12): 7602–7610. doi:10.1128/AAC.01068-15.

Ianevski, A., Giri, A.K., and Aittokallio, T. 2020. SynergyFinder 2.0: visual analytics of multi-drug combination synergies. Nucleic Acids Research **48**(W1): W488–W493. doi:10.1093/nar/gkaa216.

Isles, A., Maclusky, I., Corey, M., Gold, R., Prober, C., Fleming, P., and Levison, H. 1984. *Pseudomonas cepacia* infection in cystic fibrosis: an emerging problem. J. Pediatr. **104**(2): 206–210.

Isshiki, Y., Kawahara, K., and Zähringer, U. 1998. Isolation and characterisation of disodium (4-amino-4-deoxy-β-l-arabinopyranosyl)-(1-8)-(d-glycero-α-d-talo-oct-2-ulopyranosylonate)-(2-4)-(methyl 3-deoxy-d-manno-oct-2-ulopyranosid)onate from the lipopolysaccharide of *Burkholderia cepacia*. Carbohydrate Res **313**(1): 21–27. doi:10.1016/S0008-6215(98)00179-7.

Ito, A., Sato, T., Ota, M., Takemura, M., Nishikawa, T., Toba, S., Kohira, N., Miyagawa, S., Ishibashi, N., Matsumoto, S., Nakamura, R., Tsuji, M., and Yamano, Y. 2017. In vitro antibacterial properties of cefiderocol, a novel siderophore cephalosporin, against Gram-negative bacteria. Antimicrob Agents Chemother **62**(1). doi:10.1128/AAC.01454-17.

Jacobs, C., Huang, L.J., Bartowsky, E., Normark, S., and Park, J.T. 1994. Bacterial cell wall recycling provides cytosolic muropeptides as effectors for beta-lactamase induction. EMBO J **13**(19): 4684–4694. doi:10.1002/j.1460-2075.1994.tb06792.x.

Jacobs, C., Joris, B., Jamin, M., Klarsov, K., van Beeumen, J., Mengin-Lecreulx, D., van Heijenoort, J., Park, J.T., Normark, S., and Frère, J.-M. 1995. AmpD, essential for both β-lactamase regulation and cell wall recycling, is a novel cytosolic N-acetylmuramyl-L-alanine amidase. Mol Microbiol **15**(3): 553–559. doi:10.1111/j.1365-2958.1995.tb02268.x.

Jorgenson, M.A., and Bryant, J.C. 2021. A genetic screen to identify factors affected by undecaprenyl phosphate recycling uncovers novel connections to morphogenesis in *Escherichia coli*. Mol Microbiol **115**(2): 191–207. doi:https://doi.org/10.1111/mmi.14609.

Jorgenson, M.A., Kannan, S., Laubacher, M.E., and Young, K.D. 2016. Dead-end intermediates in the enterobacterial common antigen pathway induce morphological defects in *Escherichia coli* by competing for undecaprenyl phosphate. Mol Microbiol **100**(1): mmi.13284. NIH Public Access. doi:10.1111/mmi.13284.

Jorgenson, M.A., MacCain, W.J., Meberg, B.M., Kannan, S., Bryant, J.C., and Young, K.D. 2019. Simultaneously inhibiting undecaprenyl phosphate production and peptidoglycan synthases promotes rapid lysis in *Escherichia coli*. Mol Microbiol **112**(1): 233–248. doi:10.1111/mmi.14265.

Jorgenson, M.A., and Young, K.D. 2016. Interrupting biosynthesis of o-antigen or the lipopolysaccharide core produces morphological defects in *Escherichia coli* by sequestering undecaprenyl phosphate. J Bacteriol **198**(22): 3070–3079. doi:10.1128/JB.00550-16.

Kahan, F.M., Kahan, J.S., Cassidy, P.J., and Kropp, H. 1974. The mechanism of action of fosfomycin (phosphonomycin). Ann N Y Acad Sci **235**(0): 364–386. doi:10.1111/j.1749-6632.1974.tb43277.x.

Karp, P.D., Billington, R., Caspi, R., Fulcher, C.A., Latendresse, M., Kothari, A., Keseler, I.M., Krummenacker, M., Midford, P.E., Ong, Q., Ong, W.K., Paley, S.M., and Subhraveti, P. 2019. The BioCyc collection of microbial genomes and metabolic pathways. Brief Bioinform **20**(4): 1085–1093. Oxford Academic. doi:10.1093/bib/bbx085.

Kent, W.J. 2002. BLAT--the BLAST-like alignment tool. Genome Res **12**(4): 656–664. doi:10.1101/gr.229202.

Kitt, H., Lenney, W., and Gilchrist, F.J. 2016. Two case reports of the successful eradication of new isolates of *Burkholderia cepacia* complex in children with cystic fibrosis. BMC Pharmacol Toxicol **17**: 14-016-0054–0. doi:10.1186/s40360-016-0054-0 [doi].

Klein, K., Sonnabend, M.S., Frank, L., Leibiger, K., Franz-Wachtel, M., Macek, B., Trunk, T., Leo, J.C., Autenrieth, I.B., Schütz, M., and Bohn, E. 2019. Deprivation of the periplasmic chaperone SurA reduces virulence and restores antibiotic susceptibility of multidrug-resistant *Pseudomonas aeruginosa*. Front Microbiol **10**.

Klobucar, K., and Brown, E.D. 2022. New potentiators of ineffective antibiotics: Targeting the Gram-negative outer membrane to overcome intrinsic resistance. Curr Opin Chem Biol **66**: 102099. doi:10.1016/j.cbpa.2021.102099.

Kohanski, M.A., Dwyer, D.J., Hayete, B., Lawrence, C.A., and Collins, J.J. 2007. A common mechanism of cellular death induced by bactericidal antibiotics. Cell **130**(5): 797–810. doi:10.1016/j.cell.2007.06.049.

Kohira, N., West, J., Ito, A., Ito-Horiyama, T., Nakamura, R., Sato, T., Rittenhouse, S., Tsuji, M., and Yamano, Y. 2016. *In vitro* antimicrobial activity of a siderophore cephalosporin, S-649266, against Enterobacteriaceae clinical isolates, including carbapenem-resistant strains. Antimicrob Agents Chemother **60**(2): 729–734. doi:10.1128/AAC.01695-15.

Kuyyakanond, T., and Quesnel, L.B. 1992. The mechanism of action of chlorhexidine. FEMS Microbiol Lett **100**(1–3): 211–215. doi:10.1111/j.1574-6968.1992.tb14042.x.

Kuzuyama, T., Shimizu, T., Takahashi, S., and Seto, H. 1998. Fosmidomycin, a specific inhibitor of 1-deoxy-d-xylulose 5-phosphate reductoisomerase in the nonmevalonate pathway for terpenoid biosynthesis. Tetrahedron Letters **39**(43): 7913–7916. doi:10.1016/S0040-4039(98)01755-9.

Lahiri, S.D., Johnstone, M.R., Ross, P.L., McLaughlin, R.E., Olivier, N.B., and Alm, R.A. 2014. Avibactam and class C β-lactamases: Mechanism of inhibition, conservation of the binding pocket, and implications for resistance. Antimicrob Agents Chemother **58**(10): 5704–5713. doi:10.1128/AAC.03057-14.

Lan, P., Lu, Y., Chen, Z., Wu, X., Hua, X., Jiang, Y., Zhou, J., and Yu, Y. 2022. Emergence of high-level cefiderocol resistance in carbapenem-resistant *Klebsiella pneumoniae* from bloodstream infections in patients with hematologic malignancies in China. Microbiol Spectr **10**(2): e00084-22. doi:10.1128/spectrum.00084-22.

Landeta, C., Boyd, D., and Beckwith, J. 2018. Disulfide bond formation in prokaryotes. Nat Microbiol **3**(3): 270–280. doi:10.1038/s41564-017-0106-2.

Larson, M.H., Gilbert, L.A., Wang, X., Lim, W.A., Weissman, J.S., and Qi, L.S. 2013. CRISPR interference (CRISPRi) for sequence-specific control of gene expression. Nat Protoc **8**(11): 2180–2196. doi:10.1038/nprot.2013.132.

Lee, K., Campbell, J., Swoboda, J.G., Cuny, G.D., and Walker, S. 2010. Development of improved inhibitors of wall teichoic acid biosynthesis with potent activity against *Staphylococcus aureus*. Bioorg Med Chem Lett **20**(5): 1767–1770. doi:10.1016/j.bmcl.2010.01.036.

Liu, C., Li, C., Chen, Y., Hao, H., Liang, J., Duan, R., Guo, Z., Zhang, J., Zhao, Z., Jing, H., Wang, X., and Shao, S. 2017. Role of low-molecular-mass penicillin-binding proteins, NagZ and AmpR in AmpC β-lactamase regulation of *Yersinia enterocolitica*. Front. Cell. Infect. Microbiol. **7**. Available from https://www.frontiersin.org/article/10.3389/fcimb.2017.00425 [accessed 11 April 2022].

Loh, B., Grant, C., and Hancock, R.E. 1984. Use of the fluorescent probe 1-N-phenylnaphthylamine to study the interactions of aminoglycoside antibiotics with the outer membrane of *Pseudomonas aeruginosa*. Antimicrob. Agents Chemother. **26**(4): 546–551.

Lopatkin, A.J., Stokes, J.M., Zheng, E.J., Yang, J.H., Takahashi, M.K., You, L., and Collins, J.J. 2019. Bacterial metabolic state more accurately predicts antibiotic lethality than growth rate. Nat Microbiol: 1–9. doi:10.1038/s41564-019-0536-0.

Loutet, S.A., Mussen, L.E., Flannagan, R.S., and Valvano, M.A. 2011. A two-tier model of polymyxin B resistance in *Burkholderia cenocepacia*. Environmental Microbiology Reports **3**(2): 278–285. doi:https://doi.org/10.1111/j.1758-2229.2010.00222.x.

Loutet, S.A., and Valvano, M.A. 2011. Extreme antimicrobial peptide and polymyxin B resistance in the genus *Burkholderia*. Front Microbiol **2**: fmicb.2011.00159. doi:10.3389/fmicb.2011.00159.

Luscher, A., Moynié, L., Auguste, P.S., Bumann, D., Mazza, L., Pletzer, D., Naismith, J.H., and Köhler, T. 2018. TonB-dependent receptor repertoire of *Pseudomonas aeruginosa* for uptake of siderophore-drug conjugates. Antimicrob Agents Chemother. doi:10.1128/AAC.00097-18.

Maczuga, N., Tran, E.N.H., Qin, J., and Morona, R. 2022. Interdependence of *Shigella flexneri* O-antigen and enterobacterial common antigen biosynthetic pathways. J Bacteriol **204**(4): e0054621. doi:10.1128/jb.00546-21.

Makarov, V., Manina, G., Mikusova, K., Mollmann, U., Ryabova, O., Saint-Joanis, B., Dhar, N., Pasca, M.R., Buroni, S., Lucarelli, A.P., Milano, A., De Rossi, E., Belanova, M., Bobovska, A., Dianiskova, P., Kordulakova, J., Sala, C., Fullam, E., Schneider, P., McKinney, J.D., Brodin, P., Christophe, T., Waddell, S., Butcher, P., Albrethsen, J., Rosenkrands, I., Brosch, R., Nandi, V., Bharath, S., Gaonkar, S., Shandil, R.K., Balasubramanian, V., Balganesh, T., Tyagi, S., Grosset, J., Riccardi, G., and Cole, S.T. 2009. Benzothiazinones kill *Mycobacterium tuberculosis* by blocking arabinan synthesis. Science **324**(5928): 801–804. doi:10.1126/science.1171583.

Malinverni, J.C., and Silhavy, T.J. 2009. An ABC transport system that maintains lipid asymmetry in the gram-negative outer membrane. Proc Natl Acad Sci U S A **106**(19): 8009–8014. doi:10.1073/pnas.0903229106.

Malott, R.J., Steen-Kinnaird, B.R., Lee, T.D., and Speert, D.P. 2012. Identification of hopanoid biosynthesis genes involved in polymyxin resistance in *Burkholderia multivorans*. Antimicrob Agents Chemother **56**(1): 464–471. doi:10.1128/AAC.00602-11.

Marolda, C.L., Lahiry, P., Vinés, E., Saldías, S., and Valvano, M.A. 2006. Micromethods for the characterization of lipid A-core and O-antigen lipopolysaccharide. Methods Mol Biol **347**: 237–252. doi:10.1385/1-59745-167-3:237.

Masi, M., Réfregiers, M., Pos, K.M., and Pagès, J.-M. 2017. Mechanisms of envelope permeability and antibiotic influx and efflux in Gram-negative bacteria. Nat Microbiol **2**(3): 17001. doi:10.1038/nmicrobiol.2017.1.

Morin, M., Pierce, E.C., and Dutton, R.J. 2018. Changes in the genetic requirements for microbial interactions with increasing community complexity. eLife **7**: e37072. doi:10.7554/eLife.37072.

Moya, B., Dötsch, A., Juan, C., Blázquez, J., Zamorano, L., Haussler, S., and Oliver, A. 2009. β-lactam resistance response triggered by inactivation of a nonessential penicillin-binding protein. PLOS Pathogens **5**(3): e1000353. PLoS. doi:10.1371/journal.ppat.1000353.

Murray, C.J., Ikuta, K.S., Sharara, F., Swetschinski, L., Aguilar, G.R., Gray, A., Han, C., Bisignano, C., Rao, P., Wool, E., Johnson, S.C., Browne, A.J., Chipeta, M.G., Fell, F., Hackett, S., Haines-Woodhouse, G., Hamadani, B.H.K., Kumaran, E.A.P., McManigal, B., Agarwal, R., Akech, S., Albertson, S., Amuasi, J., Andrews, J., Aravkin, A., Ashley, E., Bailey, F., Baker, S., Basnyat, B., Bekker, A., Bender, R., Bethou, A., Bielicki, J., Boonkasidecha, S., Bukosia, J., Carvalheiro, C., Castañeda-Orjuela, C., Chansamouth, V., Chaurasia, S., Chiurchiù, S., Chowdhury, F., Cook, A.J., Cooper, B., Cressey, T.R., Criollo-Mora, E., Cunningham, M., Darboe, S., Day, N.P.J., Luca, M.D., Dokova, K., Dramowski, A., Dunachie, S.J., Eckmanns, T., Eibach, D., Emami, A., Feasey, N., Fisher-Pearson, N., Forrest, K., Garrett, D., Gastmeier, P., Giref, A.Z., Greer, R.C., Gupta, V., Haller, S., Haselbeck, A., Hay, S.I., Holm, M., Hopkins, S., Iregbu, K.C., Jacobs, J., Jarovsky, D., Javanmardi, F., Khorana, M., Kissoon, N., Kobeissi, E., Kostyanev, T., Krapp, F., Krumkamp, R., Kumar, A., Kyu, H.H., Lim, C., Limmathurotsakul, D., Loftus, M.J., Lunn, M., Ma, J., Mturi, N., Munera-Huertas, T., Musicha, P., Mussi-Pinhata, M.M., Nakamura, T., Nanavati, R., Nangia, S., Newton, P., Ngoun, C., Novotney, A., Nwakanma, D., Obiero, C.W., Olivas-Martinez, A., Olliaro, P., Ooko, E., Ortiz-Brizuela, E., Peleg, A.Y., Perrone, C., Plakkal, N., Ponce-de-Leon, A., Raad, M., Ramdin, T., Riddell, A., Roberts, T., Robotham, J.V., Roca, A., Rudd, K.E., Russell, N., Schnall, J., Scott, J.A.G., Shivamallappa, M., Sifuentes-Osornio, J., Steenkeste, N., Stewardson, A.J., Stoeva, T., Tasak, N., Thaiprakong, A., Thwaites, G., Turner, C., Turner, P., Doorn, H.R. van, Velaphi, S., Vongpradith, A., Vu, H., Walsh, T., Waner, S., Wangrangsimakul, T., Wozniak, T., Zheng, P., Sartorius, B., Lopez, A.D., Stergachis, A., Moore, C., Dolecek, C., and Naghavi, M. 2022. Global burden of bacterial antimicrobial resistance in 2019: a systematic analysis. Lancet **399**(10325): 629–655. Elsevier. doi:10.1016/S0140-6736(21)02724-0.

Nunvar, J., Hogan, A.M., Buroni, S., Savina, S., Makarov, V., Cardona, S.T., and Drevinek, P. 2019. The effect of 2-thiocyanatopyridine derivative 11026103 on *Burkholderia cenocepacia*: Resistance mechanisms and systemic impact. Antibiotics **8**(4): 159. doi:10.3390/antibiotics8040159.

Nurjadi, D., Kocer, K., Chanthalangsy, Q., Klein, S., Heeg, K., and Boutin, S. 2021. New Delhi metallo-beta-lactamase facilitates the emergence of cefiderocol resistance in *Enterobacter cloacae*. Antimicrob Agents Chemother. doi:10.1128/aac.02011-21.

Okuda, S., and Tokuda, H. 2011. Lipoprotein sorting in bacteria. Annu Rev Microbiol **65**: 239–259. doi:10.1146/annurev-micro-090110-102859.

O'Neill, J. 2014. Antimicrobial Resistance: Tackling a crisis for the health and wealth of nations. Rev Antimicrob Resist

Ortega, X., Hunt, T.A., Loutet, S., Vinion-Dubiel, A.D., Datta, A., Choudhury, B., Goldberg, J.B., Carlson, R., and Valvano, M.A. 2005. Reconstitution of O-specific lipopolysaccharide expression in *Burkholderia cenocepacia* strain J2315, which is associated with transmissible infections in patients with cystic fibrosis. Journal of Bacteriology **187**(4): 1324–1333.

Ortega, X., Silipo, A., Saldías, M.S., Bates, C.C., Molinaro, A., and Valvano, M.A. 2009. Biosynthesis and structure of the *Burkholderia cenocepacia* K56-2 lipopolysaccharide core oligosaccharide: truncation of the core oligosaccharide leads to increased binding and sensitivity to polymyxin B. J. Biol. Chem. **284**(32): 21738–21751. doi:10.1074/jbc.M109.008532.

Panta, P.R., Kumar, S., Stafford, C.F., Billiot, C.E., Douglass, M.V., Herrera, C.M., Trent, M.S., and Doerrler, W.T. 2019. A DedA family membrane protein is required for *Burkholderia thailandensis* colistin resistance. Front Microbiol **10**.

Papp-Wallace, K.M., Becka, S.A., Zeiser, E.T., Ohuchi, N., Mojica, M.F., Gatta, J.A., Falleni, M., Tosi, D., Borghi, E., Winkler, M.L., Wilson, B.M., LiPuma, J.J., Nukaga, M., and Bonomo, R.A. 2017. Overcoming an extremely drug resistant (XDR) pathogen: avibactam restores susceptibility to ceftazidime for *Burkholderia cepacia* complex isolates from cystic fibrosis patients. ACS Infect Dis **3**(7): 502–511. doi:10.1021/acsinfecdis.7b00020.

Papp-Wallace, K.M., Senkfor, B., Gatta, J., Chai, W., Taracila, M.A., Shanmugasundaram, V., Han, S., Zaniewski, R.P., Lacey, B.M., Tomaras, A.P., Skalweit, M.J., Harris, M.E., Rice, L.B., Buynak, J.D., and Bonomo, R.A. 2012. Early insights into the interactions of different β-lactam antibiotics and β-lactamase inhibitors against soluble forms of *Acinetobacter baumannii* PBP1a and *Acinetobacter* sp. PBP3. Antimicrob Agents Chemother **56**(11): 5687–5692. doi:10.1128/AAC.01027-12.

Parr, J.T., Moore, R.A., Moore, L.V., and Hancock, R.E. 1987. Role of porins in intrinsic antibiotic resistance of *Pseudomonas cepacia*. Antimicrob Agents Chemother **31**(1): 121–123. doi:10.1128/AAC.31.1.121.

Poirel, L., Rodriguez-Martinez, J.-M., Plésiat, P., and Nordmann, P. 2009. Naturally ccurring class A ß-lactamases from the *Burkholderia cepacia* complex. Antimicrob. Agents Chemother. **53**(3): 876–882. doi:10.1128/AAC.00946-08.

Powers, M.J., Simpson, B.W., and Trent, M.S. 2020. The Mla pathway in *Acinetobacter baumannii* has no demonstrable role in anterograde lipid transport. eLife **9**: e56571. doi:10.7554/eLife.56571.

Pristovsek, P., and Kidric, J. 1999. Solution structure of polymyxins B and E and effect of binding to lipopolysaccharide: an NMR and molecular modeling study. J Med Chem **42**(22): 4604–4613. doi:10.1021/jm991031b.

Pucci, M.J., Thanassi, J.A., Ho, H.T., Falk, P.J., and Dougherty, T.J. 1995. *Staphylococcus haemolyticus* contains two D-glutamic acid biosynthetic activities, a glutamate racemase and a D-amino acid transaminase. J Bacteriol **177**(2): 336–342. doi:10.1128/jb.177.2.336-342.1995.

Qi, L.S., Larson, M.H., Gilbert, L.A., Doudna, J.A., Weissman, J.S., Arkin, A.P., and Lim, W.A. 2013. Repurposing CRISPR as an RNA-guided platform for sequence-specific control of gene expression. Cell **152**(5): 1173–1183. doi:10.1016/j.cell.2013.02.022 [doi].

Rhodes, K.A., and Schweizer, H.P. 2016. Antibiotic resistance in *Burkholderia* species. Drug Resistance Updates **28**: 82–90. doi:10.1016/j.drup.2016.07.003.

Roney, I.J., and Rudner, D.Z. 2022, February 3. Two broadly conserved families of polyprenyl-phosphate transporters. bioRxiv. doi:10.1101/2022.02.03.479048.

Sabnis, A., Hagart, K.L., Klöckner, A., Becce, M., Evans, L.E., Furniss, R.C.D., Mavridou, D.A., Murphy, R., Stevens, M.M., Davies, J.C., Larrouy-Maumus, G.J., Clarke, T.B., and Edwards, A.M. 2021. Colistin kills bacteria by targeting lipopolysaccharide in the cytoplasmic membrane. Elife **10**: e65836. doi:10.7554/eLife.65836.

Sanders, C.C., Bradford, P.A., Ehrhardt, A.F., Bush, K., Young, K.D., Henderson, T.A., and Sanders, W.E. 1997. Penicillin-binding proteins and induction of AmpC beta-lactamase. Antimicrob Agents Chemother **41**(9): 2013–2015. doi:10.1128/AAC.41.9.2013.

Sanderson, T., Bileschi, M.L., Belanger, D., and Colwell, L.J. 2021, October 6. ProteInfer: deep networks for protein functional inference. bioRxiv. doi:10.1101/2021.09.20.461077.

Sass, A., Everaert, A., Acker, H.V., Driessche, F.V. den, and Coenye, T. 2018. Targeting the nonmevalonate pathway in *Burkholderia cenocepacia* increases susceptibility to certain β-lactam antibiotics. Antimicrob. Agents Chemother. **62**(5): e02607-17. doi:10.1128/AAC.02607-17.

Scoffone, V.C., Trespidi, G., Barbieri, G., Irudal, S., Perrin, E., and Buroni, S. 2021. Role of RND efflux pumps in drug resistance of cystic fibrosis pathogens. Antibiotics **10**(7): 863. doi:10.3390/antibiotics10070863.

Shionogi Inc. 2019. Antimicrobial drugs advisory committee: Cefiderocol briefing document. Food and Drug Administration. Available from https://www.fda.gov/media/131705/download [accessed 3 February 2022].

Siewert, G., and Strominger, J.L. 1967. Bacitracin: An inhibitor of the dephosphorylation of lipid pyrophosphate, an intermediate in the biogenesis of the peptidoglycan of bacterial cell walls. Proc Natl Acad Sci U S A **57**(3): 767–773.

Simpson, B.W., and Trent, M.S. 2019. Pushing the envelope: LPS modifications and their consequences. Nat Rev Microbiol **17**(7): 403–416. doi:10.1038/s41579-019-0201-x.

Sit, B., Srisuknimit, V., Hullahalli, K., Bueno, E., Cava, F., and Waldor, M.K. 2022, February 4. Candidate undecaprenyl phosphate translocases enable conditional microbial fitness and pathogenesis. bioRxiv. doi:10.1101/2022.02.04.479082.

Sonnabend, M.S., Klein, K., Beier, S., Angelov, A., Kluj, R., Mayer, C., Groß, C., Hofmeister, K., Beuttner, A., Willmann, M., Peter, S., Oberhettinger, P., Schmidt, A., Autenrieth, I.B., Schütz, M., and Bohn, E. 2020. Identification of drug resistance determinants in a clinical isolate of *Pseudomonas aeruginosa* by high-density transposon mutagenesis. Antimicrob Agents Chemother **64**(3): e01771-19. doi:10.1128/AAC.01771-19.

Spoletini, G., Etherington, C., Shaw, N., Clifton, I.J., Denton, M., Whitaker, P., and Peckham, D.G. 2019. Use of ceftazidime/avibactam for the treatment of MDR *Pseudomonas aeruginosa* and *Burkholderia cepacia* complex infections in cystic fibrosis: a case series. J Antimicrob Chemother **74**(5): 1425–1429. doi:10.1093/jac/dky558.

Sutaria, D.S., Moya, B., Green, K.B., Kim, T.H., Tao, X., Jiao, Y., Louie, A., Drusano, G.L., and Bulitta, J.B. 2018. First penicillin-binding protein occupancy patterns of β-lactams and β-lactamase inhibitors in *Klebsiella pneumoniae*. Antimicrob Agents Chemother **62**(6): e00282-18. doi:10.1128/AAC.00282-18.

Swoboda, J.G., Meredith, T.C., Campbell, J., Brown, S., Suzuki, T., Bollenbach, T., Malhowski, A.J., Kishony, R., Gilmore, M.S., and Walker, S. 2009. Discovery of a small molecule that blocks wall teichoic acid biosynthesis in *Staphylococcus aureus*. ACS Chem.Biol. **4**(10): 875–883. doi:10.1021/cb900151k.

Tayler, A.E., Ayala, J.A., Niumsup, P., Westphal, K., Baker, J.A., Zhang, L., Walsh, T.R., Wiedemann, B., Bennett, P.M., and Avison, M.B. 2010. Induction of beta-lactamase production in *Aeromonas hydrophila* is responsive to beta-lactam-mediated changes in peptidoglycan composition. Microbiology (Reading) **156**(Pt 8): 2327–2335. doi:10.1099/mic.0.035220-0.

van Teeseling, M.C.F., de Pedro, M.A., and Cava, F. 2017. Determinants of bacterial morphology: from fundamentals to possibilities for antimicrobial targeting. Front Microbiol **8**.

Trent, M.S., Ribeiro, A.A., Doerrler, W.T., Lin, S., Cotter, R.J., and Raetz, C.R. 2001a. Accumulation of a polyisoprene-linked amino sugar in polymyxin-resistant *Salmonella typhimurium* and *Escherichia coli*: Structural characterization and transfer to lipid A in the periplasm. J Biol Chem **276**(46): 43132–43144. doi:10.1074/jbc.M106962200.

Trent, M.S., Ribeiro, A.A., Lin, S., Cotter, R.J., and Raetz, C.R. 2001b. An inner membrane enzyme in *Salmonella* and *Escherichia coli* that transfers 4-amino-4-deoxy-L-arabinose to lipid A: Induction on polymyxin-resistant mutants and role of a novel lipid-linked donor. J Biol Chem **276**(46): 43122–43131. doi:10.1074/jbc.M106961200.

Van Acker, H., Gielis, J., Acke, M., Cools, F., Cos, P., and Coenye, T. 2016. The role of reactive oxygen species in antibiotic-induced cell death in *Burkholderia cepacia* complex bacteria. PLoS ONE **11**(7): e0159837. doi:10.1371/journal.pone.0159837.

Vezina, B., Petit, G.A., Martin, J.L., and Halili, M.A. 2020. Prediction of *Burkholderia pseudomallei* DsbA substrates identifies potential virulence factors and vaccine targets. PLoS One **15**(11): e0241306. doi:10.1371/journal.pone.0241306.

Walsh, C.T. 1989. Enzymes in the D-alanine branch of bacterial cell wall peptidoglycan assembly. J Biol Chem **264**(5): 2393–2396.

Wang, X., Ribeiro, A.A., Guan, Z., and Raetz, C.R.H. 2009. Identification of undecaprenyl phosphate-β-D-galactosamine in *Francisella novicida* and its function in lipid A modification. Biochemistry **48**(6): 1162–1172. doi:10.1021/bi802211k.

Weaver, A.I., Alvarez, L., Rosch, K.M., Ahmed, A., Wang, G.S., van Nieuwenhze, M.S., Cava, F., and Dörr, T. 2022. Lytic transglycosylases mitigate periplasmic crowding by degrading soluble cell wall turnover products. eLife **11**: e73178. eLife Sciences Publications, Ltd. doi:10.7554/eLife.73178.

Weaver, A.I., Murphy, S.G., Umans, B.D., Tallavajhala, S., Onyekwere, I., Wittels, S., Shin, J.-H., VanNieuwenhze, M., Waldor, M.K., and Dörr, T. 2018. Genetic determinants of penicillin tolerance in *Vibrio cholerae*. Antimicrob. Agents Chemother. **62**(10). doi:10.1128/AAC.01326-18.

Wetmore, K.M., Price, M.N., Waters, R.J., Lamson, J.S., He, J., Hoover, C.A., Blow, M.J., Bristow, J., Butland, G., Arkin, A.P., and Deutschbauer, A. 2015. Rapid quantification of mutant fitness in diverse bacteria by sequencing randomly bar-coded transposons. MBio **6**(3): e00306-00315. doi:10.1128/mBio.00306-15.

Wu, T., Malinverni, J., Ruiz, N., Kim, S., Silhavy, T.J., and Kahne, D. 2005. Identification of a multicomponent complex required for outer membrane biogenesis in *Escherichia coli*. Cell **121**(2): 235–245. Elsevier. doi:10.1016/j.cell.2005.02.015.

Xayarath, B., and Yother, J. 2007. Mutations blocking side chain assembly, polymerization, or transport of a Wzy-dependent *Streptococcus pneumoniae* capsule are lethal in the absence of suppressor mutations and can affect polymer transfer to the cell wall. J Bacteriol **189**(9). doi:10.1128/JB.01938-06.

Yang, J.H., Wright, S.N., Hamblin, M., McCloskey, D., Alcantar, M.A., Schrübbers, L., Lopatkin, A.J., Satish, S., Nili, A., Palsson, B.O., Walker, G.C., and Collins, J.J. 2019. A white-box machine learning approach for revealing antibiotic mechanisms of action. Cell **177**(6): 1649-1661.e9. doi:10.1016/j.cell.2019.04.016.

Yapa, S.W.S., Li, J., Patel, K., Wilson, J.W., Dooley, M.J., George, J., Clark, D., Poole, S., Williams, E., Porter, C.J.H., Nation, R.L., and McIntosh, M.P. 2014. Pulmonary and systemic pharmacokinetics of inhaled and intravenous colistin methanesulfonate in cystic fibrosis patients: targeting advantage of inhalational administration. Antimicrob Agents Chemother **58**(5): 2570–2579. doi:10.1128/AAC.01705-13.

Zeiser, E.T., Becka, S.A., Barnes, M.D., Taracila, M.A., LiPuma, J.J., and Papp-Wallace, K.M. 2019. Resurrecting old β-Lactams: potent inhibitory activity of temocillin against multidrug-resistant *Burkholderia* species isolates from the United States. Antimicrob Agents Chemother **63**(4): e02315-18. doi:10.1128/AAC.02315-18.

Zhanel, G.G., Zhanel, M.A., and Karlowsky, J.A. 2020. Oral and intravenous fosfomycin for the treatment of complicated urinary tract infections. Can J Infect Dis Med Microbiol **2020**: 8513405. doi:10.1155/2020/8513405.

Zheng, S., Wang, W., Aldahdooh, J., Malyutina, A., Shadbahr, T., Tanoli, Z., Pessia, A., and Tang, J. 2022. SynergyFinder Plus: Toward better interpretation and annotation of drug combination screening datasets. Genom Proteom Bioinformatics: S1672-0229(22)00008–0. doi:10.1016/j.gpb.2022.01.004.